

Host-Guest Compounds: Structure and Thermal Behaviour

by

Marie-Louise Tangouna Liambo Bissa

A thesis submitted to the Cape Peninsula University of Technology in fulfilment of
the requirements for the degree

Master of Technology in Chemistry

In the Faculty of Applied Sciences

at the

CAPE PENINSULA UNIVERSITY OF TECHNOLOGY

Supervisor: Associate Professor Ayesha Jacobs

Cape Town

June 2016

DECLARATION

I, Marie-Louise Tangouna Liambo Bissa, declare that the contents of this dissertation/thesis represent my own unaided work, and that the dissertation/thesis has not previously been submitted for academic examination towards any qualification. Furthermore, it represents my own opinions and not necessarily those of the Cape Peninsula University of Technology.

Signed

Date

ABSTRACT

Inclusion compounds of two hydroxyl hosts with a variety of guests have been investigated. These host compounds are bulky molecules and have the ability to interact with smaller organic guests to form new compounds. The host 9-(1-naphthyl)-9*H*-xanthen-9-ol (**H1**), forms inclusion compounds with pyridine (**PYR**), *N,N*-dimethylacetamide (**DMA**), morpholine (**MORP**) and *N*-methyl-2-pyrrolidinone (**NMP**). The crystal structures of **H1•NMP**, **H1•DMA** and **H1•MORP1** were successfully solved in the triclinic space group $P\bar{1}$, whereas the inclusion compound **H1•PYR** crystallised in the monoclinic space group $P2_1/c$. A different inclusion compound involving morpholine, **H1•MORP2** resulted from dissolution of **H1** in a 1:1 molar ratio of **MORP**: **DMA**. **H1•MORP2** crystallised in the space group $P\bar{1}$. All of the abovementioned inclusion compounds demonstrated a host: guest ratio of 1:1 except for **H1•MORP1** (host: guest ratio = 1: $\frac{3}{2}$). **H1** interacts with pyridine and morpholine guests via (Host)O-H...N(Guest) hydrogen bonds and via (Host)OH...O(Guest) hydrogen bonds with *N*-methyl-2-pyrrolidinone and *N,N*-dimethylacetamide.

5-(4-methylphenyl)-5*H*-dibenzo[*a,d*]cyclohepten-5-ol (**H2**) forms inclusion compounds with morpholine (**MORP**), *N*-methyl-2-pyrrolidinone (**NMP**) and dimethylsulfoxide (**DMSO**). Both **H2•DMSO** and **H2•NMP** crystallised in $P2_1/n$ with (Host)OH...O(Guest) hydrogen bonds whereas the crystal structure of **H2•MORP** solved in $P\bar{1}$ demonstrating (Host)OH...N(Guest) linkages. A crystal structure of the apohost (**H2**) was solved in $P\bar{1}$ with **H2** molecules forming (Host)O-H...O(Host) hydrogen bonds.

The crystal structures of the host-guest compounds were elucidated using single crystal X-ray diffraction methods. Thermogravimetry (TG), differential scanning calorimetry (DSC) and hot stage microscopy (HSM) were used to study the thermal behaviour of the compounds. The compounds were also characterized using powder X-ray diffraction (PXRD) and Fourier transform infrared (FTIR) spectroscopy. The selectivity of **H1** and **H2** towards mixtures of guests was determined whereby the respective hosts were dissolved in equimolar mixtures of the guests. The resultant crystals were analysed and the selectivity trend for **H1**, was established as **NMP** > **MORP** > **DMA** > **PYR**. For **H2** the selectivity trend was **NMP** > **MORP** > **DMSO**.

Hirshfeld surface analysis was used to calculate the contribution of the intermolecular interactions in the crystal structures. Fingerprint plots showing each of the contributions were generated and comparisons between the crystal structures are discussed.

ACKNOWLEDGEMENTS

I wish to thank:

- **God, for his love, grace and mercy,**
- **My supervisor Associate Professor Ayesha Jacobs, for her patience, help and support,**
- **My family, friends and colleagues for their support and encouragement**
- **The staff of the Department of Chemistry, Cape Peninsula University of Technology.**

PUBLICATION

Parts of this thesis has been published:

- ❖ Jacobs, A., Tangouna Liambo Bissa, M-L., Taljaard, J.H. (2015) Inclusion compounds of 5-(4-methylphenyl)-5*H*-dibenzo[a,d]cyclohepten-5-ol with dimethylsulfoxide, morpholine and *N*-methyl-2-pyrrolidinone. *J. Chem. Crystallogr.*, 45:330-337.

DEDICATION

I dedicate this thesis to my family.

TABLE OF CONTENTS

DECLARATION	ii
ABSTRACT	iii
ACKNOWLEDGEMENTS	iv
PUBLICATION	v
DEDICATION	vi
TABLE OF CONTENTS	vii
ATOM COLOUR SCHEME	xx
CHAPTER 1: INTRODUCTION	1
1.1 Supramolecular chemistry.....	1
1.2 Host-guest chemistry	3
1.3 Applications of Host-Guest Chemistry.....	7
1.4 Interactions in supramolecular chemistry	8
1.4.1 Non-covalent interactions.....	8
1.4.1.1 Hydrogen bond	9
1.4.1.2 π - π interactions	12
1.5 Crystal engineering	13
1.6 Objectives of the study.....	14
References	15
CHAPTER 2: EXPERIMENTAL METHODS AND MATERIALS	18
2.1 Host compounds used in the study	18
2.2 Guest compounds.....	20
2.3 Crystal growth.....	21

2.4	Thermal analysis.....	21
2.5	Powder X-ray diffraction (PXRD)	22
2.6	Single crystal X-ray diffraction	22
2.7	Infrared (IR) spectroscopy.....	23
2.8	Selectivity experiments.....	24
2.9	Hot stage microscopy (HSM).....	24
2.10	CrystalExplorer.....	24
2.11	Computing packages.....	25
	References	26

CHAPTER 3: H1 AND ITS INCLUSION COMPOUNDS..... 28

3.1	Inclusion compound of H1 and pyridine (H1•PYR)	30
3.1.1	Thermal analysis	30
3.1.2	Hot stage microscopy (HSM).....	31
3.1.3	IR spectroscopy.....	32
3.1.4	Powder X-ray diffraction (PXRD)	34
3.1.5	Crystal structure analysis	35
3.2	Inclusion compound of H1 and <i>N</i> -methyl-2-pyrrolidinone (H1•NMP)	41
3.2.1	Thermal analysis	41
3.2.2	Hot stage microscopy (HSM).....	42
3.2.3	IR spectroscopy	43
3.2.4	Powder X-ray diffraction (PXRD)	44
3.2.5	Crystal structure analysis	45
3.3	Inclusion compound of H1 and <i>N</i> -dimethylacetamide (H1•DMA).....	51
3.3.1	Thermal analysis.....	51
3.3.2	Hot stage microscopy (HSM).....	53

3.3.3	IR spectroscopy.....	54
3.3.4	Powder X-ray diffraction (PXRD).....	55
3.3.5	Crystal structure analysis.....	56
3.4	Inclusion compounds of H1 and morpholine (H1•MORP1 and H1•MORP2).....	64
3.4.1	H1•MORP1.....	64
3.4.1.1	Thermal analysis.....	64
3.4.1.2	Hot stage microscopy (HSM).....	66
3.4.1.3	IR spectroscopy.....	67
3.4.1.4	Powder X-ray diffraction (PXRD).....	68
3.4.1.5	Crystal structure analysis.....	69
3.5	H1•MORP2.....	76
3.5.1	Thermal analysis.....	76
3.5.2	Hot stage microscopy (HSM).....	77
3.5.3	IR spectroscopy.....	79
3.5.4	Crystal structure analysis.....	80
3.6	Summary of thermal analysis results of H1 and its inclusion compounds.....	88
3.7	Selectivity experiments.....	89
3.8	Torsion angles for the host molecule H1.....	90
References	92

CHAPTER 4: H2 AND ITS INCLUSION COMPOUNDS..... 92

4.1	Inclusion compound of H2 and dimethylsulfoxide (H2•DMSO).....	95
4.1.1	Thermal analysis.....	95
4.1.2	Hot stage microscopy (HSM).....	95
4.1.3	IR spectroscopy.....	98
4.1.4	Powder X-ray diffraction (PXRD).....	99
4.1.5	Crystal structure analysis.....	100

4.2	Inclusion compound of H2 and <i>N</i> -methyl-2-pyrrolidinone (H2•NMP)	105
4.2.1	Thermal analysis.....	105
4.2.2	Hot stage microscopy (HSM).....	106
4.2.3	IR spectroscopy.....	108
4.2.4	Powder X-ray diffraction (PXRD)	109
4.2.5	Crystal structure analysis.....	110
4.3	Inclusion compound of H2 and morpholine (H2•MORP).....	115
4.3.1	Thermal analysis	115
4.3.2	Hot stage microscopy (HSM).....	116
4.3.3	IR spectroscopy	117
4.3.4	Powder X-ray diffraction (PXRD).....	118
4.3.5	Crystal structure analysis.....	119
4.4	Crystal structure of the apohost H2	126
4.5	Torsion angles for the host molecule H2	132
4.6	Selectivity experiments.....	133
	References	135

CHAPTER 5: HIRSHFELD SURFACE ANALYSIS OF THE INCLUSION COMPOUNDS OF H1 **136**

References	142
-------------------------	------------

CHAPTER 6: HIRSHFELD SURFACE ANALYSIS OF THE INCLUSION COMPOUNDS OF H2..... **143**

References	147
-------------------------	------------

CHAPTER 7: CONCLUSION..... **148**

LIST OF FIGURES

CHAPTER 1: INTRODUCTION

Figure 1.1: Comparison between molecular and supramolecular chemistry.....	2
Figure 1.2: A host binds a guest in order to produce a host-guest complex (a supermolecule).....	4
Figure 1.3: Demonstration of the difference between a cavitate and a clathrate	6
Figure 1.4: Various types of hydrogen bonding geometries: (a) linear; (b) bent; (c) donating bifurcated; (d) accepting bifurcated; (e) trifurcated; (f) three-centre bifurcated	10
Figure 1.5: Off-set face-to-face π - π stacking.....	12
Figure 1.6: Edge-to-face π - π interaction	13

CHAPTER 2: EXPERIMENTAL METHODS AND MATERIALS

Figure 2.1: Schematic representation of H1	19
Figure 2.2: Schematic representation of H2	19
Figure 2.3: Flow diagram of a single crystal X-ray analysis.....	23

CHAPTER 3: H1 AND ITS INCLUSION COMPOUNDS

Figure 3.1: Numbering scheme of H1	29
Figure 3.2: DSC curve of the host compound H1	30
Figure 3.3: DSC and TG curves of H1•PYR	31
Figure 3.4: Thermal decomposition of the crystal H1•PYR	32
Figure 3.5: IR spectra of (a) H1 and (b) H1•PYR	33
Figure 3.6: PXRD patterns of (a) H1•PYR calculated from LAZYPULVERIX, (b) ground product and (c) H1	34
Figure 3.7: Asymmetric unit of H1•PYR	37

Figure 3.8: Hydrogen bonding in H1•PYR	38
Figure 3.9: C-H••• π interactions in H1•PYR	39
Figure 3.10: Packing diagram of H1•PYR viewed along [100], only the hydrogen atoms involved in hydrogen bonding are shown.	40
Figure 3.11: Channels in which PYR guests are located.	40
Figure 3.12: DSC and TG traces of H1•NMP	41
Figure 3.13: HSM photographs of H1•NMP	42
Figure 3.14: IR spectra of (a) H1 and (b) H1•NMP	44
Figure 3.15: PXRD patterns of (a) H1•NMP calculated from LAZYPULVERIX, (b) H1•NMP ground product and (c) H1	45
Figure 3.16: Asymmetric unit of H1•NMP	47
Figure 3.17: Hydrogen bonding in H1•NMP ; for clarity the H atoms not involved in hydrogen bonding have been omitted.	48
Figure 3.18: C-H••• π interactions in H1•NMP	49
Figure 3.19: Packing diagram of H1•NMP viewed along [001].....	51
Figure 3.20: The cavities in which the NMP guests are located.....	51
Figure 3.21: DSC and TG curves of H1•DMA	52
Figure 3.22: HSM photographs of H1•DMA	53
Figure 3.23: IR spectra of (a) H1 and (b) H1•DMA	55
Figure 3.24: PXRD patterns of (a) H1•DMA calculated from LAZYPULVERIX, (b) ground product and (c) H1	56
Figure 3.25: Asymmetric unit of H1•DMA	58
Figure 3.26: Disordered DMA guest with hydrogen atoms omitted.....	59
Figure 3.27: Hydrogen bonding in H1•DMA	60
Figure 3.28: C-H••• π interactions between host molecules.	61
Figure 3.29: Packing diagram of H1•DMA along [010], only the major component of the disordered DMA guest is shown for clarity.	62
Figure 3.30: Cavities in which the DMA guests are located.....	63
Figure 3.31: DSC and TG curves for H1•MORP1	65
Figure 3.32: Thermal decomposition of the crystal H1•MORP1	66
Figure 3.33: IR spectra of (a) H1 and (b) H1•MORP1	68

Figure 3.34: PXRD patterns of (a) H1•MORP1 calculated from LAZYPULVERIX, (b) ground product and (c) H1	69
Figure 3.35: Asymmetric unit of H1•MORP1	71
Figure 3.36: Hydrogen bonding in H1•MORP1	72
Figure 3.37: C-H••• π interactions in H1•MORP1	73
Figure 3.38: Packing diagram of H1•MORP1 viewed along [001]	74
Figure 3.39: Channels in which the MORP guests are located.	75
Figure 3.40: Space filling diagram along [001] with the MORP guests omitted	76
Figure 3.41: TG and DSC curves of H1•MORP2	77
Figure 3.42: Thermal decomposition of the crystal H1•MORP2	78
Figure 3.43: IR spectra of (a) H1 and (b) H1•MORP2	80
Figure 3.44: Asymmetric unit of H1•MORP2	82
Figure 3.45: Hydrogen bonding in H1•MORP2	83
Figure 3.46: C-H••• π interactions in H1•MORP2	84
Figure 3.47: Packing diagram of H1•MORP2 along [001], only the major component of the disordered MORP guest is shown for clarity.	85
Figure 3.48: Channels in which the MORP guests are located.	86
Figure 3.49: Packing diagram of (a) H1•MORP1 and (b) H1•MORP2 . Channels of (c) H1•MORP1 and (d) H1•MORP2 along [100] with the guest omitted	87
Figure 3.50: Torsion angles (τ_1 , τ_2 and τ_3) analysed for the host molecule H1	90

CHAPTER 4: H2 AND ITS INCLUSION COMPOUNDS

Figure 4.1: Numbering scheme of H2	94
Figure 4.2: DSC curve of the host compound H2	95
Figure 4.3: TG and DSC curves of H2•DMSO	96
Figure 4.4: Thermal decomposition of the crystal H2•DMSO	97
Figure 4.5: IR spectra of (a) H2 and (b) H2•DMSO	99

Figure 4.6: PXRD patterns of (a) H2•DMSO calculated from LAZYPULVERIX, (b) ground product and (c) H2	100
Figure 4.7: Asymmetric unit of H2•DMSO	102
Figure 4.8: Hydrogen bonding and C-H••• π in H2•DMSO	103
Figure 4.9: Packing diagram of H2•DMSO viewed along [010].....	104
Figure 4.10: Space filling diagram along [010] with the DMSO guests omitted.....	104
Figure 4.11: Voids (blue) occupied by DMSO guests in H2•DMSO	105
Figure 4.12: TG and DSC curves of H2•NMP	106
Figure 4.13: Thermal decomposition of the crystal H2•NMP	107
Figure 4.14: IR spectra of (a) H2 and (b) H2•NMP	109
Figure 4.15: PXRD patterns of (a) H2•NMP calculated from LAZYPULVERIX, (b) ground product and (c) H2	110
Figure 4.16: Asymmetric unit of H2•NMP	112
Figure 4.17: Hydrogen bonding and C-H••• π interactions in H2•NMP	113
Figure 4.18: Packing diagram of H2•NMP viewed along [010].....	114
Figure 4.19: Cavities in which the NMP guests are located.....	114
Figure 4.20: TG and DSC curves of H2•MORP	115
Figure 4.21: Thermal decomposition of the crystal H2•MORP	116
Figure 4.22: IR spectra of (a) H2 and (b) H2•MORP	118
Figure 4.23: PXRD patterns of (a) H2•MORP calculated from LAZYPULVERIX, (b) ground product and (c) H2	119
Figure 4.24: Asymmetric unit of H2•MORP	121
Figure 4.25: Hydrogen bonding in H2•MORP	122
Figure 4.26: C/N-H••• π (centroid) interactions in H2•MORP (only the interactions involving the major component of the disordered MORP guest are shown for clarity).....	123
Figure 4.27: Packing diagram along [010], only the major component of the disordered MORP guests is shown for clarity	124
Figure 4.28: Space filling diagram along [010] with the MORP guests omitted.....	125
Figure 4.29: Channels in which the MORP guests are located.....	126
Figure 4.30: Asymmetric unit of H2	128
Figure 4.31: Hydrogen bonding in H2	129

Figure 4.32: C-H••• π (centroid) and O-H••• π (centroid) hydrogen bonding in H2	130
Figure 4.33: Packing diagram of H2 along [100].....	121
Figure 4.34: Torsion angle (τ_1 , τ_2 and τ_3) analyses for the host molecule H2	134

CHAPTER 5: HIRSHFELD SURFACE ANALYSIS OF THE INCLUSION COMPOUNDS OF H1

Figure 5.1: Fingerprint plots for different interactions present in H1•PYR	137
Figure 5.2: Fingerprint plots for different interactions present in H1•NMP	138
Figure 5.3: Fingerprint plots for different interactions in H1•DMA	139
Figure 5.4: Fingerprint plots for different interactions in H1•MORP1	140
Figure 5.5: Fingerprint plots for different interactions in H1•MORP2	141

CHAPTER 6: HIRSHFELD SURFACE ANALYSIS OF THE INCLUSION COMPOUNDS OF H2

Figure 6.1: Fingerprint plots for all the interactions in H2•DMSO	144
Figure 6.2: Fingerprint plots for all the interactions in H2•NMP	145
Figure 6.3: Fingerprint plots for all the interactions in H2•MORP	146

LIST OF TABLES

CHAPTER 1: INTRODUCTION

Table 1.1: Timeline events in supramolecular chemistry.....	3
Table 1.2: Summary of non-covalent interactions	8
Table 1.3: Characteristics of very strong, strong and weak hydrogen bond interactions	11

CHAPTER 2: EXPERIMENTAL METHODS AND MATERIALS

Table 2.1: Physical properties of guest compounds.....	20
---	-----------

CHAPTER 3: H1 AND ITS INCLUSION COMPOUNDS

Table 3.1: Results of the thermal analysis of H1•PYR	31
Table 3.2: Positions and assignments of peaks in H1 and H1•PYR	33
Table 3.3: Crystal data and refinement parameters of H1•PYR	36
Table 3.4: Hydrogen bonding details of H1•PYR	37
Table 3.5: C-H••• π parameters of H1•PYR	38
Table 3.6: Thermal analysis results of H1•NMP	42
Table 3.7: Positions and assignments of peaks in H1 and H1•NMP	43
Table 3.8: Crystal data and refinement parameters of H1•NMP	46
Table 3.9: Hydrogen bonding details of H1•NMP	48
table 3.10: C-H••• π parameters of H1•NMP	48
Table 3.11: Thermal analysis for H1•DMA	52
Table 3.12: Positions and assignments of peaks in H1 and H1•DMA	54
Table 3.13: Crystal data and refinement parameters of H1•DMA	57
Table 3.14: Hydrogen bonding details in H1•DMA	59

Table 3.15: Thermal analysis results of H1•MORP1	65
Table 3.16: Positions and assignments of peaks in H1 and H1•MORP1	67
Table 3.17: Crystal data and refinement parameters of H1•MORP1	70
Table 3.18: Hydrogen bonding details of H1•MORP1	72
Table 3.19: Thermal analysis results of H1•MORP2	77
Table 3.20: Positions and assignments of peaks in H1 and H1•MORP2	79
Table 3.21: Crystal data and refinement parameters of H1•MORP2	81
Table 3.22: Hydrogen bonding in H1•MORP2	83
Table 3.23: Summary of thermal results of H1 and its inclusion compounds	88
Table 3.24: Summary of the selectivity experiments	89
Table 3.25: Selected geometrical parameters of the host molecule H1	91

CHAPTER 4: H2 AND ITS INCLUSION COMPOUNDS

Table 4.1: Thermal analysis results of H2•DMSO	96
Table 4.2: Positions and assignments of peaks in H2 and H2•DMSO	98
Table 4.3: Crystal data of H2•DMSO	101
Table 4.4: Hydrogen bonding details of H2•DMSO	102
Table 4.5: C-H••• π parameters of H2•DMSO	103
Table 4.6: Thermal analysis results of H2•NMP	106
Table 4.7: Positions and assignments of peaks of H2 and H2•NMP	108
Table 4.8: Crystal data of H2•NMP	111
Table 4.9: Hydrogen bonding details of H2•NMP	112
Table 4.10: C-H••• π parameters of H2•NMP	113
Table 4.11: Thermal analysis results of H2•MORP	115

Table 4.12: Positions and assignments of peaks in H2 and H2•MORP	117
Table 4.13: Crystal data of H2•MORP	120
Table 4.14: Hydrogen bonding details of H2•MORP	122
Table 4.15: Crystal data and refinement parameters of H2	127
Table 4.16: Hydrogen bonding details of H2	129
Table 4.17: Summary of thermal analysis data of H2 and its inclusion compounds	132
Table 4.18: Summary of selectivity experiments.....	133
Table 4.19: Selected geometrical parameters of the host molecule H2	134

CHAPTER 5: HIRSHFELD SURFACE ANALYSIS OF THE INCLUSION COMPOUNDS OF H1

Table 5.1: Summary of the percentage of various intermolecular contacts contributed to the Hirshfeld surface contacts of H1 in its inclusion compounds.....	136
---	------------

CHAPTER 6: HIRSHFELD SURFACE ANALYSIS OF THE INCLUSION COMPOUNDS OF H2

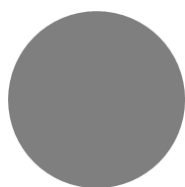
Table 6.1: Summary of the percentage of various intermolecular contacts contributed to the Hirshfeld surface of H2 in its inclusion compounds.....	143
--	------------

LIST OF APPENDICES

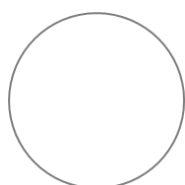
APPENDIX A: DSC RESULTS FOR SELECTIVITY EXPERIMENTS OF H1.....	150
Figure A1 DSC curve for H1: PYR/NMP	150
Figure A2 DSC of H1•PYR (red), H1•NMP (blue) and H1:PYR/NMP (green).....	151
Figure A3 DSC for H1: PYR/MORP	152

Figure A4	DSC of H1•MORP1 (turquoise), H1•MORP2 (green), H1•PYR (red) and H1:PYR/MORP (blue).....	152
Figure A5	DSC of H1: MORP/NMP	153
Figure A6	DSC of H1•MORP1 (blue), H1•MORP2 (green), H1•NMP (aqua) and H1:MORP/NMP (red).....	153
Figure A7	DSC of H1: DMA/NMP	154
Figure A8	DSC of H1•DMA (blue), H1•NMP (green) and H1:DMA/NMP (red).....	154
Figure A9	PXRD patterns of (a) H1:DMA/NMP and (b) H1•NMP calculated from LAZYPULVERIX.....	155
Figure A10	DSC of H1:DMA:PYR	156
Figure A11	DSC of H1•PYR (blue), H1•DMA (red) and H1:DMA/PYR (green).....	156
Figure A12	DSC of H1:DMA/MORP	157
Figure A13	DSC of H1•MORP1 (blue), H1•DMA (red) and H1:MORP/DMA (green)..	158
APPENDIX B: SELECTIVITY EXPERIMENTS OF H2.....		159
Figure B1	DSC of H2:DMSO/MORP	159
Figure B2	DSC of H2•MORP (blue), H2•DMSO (red) and H2:DMSO/MORP (green)	160
Figure B3	DSC of H2:DMSO/NMP	161
Figure B4	DSC of H2•DMSO (red), H2•NMP (blue) and H2:DMSO/NMP (green).....	162
Figure B5	DSC of H2:NMP/MORP	162
Figure B6	DSC of H2•MORP (blue), H2•NMP (red) and H2:NMP/MORP (green).....	163

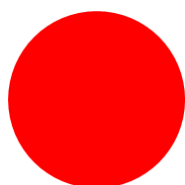
ATOM COLOUR SCHEME



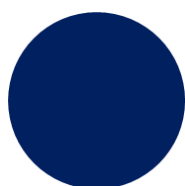
CARBON



HYDROGEN



OXYGEN



NITROGEN



SULFUR

1. Chapter 1-Introduction

1.1 Supramolecular Chemistry

In contrast to the field of molecular chemistry, which is based on atoms linked by covalent bonds, supramolecular chemistry is the chemistry of the intermolecular bond.^[1-3] Supramolecular chemistry aims to develop highly complex chemical systems from components which act together by non-covalent intermolecular interactions.^[4] The comparison between the fields of molecular and supramolecular chemistry according to Lehn is shown in Figure 1.1.

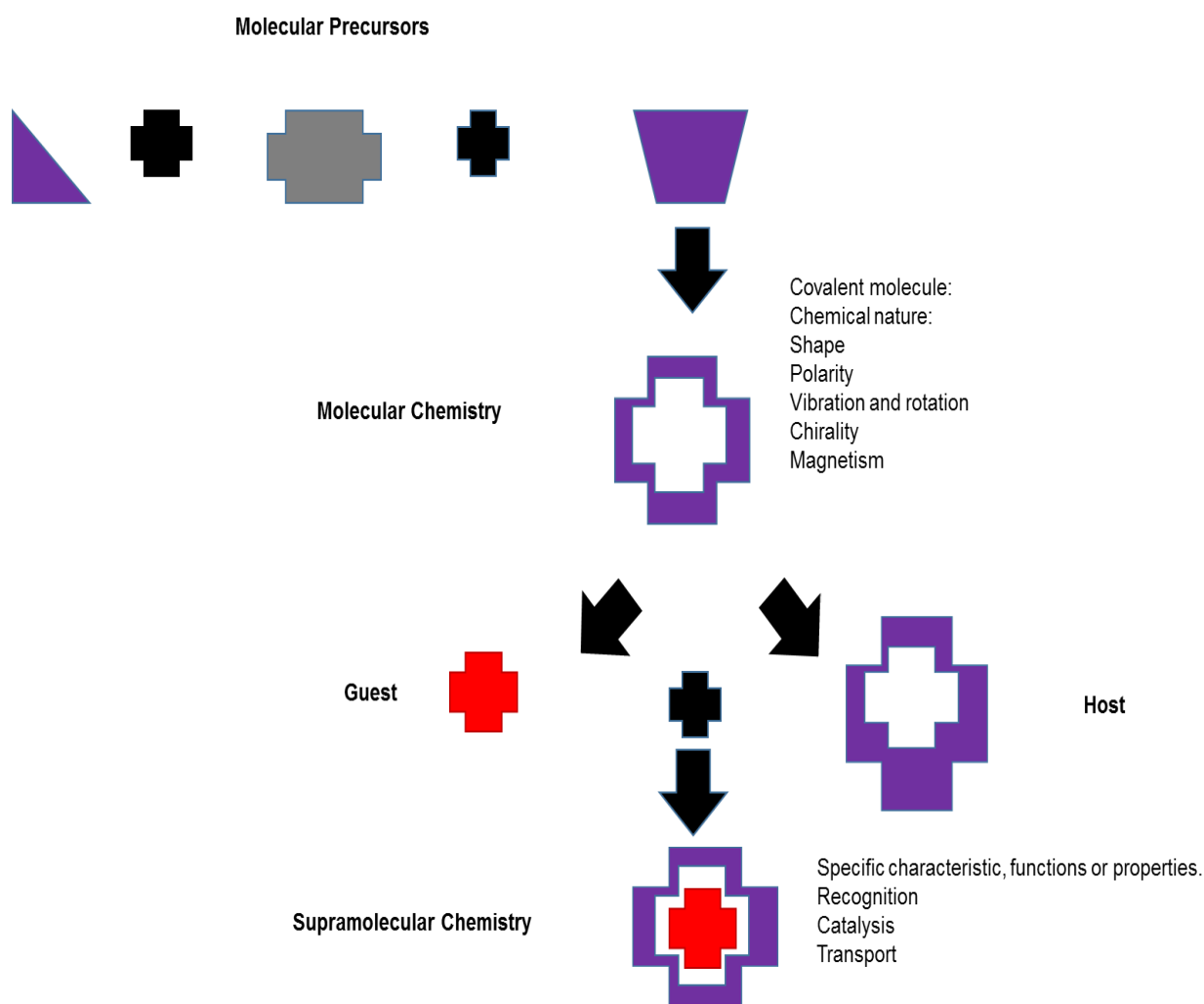


Figure 1.1: Comparison between molecular and supramolecular chemistry. ^[5]

Supramolecular chemistry is defined as the chemistry “beyond the molecule”, as chemistry of tailor-shaped intermolecular interactions. ^[3] It has been defined by Lehn as “the chemistry of molecular assemblies and of the intermolecular bond”. ^[6] A supramolecular compound (supermolecule) is the unit under study in supramolecular chemistry. At the end of the 1960s and in the beginning of the 1970s, Cram, Lehn and Pedersen had developed research which had established the basis for the development of supramolecular chemistry as a recognised discipline. Due to their work in the area of chemistry, they were awarded the chemistry Nobel Prize in 1986. ^[2, 7, 8] Supramolecular chemistry has over the years grown exponentially and become a major field, as indicated by the large number of articles, review and books. ^[1, 9-13]

Table 1.1: Timeline events in supramolecular chemistry. ^[14, 15]

Year	Author	Event
1810	Humphry Davy	Discovery of the chlorine hydrate
1823	Michael Faraday	Formula of the chloride hydrate
1849	F. Wöhler	Preparation of the β -quinol H ₂ S clathrate
1891	Villiers and Hebd	Cyclodextrin inclusion compounds
1893	Alfred Werner	Co-ordination chemistry
1894	Emil Fischer	Introduction of the lock and key concept
1906	Paul Ehrlich	Introduction of the concept of receptor
1940	M.F Bengen	Urea channel inclusion compounds
1948	H.M Powell	Introduction of the term "clathrate"
1953	Watson and Crick	Structure of DNA
1956	Hodgkin	X-ray crystal structure of vitamin B ₁₂
1961	N.F Curtis	First Schiff's macrocycle from acetone and ethylene diamine
1964	Busch and Jäger	Schiff's base macrocycles
1967	Charles Pedersen	Determination of crown ethers
1968	Park and Simmonds	Katapinand anion hosts
1969	Jean-Marie Lehn	Synthesis of the first cryptands
1969	Jerry Atwood	Liquid clathrates from alkyl aluminium salts
1978	Jean-Marie Lehn	Introduction of the term 'Supramolecular Chemistry'
1979	Gokel and Gokahara	Development of the lariat ethers as a subclass of host compounds
1981	Vögtle and Weber	Podand hosts and development of nomenclature
1987	Lehn, Cram, and Pedersen	Award of the Nobel prize in the field of supramolecular chemistry

1.2 Host-Guest Chemistry

Supramolecular chemistry has grown exponentially with the development of host-guest chemistry. Host-guest chemistry focuses on the molecular interactions between a bulky molecule (the host) and a smaller molecule (the guest). ^[16] The nature of the interactions is dependent on the functional groups present on the host and the guest molecule, and is usually dominated by hydrogen bonding. It is the study of the inclusion compounds between the host and the guest. In host-guest chemistry, the molecule under study is a host-guest

complex or supermolecule. Generally, a host-guest complex is formed when the host binds the guest.^[17] Commonly, the host is a large organic molecule containing convergent binding sites. A guest may be a molecule or ion containing divergent sites.^[18]

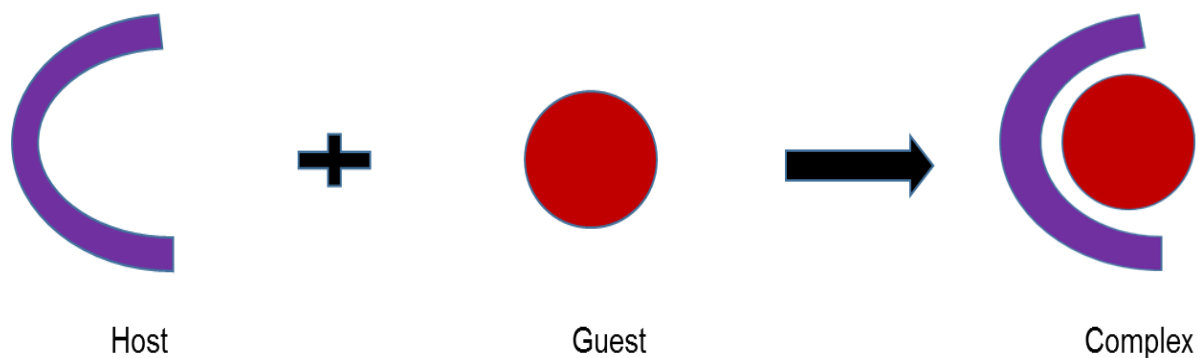


Figure 1.2: A host binds a guest in order to produce a host-guest complex (a supermolecule).

Host compounds can be classified into two major types:

- 1) Cavitands: They may be described as hosts possessing permanent intermolecular cavities.^[19]
- 2) Clathrands: They are hosts having extramolecular cavities.^[19]

In 1948 at the University of Oxford, Powell defined the term clathrate as a kind of inclusion compound in which two or more components are associated without ordinary chemical union, but through complete enclosure of one molecule in a suitable structure formed by another.^[20]

● Inclusion compounds

Inclusion compounds are defined as a unique form of chemical complex in which one molecule (guest) is surrounded within another molecule (host or host structure).^[21] In 1886 inclusion compounds were first mentioned in a study by Mylius. The studies by Mylius were based on the inclusion compounds of hydroquinone with several volatile compounds.^[22]

Mylius conducted research on the interactions of hydroquinone with formic acid and came to the conclusion that the chemical he obtained was not an accurate chemical compound. ^[22]

Supramolecular host-guest compounds can be classified into two types: ^[23]

- A) Molecular inclusion
- B) Crystal lattice inclusion

Figure 1.3 demonstrates the difference between a cavitare and a clathrate. A cavitare is formed by the inclusion of a guest into the cavity of the host molecule (a) whereas a clathrate results from the inclusion of guest molecules in voids formed between host molecules in a lattice (b).

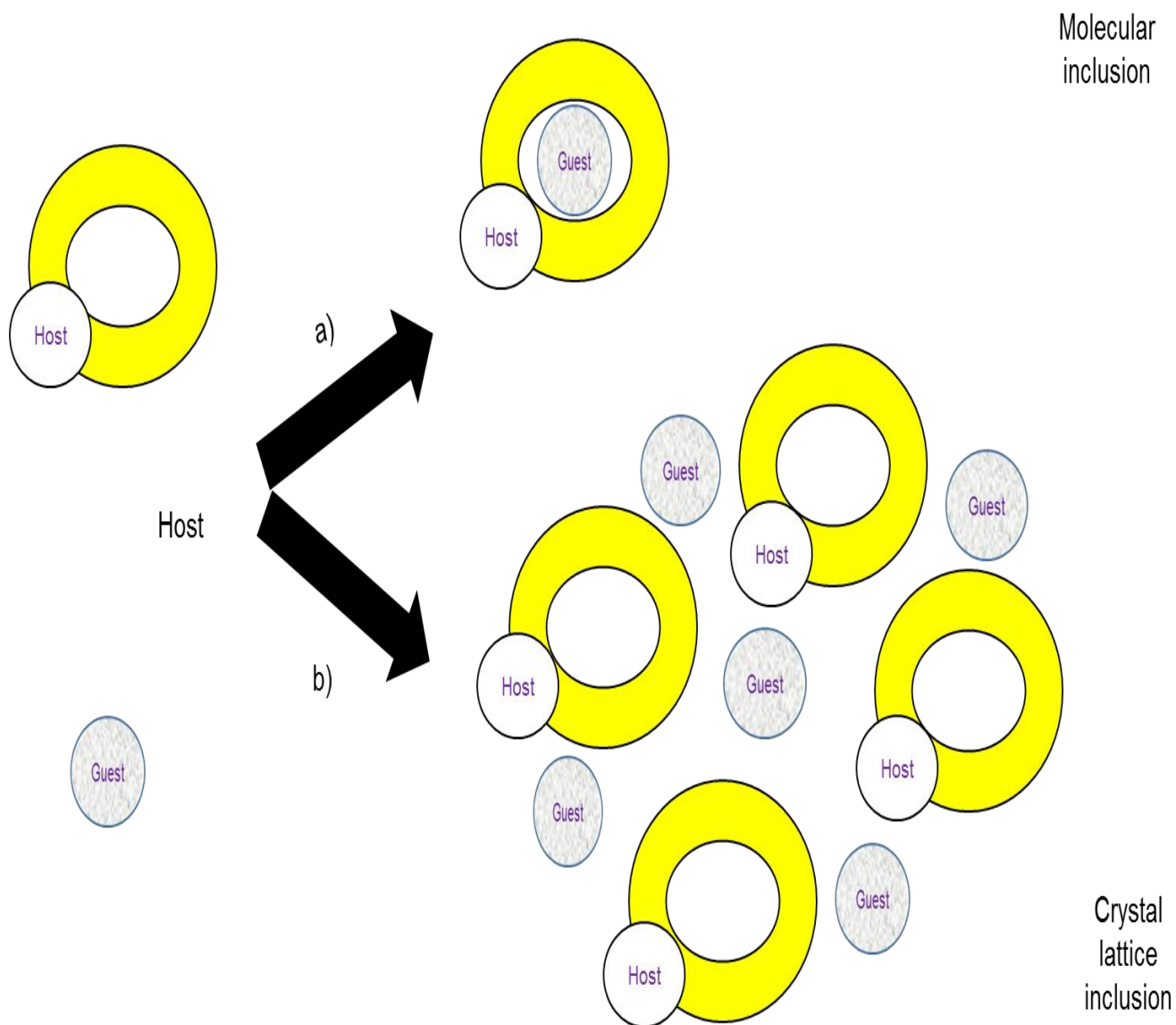
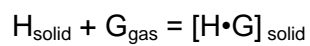


Figure 1.3: Demonstration of the difference between a cavitate and a clathrate. ^[23]

The formation of an inclusion compound is given by the following equation:

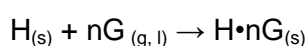


where: H_{solid} = solid host (H) and G_{gas} = gaseous guest (G)

• Selectivity

The preference of a host for a particular guest can be studied by selectivity experiments whereby the host is exposed to a mixture of guests. Typical competition experiments involve the host being dissolved in a mixture of two or more guests where the total guest mixture is in excess. The selectivity that a host compound shows towards a given guest from a mixture of guests has become a very important domain in the field of crystal engineering. [24, 25]

When a host (H) reacts with a guest (G), the formation of a solid host-guest complex may be written in terms of the following equation:



The thermodynamic selectivity when the host is exposed to two or more guests can then be defined as the ratio of the equilibrium constants. [26] The concept of a selectivity coefficient, $K_{B:A}$ is defined as:

$$K_{B:A} = (K_{B:A})^{-1} = Z_A/Z_B \cdot X_B/X_A$$

where A and B represents the two guests, and X_A and X_B are the mole fractions of each of the guests in the liquid mixture. Z_A and Z_B are the mole fractions of the guests in the crystal. [26, 27]

1.3 Applications of Host-Guest Chemistry

Host-guest chemistry has been utilized in many fields. One of the applications is in the removal of hazardous materials from the environment. [28] The host-guest complexes can have different sizes and shape in order to trap a range of chemical guests. One example is *p*-tert-butylcalix [4]arene, which has the ability to remove a cesium ion (cesium-137) a radioactive material from nuclear waste. [29] Host-guest chemistry has also been utilized in the removal of carcinogenic aromatic amines from water. [29] Another application of host-guest chemistry is in biological chemistry. The hosts in biological chemistry are the antibodies of the immune system; genes, receptor sites of enzymes and ionophores. The guests are drugs, substrates, inhibitors, co-factors and antigens. [30] Host-guest complexes

have been used to enhance the delivery of oral drugs and the amount of drug dissolution.^[31] Host-guest chemistry plays and will continue to play an important role in our everyday lives.

1.4 Interactions in Supramolecular Chemistry

1.4.1 Non-covalent interactions

Intermolecular interactions are considered as the heart of crystal engineering.^[32] They play an important role in supramolecular chemistry and help to combine individual molecules (host and guest molecules) into a host-guest complex. A large number and variety of intermolecular interactions have been used in crystal engineering.^[33]

There are many types of non-covalent interactions that occur in supramolecular systems (Table 1.2).

Table 1.2: Summary of non-covalent interactions.^[15, 34]

Non-covalent interactions	Strength (kJmol ⁻¹)	Example
Hydrogen bonding	4-120	DNA
van der Waals	< 5 kJmol ⁻¹ but variable depending on the surface area	Argon; packing in molecular crystals
π – π interactions	0-50	Benzene and graphite
Cation- π interactions	5-80	K ⁺ in benzene
Ion-ion	200-300	Tetrabutylammonium chloride
Ion-dipole	50-200	Sodium [15] crown-5
Dipole-dipole	5-50	Acetone
Hydrophobic	Related to solvent-solvent interaction energy	Cyclodextrin inclusion compounds

1.4.1.1 Hydrogen bond

Hydrogen bonding has become the most important intermolecular interaction in the field of supramolecular chemistry, because of their relative strength and directional nature. ^[35] Hydrogen bonds can be defined as an attractive interaction between the hydrogen atoms attached to an electronegative atom or electron-withdrawing group (donor) with another electronegative atom (acceptor) of a neighbouring molecule. A hydrogen bond can be characterized by:

- ❖ A weak to medium interaction ^[36]
- ❖ An electron transfer between the donor and the acceptor
- ❖ A desired geometry ^[37-39]

Hydrogen bonds of the type X-H...A are the most common. Desiraju has defined this type of hydrogen bond as “an interaction wherein a hydrogen atom is attracted to two atoms, X and A, rather than just one and so acts like a bridge between them”. ^[35]

Generally, a hydrogen bond is represented in the form D-H...A (D = donor and A = acceptor). ^[40] Various types of hydrogen bonding geometries are shown below in Figure 1.4.

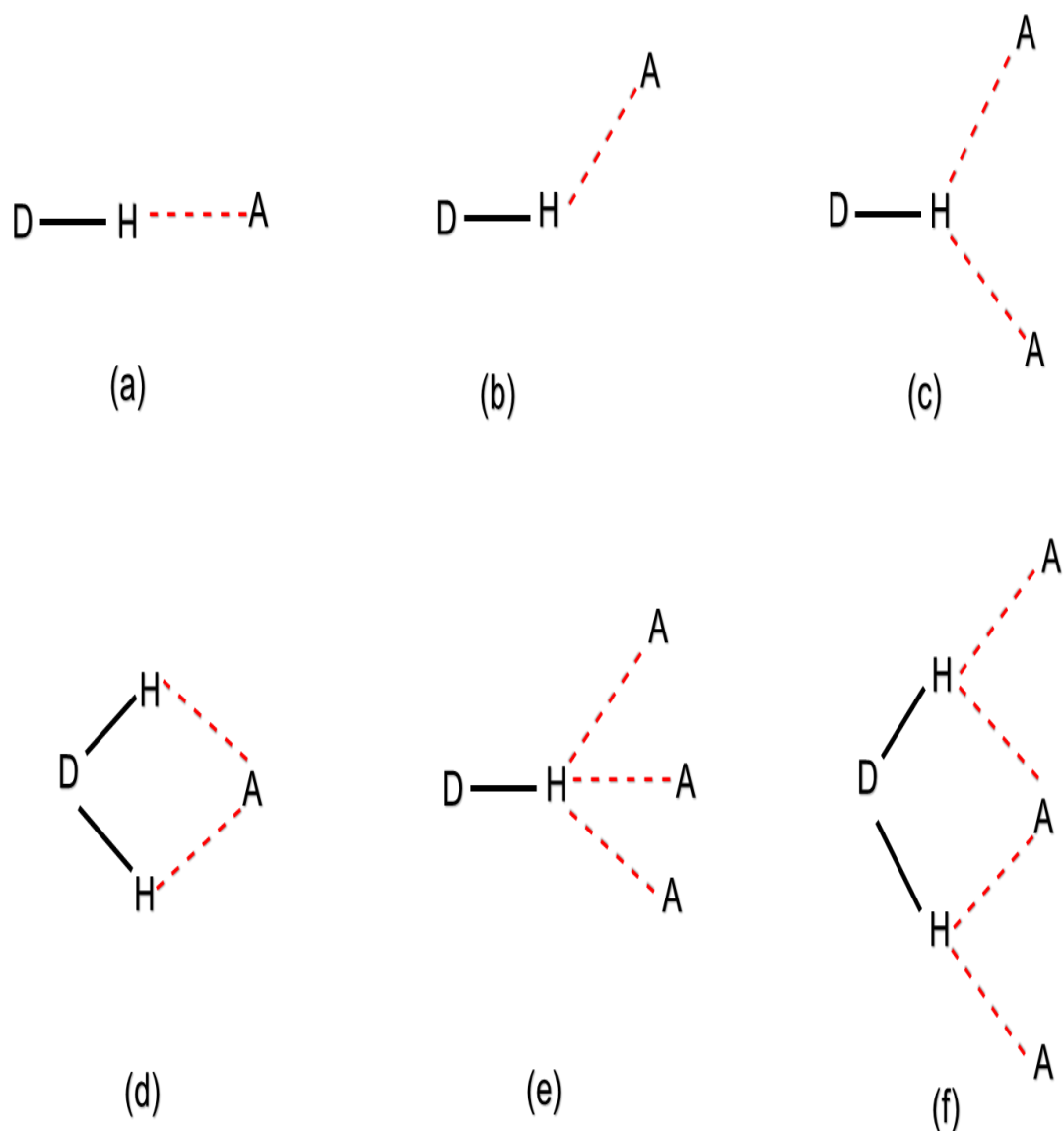


Figure 1.4: Various types of hydrogen bonding geometries: (a) linear; (b) bent; (c) donating bifurcated; (d) accepting bifurcated; (e) trifurcated; (f) three-centre bifurcated. ^[40, 41]

Hydrogen bonds of the type O-H...O or N-H...O have been mostly researched because of their strength and they are considered as strong hydrogen bonds. However there is also a group of weak interactions (O-H... π , C-H...O, N-H... π , C-H...F-C) which play an important role in crystallography. ^[41-43] There are different categories of hydrogen bonding: very strong, strong and weak hydrogen bonding. Table 1.3 summarizes these types of hydrogen bonds and their characteristics.

Table 1.3: Characteristics of very strong, strong and weak hydrogen bond interactions. ^[44, 45]

Strength	D-H...A	d(D...A) (Å)	d(H...A) (Å)	D-H...A (°)
Very strong	[F-H-F]	2.2-2.5	1.2-1.5	175-180
Strong	O-H...O-H	2.6-3.0	1.6-2.2	145-180
	O-H...N-H	2.6-3.0	1.7-2.3	140-180
	N-H...O=C	2.8-3.0	1.8-2.3	150-180
	N-H...O-H	2.7-3.1	1.9-2.3	150-180
	N-H...N-H	2.8-3.1	2.0-2.5	135-180
Weak	C-H...O	3.0-4.0	2.0-3.0	110-180

► **Very strong hydrogen bonds:** They are usually characterised with bond energies in the range of 60-120 kJmol⁻¹ and have d(D...A) distances in the range of 2.2-2.5 Å with a D-H...A (°) angle of 175-180°.

► **Strong hydrogen bonds:** They are the most common type of hydrogen bonds. They are easily recognised because of their physical properties which distinguish them from other type of hydrogen bonds. ^[46] The most structure determining interactions are the strong hydrogen bonds of the type N-H...O and O-H...O. ^[47] These hydrogen bonds are characterised by a d(D...A) distances in the range from 2.6-3.1 Å, D-H...A (°) angles from 135-180° and bond energies in the range of 16-60 kJmol⁻¹.

► **Weak hydrogen bonds:** This type of hydrogen bond was defined by Desiraju as “an interaction X-H...A wherein a hydrogen atom forms a bond between two structural moieties X and A, of which one or even both are of moderate to low electronegativity”. ^[42] They are characterised by a d(D...A) (Å) distance from 3.1-4.0 Å and a D-H...A (°) angle from 110-180°.

1.4.1.2 π - π interactions

π - π interactions result due to the partial overlapping of aromatic rings. ^[48] This is made possible due to the fact that aromatic rings are planar. ^[49] These interactions usually depend on the stacking arrangements between molecules and their strength is generally strong. ^[50-51] For many years, C-H $\cdots\pi$ interactions between a hydrogen atom and the π -system have been neglected, however these have recently gained interest in research. ^[51] One of the aromatic rings involved in the π - π interaction is considered as the electron-rich (donor) and the other aromatic ring is the electron-deficient (acceptor). ^[52] There are two major orientations in π - π interactions: the off-set face-to-face (stacked) and the edge-to-face π - π interactions.

- **Off-set face-to-face π - π stacking:** The molecules are parallel to each other. The distance between the off-set and parallel packed aromatics rings is 3.3-3.8 Å. (Figure 1.5).

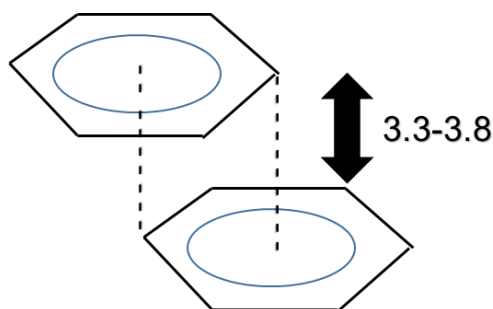


Figure 1.5: Off-set face-to-face π - π stacking. ^[52]

- **Edge-to-face π - π interaction:** This kind of π - π interaction is normally observed in structures having small aromatic molecules (Figure 1.6).

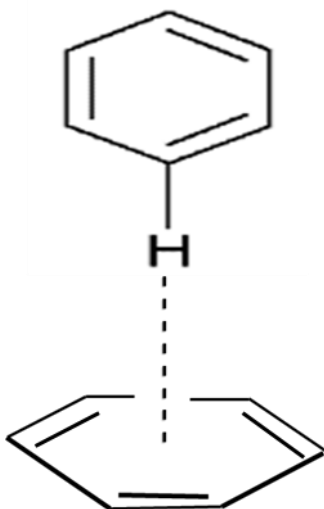


Figure 1.6: Edge-to-face π - π interaction.^[52]

1.5 Crystal engineering

Crystal engineering was defined by Desiraju as “ the understanding of intermolecular interactions in the context of crystal packing and the utilization of such understanding in the design of new solids with desired physical and chemical properties”.^[44, 53]

Crystal engineering was first given an identity in 1962 by Von Hippel^[54] and then introduced in 1955 by Pepinsky,^[55] but the field was employed by Schmidt.^[56] It has become an initial and very fundamental step leading to the fabrication of a material and it implies the design, the preparation and the characterization of crystalline species.^[57] Recently, crystal engineering has been the focus in the determination and analysis of crystal structures and in the construction of new materials with interesting properties. Furthermore the introduction of modern crystallographic techniques has assisted in the progress in crystal engineering and this includes studies in crystal structure prediction.

1. 6 Objectives of the study

- ❖ Form inclusion compounds using the following hosts with a range of guests:
 - 9-(1-naphthyl)-9*H*-xanthen-9-ol (**H1**)
 - 5-(4-methylphenyl)-5*H*-dibenzo[a,d]cyclohepten-5-ol (**H2**)
- ❖ Characterise resultant inclusion compounds using:
 - Single crystal X-ray diffraction
 - Thermogravimetry (TGA)
 - Differential scanning calorimetry (DSC)
 - Hot stage microscopy (HSM)
 - FTIR spectroscopy
- ❖ Thereafter the intermolecular interactions between the hosts and the guest molecules were studied.
- ❖ Competition experiments were investigated in order to determine the selectivity of each host towards mixtures of guests.
- ❖ Hirshfeld surface analysis was used to quantify the intermolecular contacts in the structures.

References

1. Lehn, J.M. (1995) *Supramolecular Chemistry: Concepts and Perspectives*. VCH, Weinheim.
2. Lehn, J.M. (1988) *Angew. Chem. Int. Ed. Engl.*, 27: 89-112.
3. Lehn, J.M., Atwood, J.L., Davies, J.E.D., MacNicol, D.D. & Vögtle, F. (1996) *Comprehensive Supramolecular Chemistry*. Pergamon/ Elsevier Oxford.
4. Lehn, J.M. (2002) *Proc. Natl. Acad. Sci. USA*, 99: 4763-4768.
5. Lehn, J.M. (1995) *Supramolecular Chemistry*. VCH, Weinheim.
6. Lehn, J.M. (1978) *Pure Appl. Chem.*, 50:871-892.
7. Steed, J.W. & Atwood, J.L. (2000) *Supramolecular Chemistry*. Wiley.
8. Beer, P.D., Gale, P.A. & Smith, D.K. (1999) *Supramolecular Chemistry*. OCP.
9. Lindsey, J.S. (1991) *New J. Chem.*, 15: 153-180.
10. Whitesides, G.M., Mathias, J.P. & Seto, C.T. (1991) *Science*, 254: 1312-1319.
11. Philip, D. & Stoddart, J.F. (1996) *Angew. Chem. Int. Ed. Engl.*, 35: 1154-1196.
12. Reinhoudt, D.N., Stoddart, J.F. & Ungaro, R. (1998) *Chem. Euro. J.*, 4: 1349-1351.
13. De Mendoza, J. (1998) *Chem. Euro. J.*, 4: 1373-1377.
14. Steed, J.W. (2004) *Supramolecular Chemistry: Definition*. Encyclopedia of Supramolecular Chemistry. New York, Taylor and Francis, 2:1401-1411.
15. Steed, J.W., Turner, D.R. & Wallace, K.J. (2007) *Core Concepts in Supramolecular Chemistry and Nanochemistry*. John Wiley & Sons, Ltd.
16. Jacobs, A., Tangouna, M-L. & Taljaard, J.H. (2015) *J. Chem. Crystallogr.*, 45: 330-337.
17. Steed, J.W. & Atwood, J.L. (2000) *Supramolecular Chemistry*. P.3-4, Wiley.
18. Cram, D.J. (1986) *Angew. Chem. Int. Ed.*, 25:1039-1134.
19. Vögtle, F. (1991) *Supramolecular Chemistry*. John Wiley & Sons, Ltd: Chichester.
20. Powell, H.M. (1948) *J. Chem. Soc.*, 61-73.
21. Sylvan, G.F. (1975) *J. Pharma. Sci.*, 64:1585-1604.
22. Mylius, F. (1886) *Chem. Ber.*, 19:999.
23. Vögtle, F. (1985) *Angew. Chem. Int. Ed. Engl.*, 24: 727-742.
24. Báthori, N.B. & Nassimbeni, L.R. (2011) *CrystEngComm.*, 13:3156-3161.
25. Schneider, H.J. & Yatsimirsky, A.K. (2008) *Chem. Soc. Rev.*, 37: 263-277.
26. Ramon, G., Jacobs, A., Masuku, L.Z.N. & Nassimbeni, L.R. (2009) *CrystEngComm.*, 11:2332-2337.
27. Jacobs, A., Nassimbeni, L.R., Nokalo, K.L., Su, H & Taljaard, J.H. (2008) *Cryst. Growth & Des.*, 8:1301-1305.

28. Hughes, E., Jordan, J., Gullion, T. (2001) Structural Characterisation of the [Cs(p-tert-butylcalix[4]arene-H) (Me CN)] Guest-Host system by ¹³C-¹³³Cs REDOR NMR. *Phys.Chem.*, 25:5997-5891.
29. Endermir, S., Bahadir., Yilmaz, M. (2009) Extraction of Carcinogenic Aromatic Amines from Aqueous Solution Using Calix [n] arene Derivatives as Carriers. *J. Hazard. Mat.*, 168-1170:1176.
30. Cheng, Y., Rao, T., He, X., Xu, T. (2008) Pharmaceutical applications of dendrimers: promising nanocarriers for drug discovery. *Frontiers in Bioscience.*, 13:1447-1471.
31. Wenz, G. (2000) An Overview of Host-Guest Chemistry and its Application to Nonsteroidal Anti-Inflammatory Drugs. *Drug Investig.*, 19:21-25.
32. Aakeröy, C.B., Champness, N.R. & Janiak, C. (2010) *CrystEngComm.*, 12:22-43.
33. Desiraju, G.R. (2010) *J. Chem. Sci.*, 122: 667-675.
34. Albrecht, M. (2007) *Naturwissenschaftler.*, 94:951-966.
35. Desiraju, G.R. (2002) *Acc. Chem. Res.*, 35:565-573.
36. Hibbert, F. & Emsley, J. (1990) *Adv. Phys. Org. Chem.*, 26:255-375.
37. MacDonald, J.C. & Whitesides, G.M. (1994) *Chem. Rev.*, 94:2383-2420.
38. Koch, U. & Popelier, P.L.A. (1995) *J. Phys. Chem.*, 99:9747-9754.
39. Desiraju, G.R. (2004) Hydrogen Bonding. *Encyclopedia of Supramolecular Chemistry*, 1:658-664. New York, Taylor and Francis.
40. Clyburne, J.A.C., Hamilton, T. & Jenkins, H.A. (2001) *Crystal Engineering*, 4: 1-9.
41. Desiraju, G.R. & Steiner, T. (1999) *The Weak Hydrogen Bond in Structural Chemistry and Biology*, Oxford University Press, Oxford.
42. Jeffrey, G.A. & Saenger, W. (1994) Springer-Verlag, Berlin.
43. Desiraju, G.R., Vital, J.J. & Ramanan, A. (2004) *Crystal Engineering: a textbook*. World Scientific, Singapore.
44. Jeffrey, G.A. (1997) *An Introduction to Hydrogen Bonding*. New York, Oxford University Press, Chapter 2.
45. Moore, M. & Stezowski, J.J. (1995) *Cryst. Rev. CRRVEN.*, 4:211-282.
46. Thakur, T.S., Dubey, R. & Desiraju, G.R. (2014) *IUCrJ.*, 2:159-160.
47. Hunter, C.A. & Sanders, J.K.M. (1990) *J. Am. Chem. Soc.*, 112:5525-5534.
48. Baroak, N., Sarma, R.J. & Baruah, J.B. (2003) *Cryst. Growth & Des.*, 3:639-641.
49. Gabriel, G.J. & Iverson, B.L. (2002) *J. Am. Chem. Soc.*, 124:15174-15175.
50. Zheng, S.L. & Coppens, P. (2005) *Cryst. Growth & Des.*, 5: 2050-2059.
51. Malone, J.F., Murray, C.M., Charlton, M.H., Docherty, R. & Lavery, A.J. (1997) *J. Chem. Soc., Faraday Trans.*, 93:3429-3436.
52. Schneider, H.J. (2004) Van der Waals Forces. *Encyclopedia of Supramolecular Chemistry*, 2:1550-1555. New York, Taylor and Francis.

53. Desiraju, G.M. (1989) *Crystal Engineering, the Design of Organic Solids*. Elsevier: Amsterdam.
54. Von Hippel, A.R. (1955) *Science*, 138:91-108.
55. Pepinsky, R. (1955) *Phys. Rev.*, 97:100.
56. Schmidt, G.M.J. (1971) *Pure Appl. Chem.*, 27:647-678.
57. Krawczuk, A. & Macchi, P. (2014) *Chem. Cent. J.*, 8:68.

2. CHAPTER 2- Experimental methods and materials

2.1 Host Compounds used in the study

9-(1-naphthyl)-9*H*-xanthenol-9-ol (**H1**) and 5-(4-methylphenyl)-5*H*-dibenzo [a,d]cyclohepten-5-ol (**H2**) are the hosts compounds used in this study. The host compounds were synthesized by an organic chemist Dr Jana H. Taljaard and were used without further purification. The synthesized of **H1** was done by using the method of Dilthey, Quint and Heinen. ^[1] **H2** was synthesized using a Grignard reaction of the starting material, dibenzosuberone.^[2] Both host compounds are bulky molecules and contain a hydroxyl group which is capable of forming hydrogen bonds with suitable guests.

H1 is a xanthenol host composed of a xanthene and a naphthalene moiety. Xanthenol hosts are very popular hosts in crystal engineering and have been shown to form inclusion compounds with a variety of guests.

- ❖ The host 9-(3-trifluoromethyl)-9*H*-xanthene-9-ol forms inclusion compounds with acetone and tetrahydrofuran.^[3]
- ❖ The host 9-(4-methylphenyl)-9*H*-xanthen-9-ol forms inclusion compounds with the guests cyclohexane, benzene, 1,4-dioxane, cyclohexanone, *N,N*-dimethylformamide and *N,N*-dimethylacetamide.^[4]
- ❖ The host compound 9-(4-methoxyphenyl)-9*H*-xanthen-9-ol has been found to form inclusion compounds with 18 different guests (morpholine^[5], aniline^[6], naphthalene^[7], anthracene^[7], phenanthrene^[7], pyrene^[7], β -naphthol^[7], *p*-xylene^[8], benzene^[8], *o*-xylene^[8], *m*-xylene^[8], 8-hydroxyquinoline^[9], acridine^[9], 1-naphthylamine^[9], triethylenediamine^[9], *N,N*-dimethylformamide^[10], 1,4-dioxane^[10] and cyclohexane^[10]. Some of the inclusion compounds are formed via solid-solid reactions.^{[7],[9]}
- ❖ The host 9-(3-methoxyphenyl)-9*H*-xanthen-9-ol forms inclusion compounds with morpholine^[5] and aniline^[6].
- ❖ The host 9-(3-chlorophenyl)-9*H*-xanthen-9-ol forms inclusion compounds with benzene, toluene, *p*-xylene and pyridine.^[11]
- ❖ The host compound 9-(1-naphthyl)-9*H*-xanthenol-9-ol has been reported previously to form inclusion compounds with acetone and with dioxane^[12, 13]

H2 is composed of an extensive aromatic system utilising a dibenzosuberonyl moiety and an additional *p*-tolyl group attached to the central seven membered ring. Dibenzosuberonyl alcohols have been used previously to form complexes with metals.^[14, 15] The wheel and axle host 1, 4-bis(5*H*-dibenzo(a,d)cyclohepten-5-yl)buta-1,3-diyne which has two bulky dibenzosuberonyl alcohol groups on either end separated by a linear spacer, forms inclusion compounds with acetone and pyridine.^[16] Inclusion compounds of the host 5-(4-methoxyphenyl)-5*H*-dibenzo[a,d]cyclohepten-5-ol with benzene, bromobenzene, *p*-xylene and pyridine have also been reported.^[17]

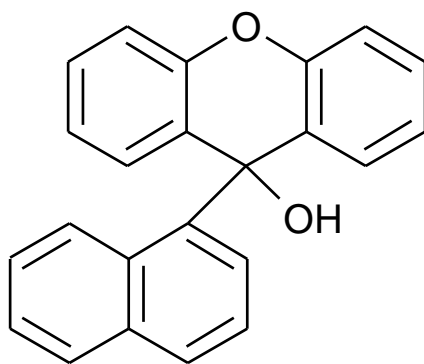


Figure 2.1: Schematic representation of H1.

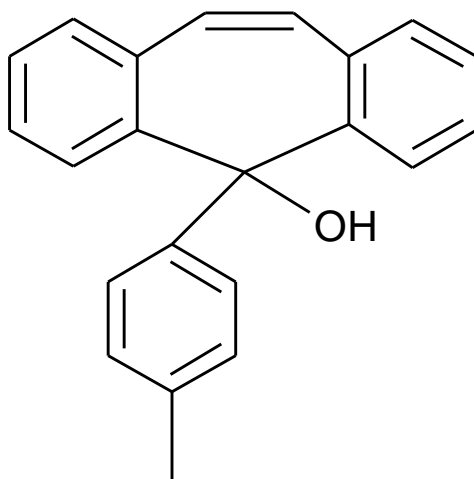
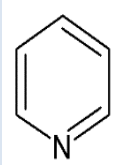
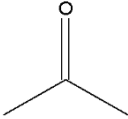
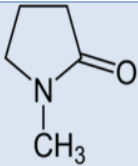
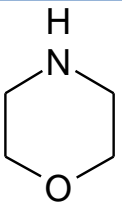
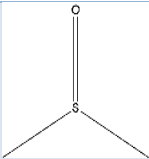
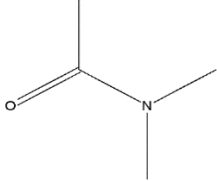


Figure 2.2: Schematic representation of H2.

2.2 Guest Compounds

The guest compounds were purchased from Sigma Aldrich and used directly. The physical properties of the guests are summarised in Table 2.1.

Table 2.1: Physical properties of guest compounds.

Guest compounds	Structures	Abbreviation	Molar mass (g mol ⁻¹)	Boiling point (°C)
Pyridine		PYR	79.1	115
Acetone		ACE	58.1	56
<i>N</i> -Methyl-2-Pyrrolidinone		NMP	99.1	204
Morpholine		MORP	87.1	129
Dimethylsulfoxide		DMSO	78.1	189
<i>N,N</i> -Dimethylacetamide		DMA	87.1	165

2.3 Crystal Growth

A number of techniques are available for the crystallization of small organic molecules such as diffusion methods, slow cooling, slow evaporation and other techniques. ^[18, 1] In this work all of the crystals were obtained using the slow evaporation technique. Inclusion compounds were obtained by dissolving 30 mg of the host in the respective liquid guest with stirring until the solution became clear. The solutions were heated gently and left to crystallise at room temperature. Crystals were obtained after 3 to 4 weeks for some and for others, after 8 weeks. Crystals of the apohost (**H2**) were obtained after 1 week via solvent evaporation of a concentrated solution of the host **H2** in acetone.

2.4 Thermal Analysis

The thermal analysis conducted involved both thermogravimetry (TG) and differential scanning calorimetry (DSC). Both were performed on a Perkin-Elmer Pyris 6 system under nitrogen purge gas with a flow rate of 20 mLmin⁻¹. Samples were taken from the mother liquor and crushed on filter paper to dry. The samples for the analysis were between 3 to 5 mg. Thermal analysis was used to determine the thermal decomposition of each of the compounds.

The samples for the DSC experiments were placed in vented aluminium pans with covers and for TG an open pan was used. DSC was used to measure the onset temperature of the inclusion compound decomposition. Two pans are used in the analysis, the sample pan and the reference pan which is an empty pan. Both pans were heated from 30-300 °C at 10 °Cmin⁻¹ during analysis.

Volatile guests are released as the sample is heated and TG analysis is employed to measure the percentage mass loss as a function of temperature or time. Both DSC and TG are important analytical techniques used to determine a material's thermal stability.

2.5 Powder X-ray Diffraction (PXRD)

PXRD is an important technique for the identification of compounds. Samples were ground until they became fine powders and were then placed in sample holders. The PXRD patterns of the compounds were measured using a Bruker D2 PHASER diffractometer with Cu-K α radiation.

When the crystal is bombarded with X-rays it results in a diffraction pattern characteristic of the structure. A diffraction pattern plots intensity against the angle of the detector, 2θ . PXRD was used to identify the products from the grinding experiments. In these experiments 2-3 drops of liquid guest was added to 30 mg of host and the mixtures were ground for 15 min. The experimental PXRD patterns of the ground products were compared to the calculated pattern obtained from LAZYPULVERIX.^[19]

2.6 Single Crystal X-Ray Diffraction

Single crystal X-ray diffraction has been the most straightforward and significant technique in the structural determination of crystalline materials for understanding their structure property relationships.^[20] It is a technique which provides information about the crystal structure and is the most accurate method used for the determination of crystal structures. Four of the major steps involved in an X-ray study are: crystallization, data collection, structure solution and refinement or validation (Figure 2.3).^[21]

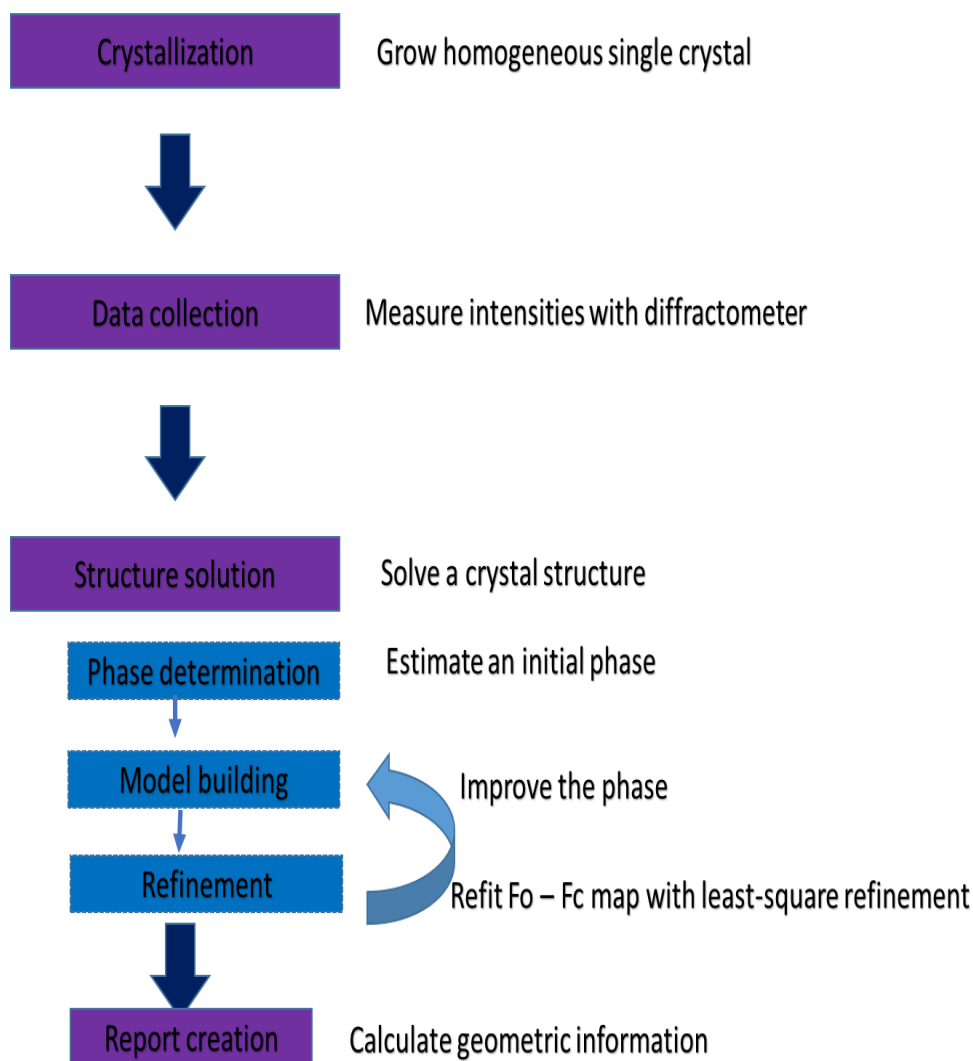


Figure 2.3: Flow diagram of a single crystal X-ray analysis. ^[22]

Structures were solved using SHELXS-97^[23] which was run on a graphical user interface, X-SEED.^[24] The SHELXL-97^[25] program was used to refine the structures.

2.7 Infrared (IR) Spectroscopy

For the molecular characterization of compounds, Fourier transform infrared (FTIR) spectra were collected using a Perkin Elmer Spectrum Two FTIR spectrometer. Spectrum Two has many advantages as it is fast and perfectly suitable for everyday analysis to give accurate results. Spectra were collected in the infrared range of 400 – 4000 cm^{-1} at a spectral resolution of 4 cm^{-1} .

2.8 Selectivity Experiments

The host compound was dissolved in a mixture of two guests with the mole fraction of each guest, $X_{\text{guest}} = 0.5$, followed by gentle heating on a hot plate. The total guest mixture was in excess. The dilute solutions were then closed with pierced parafilm and left to slowly evaporate at room temperature. The resultant precipitates were analysed using either TG, DSC or PXRD.

2.9 Hot stage microscopy

Also known as thermo microscopy or thermal microscopy (TM), hot stage microscopy (HSM) combines thermal and microscopy analysis to allow the study and physical characterization of materials as a function of temperature and time.^[26] In our study, to observe the crystals under a transmitted light microscope, a MEIJI TECHNO EMZ-8TR was used, and the images were then recorded with a CANON DS 1261911 Camera. Silicone oil was used to cover the crystals to observe the guest released upon heating. As soon as a transformation of the crystals was observed, a photograph of the event was taken and the temperature was recorded.

2.10 CrystalExplorer

CrystalExplorer^[27] has become a very important tool in crystallography. It is used to calculate the relative contribution of each intermolecular interaction in a molecular crystal using Hirshfeld surfaces.^[28] Hirshfeld surface analysis is an effective tool for exploring crystal packing modes and intermolecular interactions, as they provide a visual picture of intermolecular interactions and of the molecular shapes in a crystalline environment.^[29] All of the intermolecular interactions in a crystal can then be visualised using the Hirshfeld surface.^[30] The position of atoms and molecules in the crystal structure can be reflected and information on intermolecular interactions between molecules is given.^[31] All intermolecular interactions are shown in a 2D fingerprint plot.^[32]

2.11 Computing Packages

- LAZYPULVERIX^[33]: calculates the theoretical powder X-Ray diffraction pattern from single crystal data.
- PovRay^[34]: renders graphics for structures.
- POVLabel^[35]: a component of X-SEED used to edit the atomic labels of POV-RAY images.
- Xprep^[36]: processing of Bruker diffraction data. SHELX input files can be set up and the space group determined.
- PLATON^[37]: the structure molecular parameters are calculated using this software.
- ConQuest^[38]: program which uses the Cambridge Structural Database (CSD). The CSD is an important tool for crystal engineering. It is a means of checking all the structural data that have been deposited either as part of journal articles or as private communications.
- Mercury^[39]: software which gives a more comprehensive range of tools for the visualization, exploration and analysis of crystal packing. It has the ability to:
 - calculate voids
 - measure angles and torsion angles
 - locate and display intermolecular hydrogen bonds
 - calculate, display and save powder diffraction patterns for a structure
 - display the space group.

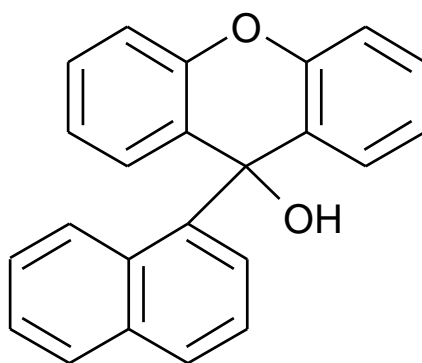
References

1. Diltthey, W., Quint, F. & Heinen, J. (1939) *J. Prakt. Chem.*, 152:49-98.
2. Nassimbeni LR, Ramon G, Taljaard JH. (2009) *Cryst. Growth Des.*, 9:88-94
3. Nassimbeni, L.R., Su, H., Patel, L.D. (2014) *J. Chem. Cryst.*, 44:190-193.
4. Faleni, N., Jacobs, A., Taljaard, J.H. (2009) *J. Chem. Cryst.*, 39:285-292.
5. Sayed, A., Jacobs, A., Taljaard, J.H. (2003) *J. Chem. Cryst.*, 43:325-330.
6. Jacobs, A., Nassimbeni, L.R & Taljaard, J.H. (2006) *CrystEngComm.*, 7:731-734.
7. Curtis, E., Nassimbeni, L.R., Su, H. & Taljaard, J.H. (2006) *Cryst. Growth & Des.*, 6:2716-2719.
8. Jacobs, A., Nassimbeni, L.R., Su, H. & Taljaard, B. (2005) *Org. Biomol. Chem.*, 3:1319-1322.
9. Jacobs, A., Nassimbeni, L.R., Nohako, K.L., Ramon, G. & Taljaard, J.H. (2009) *New J. Chem.*, 33:1960-1964.
10. Jacobs, A., Faleni, N., Nassimbeni, L.R. & Taljaard, J.H. (2007) *Cryst. Growth & Des.*, 7:1003-1006.
11. Ramon, G., Coleman, A.W., Nassimbeni, L.R. & Taljaard, B. (2005) *Cryst. Growth & Des.*, 5:2331-2335.
12. Jacobs, A., Nassimbeni, L.R., Taljaard, J.H. (2006) *Acta Cryst.*, E62:o825-o827.
13. Jacobs, A., Nassimbeni, L.R. & Taljaard, B. (2004) *Acta Cryst.*, C60:0668-0670.
14. Brusey SA, Banide EV, Dorrich S, O'Donohue P, Ortin Y, Muller-Bunz H, Long C, Evans P, McGlinchey MJ. (2009) *Organomet.* 28:6308-6319
15. Banide EV, Müller-Bunz H, Manning AR, Evans P, McGlinchey MJ. (2007) *Angew. Chem. Int. Ed.*, 46:2907-2910.
16. Jacobs, A., Masuku, K.L.Z., Nassimbeni, L.R., Tarjaard, J.H. (2008) *CrystEngComm.*, 10:322-326.
17. Holden, A., Singer, P. (1960) *Crystals and Crystal Growing*. Anchor Books. Doubleday, New York.
18. Laudise, R.A. (1970) *The Growth of Single Crystal*. Solid State Physical Electronics Series Inc, New Jersey.
19. Yvon, K., Jeitschko, W., Parth, E. (1977) *Appl. Cryst.*, 10: 73-74.
20. Zang, J-P., Liao, P-Q., Zhou, H-L., Lin, R-B., Chen, X-M. (2014) *Chem. Soc. Rev.*, 43:5789-5814.
21. Deschamps, J.R. (2010) *X-ray crystallography of chemical compounds*. Life Science, 8:585-589. Elsevier.
22. Hasegawa, K. (2012) *Introduction to single crystal X-ray analysis*. *The Rigaku J.*, 28:1.

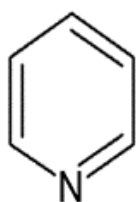
23. Sheldrick, G.M. (2008) A short history of SHELX. *Acta Cryst., Section A*: 112-122.
24. Barbour, L.J. (2003) X-seed, Graphical interface for SHELX program, *J. Supramol. Chem.*, 1:189.
25. Sheldrick, G.M. (1997) Program for crystal structure determination. University of Göttingen, Germany.
26. Stieger, N., Aucamp, M., Zhang, S-W., De Villiers, M.M. (2012) Hot-stage Optical Microscopy as an Analytical Tool to Understand Solid-state Changes in Pharmaceutical Materials. *American pharmaceutical review*.
27. Wolff, S.K., Grimwood, D.J., McKinnon, J.J., Jayatilaka, D. & Spackman, M.A. (2007) Crystal Explorer 2.1. University of Western Australia, Perth.
28. Hirshfeld, F.L. (1977). *Theor. Chim. Acta*, 44:129-138.
29. Mohammed, Y.H.I., Naveen, S., Zabiulla., Al-Ghorbani, M., Mamatha, S.V., Manjunath, H.R., Lokanath, N.K & Khanum, S.A. (2016) *Der. Pharma. Chem.*, 8(4):219-225.
30. Spackman, M.A. & McKinnon, J.J. (2002) *CrystEngComm.*, 378-392.
31. McKinnon, J.J., Mitchell, A.S. & Spackman, M.A. (1998) *Chem. Eur. J.*, 4:2136-2141.
32. McKinnon, J.J., Jayatilaka, D. & Spackman, M.A. (2007) *Chem. Comm.*, 3814-3816.
33. Yvon, K., Jeitschko, W. & Parthe, E. (1997) *Appl. Cryst.*, 10:73-74.
34. PoV-Ray for Windows: The persistence of Vision Development Team: © 1991-1999.
35. Barbour, L. J. (2001) X-Seed - A Software Tool for Supramolecular Crystallography, *J. Supramol. Chem.*, 1:189-191.
36. XPREP: Data Preparation & Reciprocal Space Group Exploration: Version 5.1/NT: © 1997: Bruker Analytical X-ray Systems.
37. Spek, A.L. (2009) *Acta Cryst.*, D65, 148-155.
38. Allen, F.H. (2002) *Acta Cryst., B*, 58-380.
39. Macrae, C.F., Edgington, P.R., McCabe, P., Pidcock, E., Shields, G.P., Taylor, R., Towler, M. & van de Streek, J. (2006) *J. Appl. Cryst.*, 39: 453-457.

3. CHAPTER 3- H1 AND ITS INCLUSION COMPOUNDS.

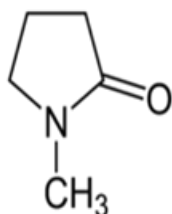
The host 9-(1-naphthyl)-9*H*-xanthen-9-ol (**H1**) forms inclusion compounds with pyridine (**PYR**), *N*-methyl-2-pyrrolidinone (**NMP**), *N,N*-dimethylacetamide (**DMA**) and morpholine (**MORP**). The host numbering scheme is given in Figure 3.1 and the DSC curve of **H1** (Figure 3.2) shows a single endotherm which corresponds to the melt of the host compound at $T_{on} = 464.7$ K



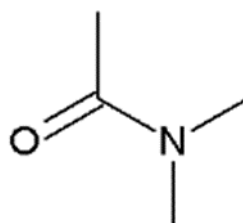
9-(1-naphthyl)-9*H*-xanthen-9-ol (H1)



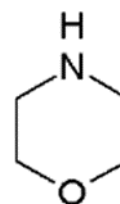
Pyridine
(PYR)



N-Methyl-2-Pyrrolidinone
(NMP)



N,N-dimethylacetamide
(DMA)



Morpholine
(MORP)

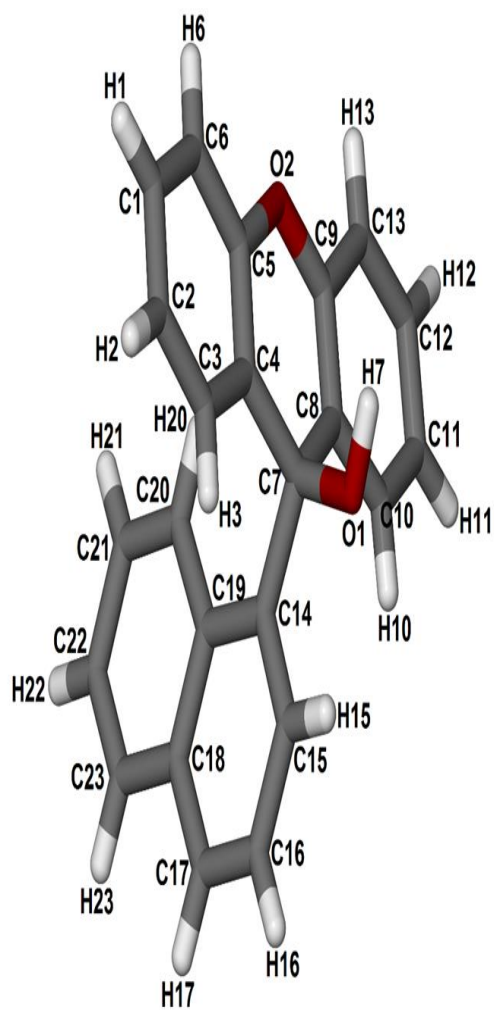


Figure 3.1: Numbering scheme of H1.

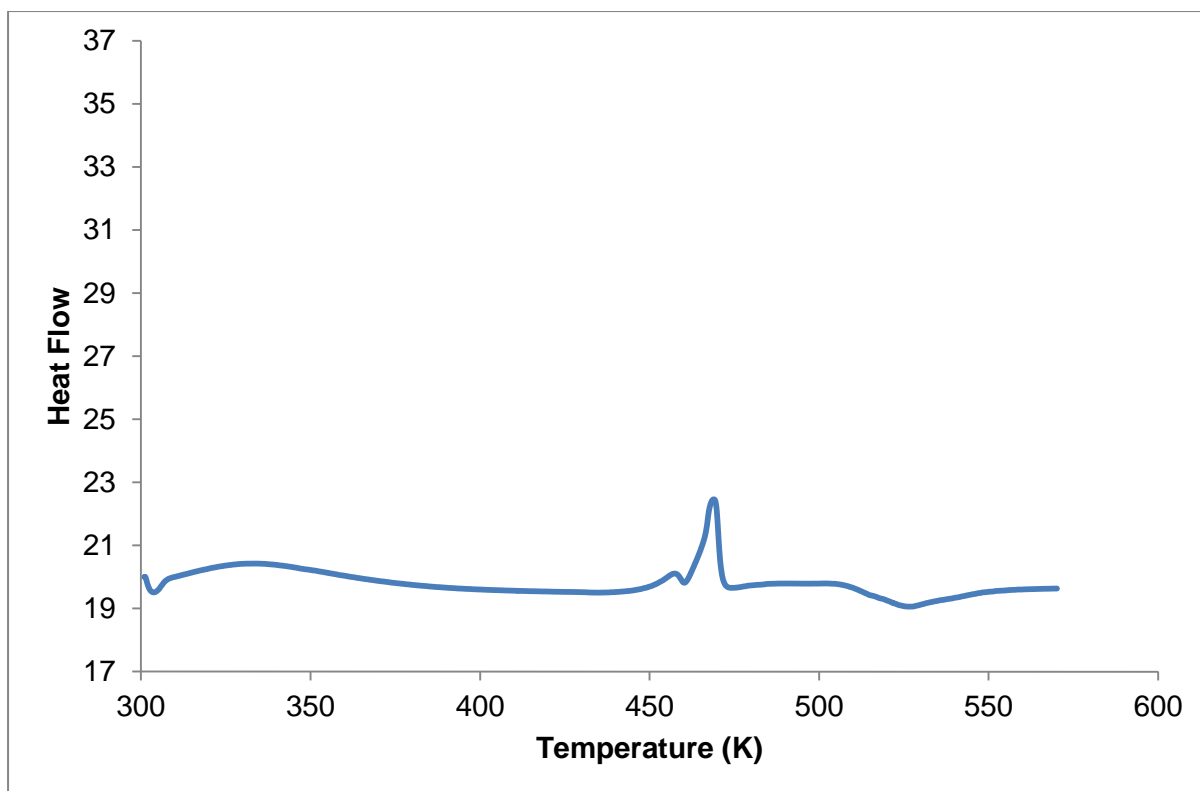


Figure 3.2: DSC curve of the host compound H1.

3.1 Inclusion compound of H1 and pyridine (H1•PYR)

3.1.1 Thermal analysis

Figure 3.3 shows the DSC and the TG of **H1•PYR**. The TG shows a single mass loss step of 18.8 % which corresponds to the loss of one mole of pyridine, confirming a host: guest ratio of 1:1. The DSC shows two endotherms; the first endotherm is due to the release of the guest which occurs at a $T_{\text{onset}} = 383.1$ K and the second endotherm which occurs at $T_{\text{onset}} = 469.9$ K, corresponds to the melt of the host. A summary of the thermal data is given in Table 3.1.

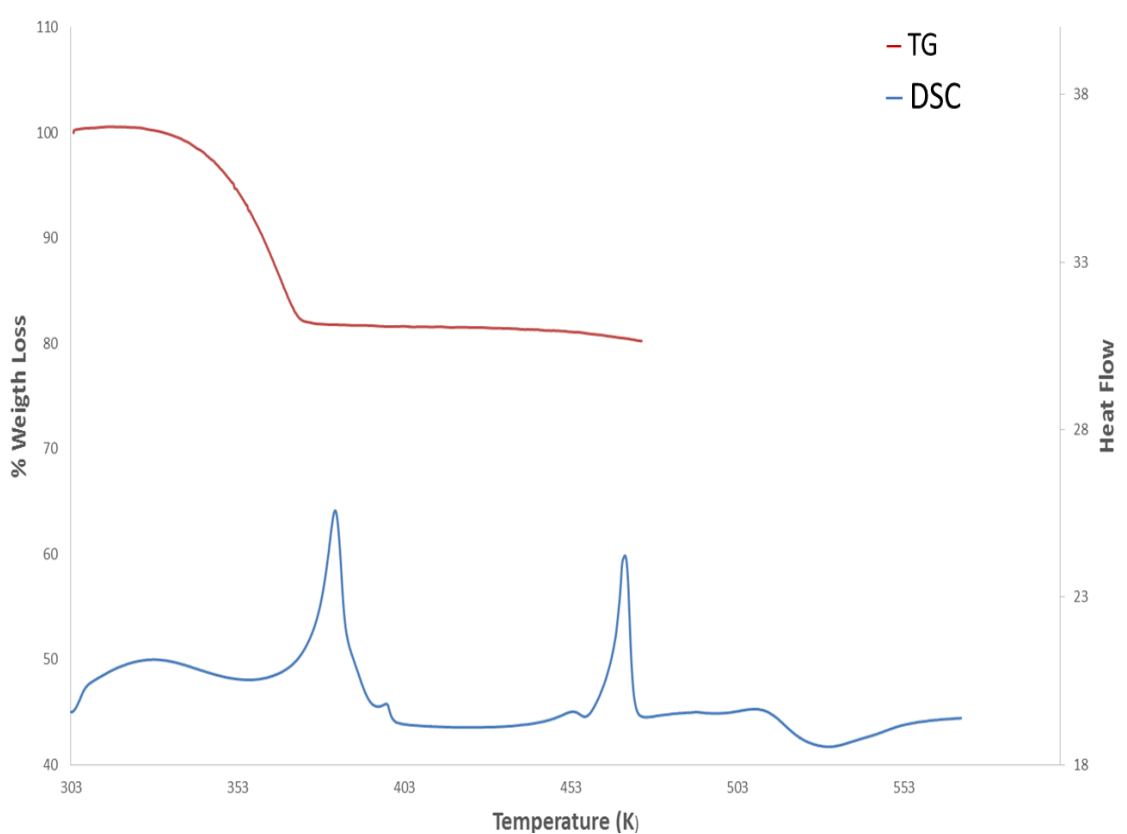


Figure 3.3: DSC and TG curves of H1•PYR.

Table 3.1: Results of the thermal analysis of H1•PYR.

Boiling point of PYR (K)	388.2
Host : Guest ratio	1 : 1
TG calculated % weight loss	19.6
TG experimental % weight loss	18.8
DSC Endotherm 1 T_{onset} (K)	375.9
DSC Endotherm 2 T_{onset} (K)	469.9

3.1.2 Hot stage microscopy (HSM)

The crystals were immersed in silicone oil and were observed over a temperature range, with the initial temperature at 300 K. The results are shown in Figure 3.4.

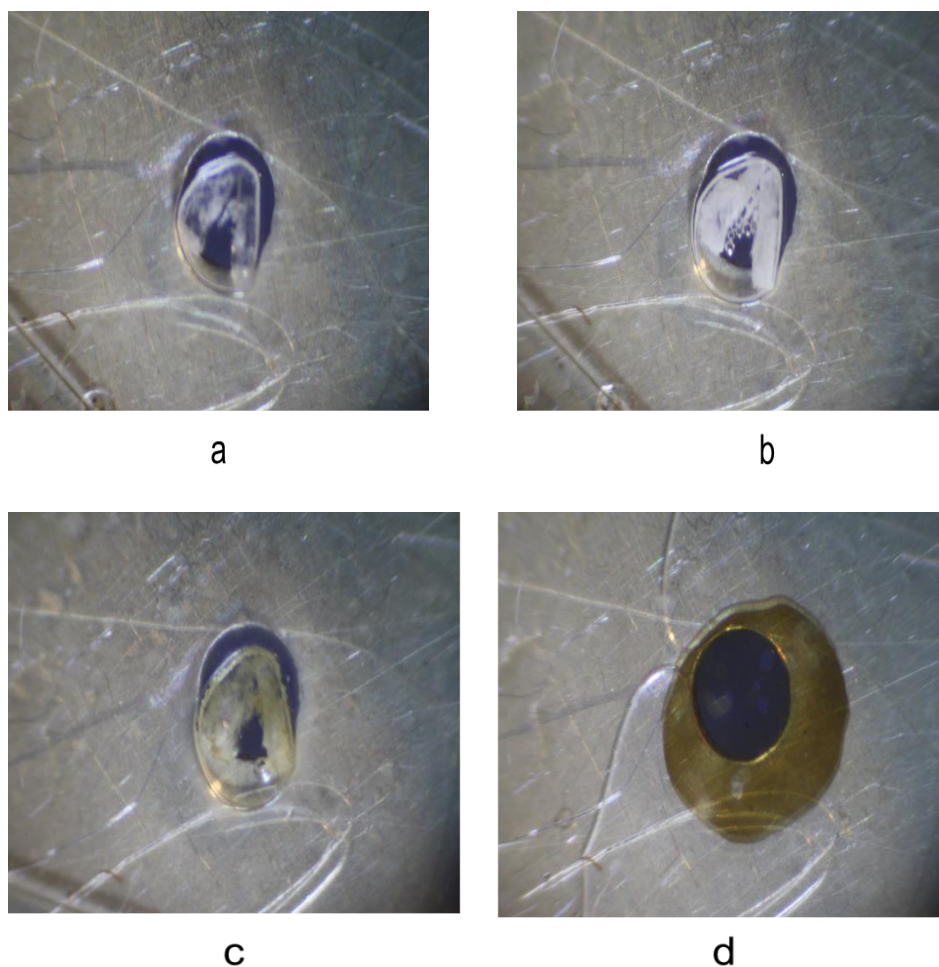


Figure 3.4: Thermal decomposition of the crystal H1•PYR: (a) crystal immersed in silicone oil at 300 K, (b) bubbles form and the crystal starts to become opaque at 413 K, (c) crystal starts melting at 472 K, (d) crystal is completely melted at 479 K.

3.1.3 IR spectroscopy

IR spectroscopy was used to characterise the compound **H1•PYR**. The spectra of **H1** and **H1•PYR** are shown below in Figure 3.5. IR positions and the assignment of peaks are given in Table 3.2. The IR spectrum of **H1•PYR** demonstrates the formation of a new compound by the presence of a new broad band observed at 3045 cm^{-1} . This band is assigned to the hydrogen bonded O-H present in **H1•PYR**. The peak at 3507 cm^{-1} in the spectrum of **H1** and at 2834 cm^{-1} in the spectrum of **H1•PYR** are assigned to the free OH stretch.

Table 3.2: Positions and assignment of peaks in H1 and H1•PYR.

H1	H1•PYR	Assignment
3507	2834	Free OH stretch
-	3045	Hydrogen bonded OH
-	1573, 1601	C=N stretch
1477, 1509, 1574, 1601	1476, 1510	Aromatic C=C stretch
1099, 1126, 1205, 1234, 1291	1099, 1126, 1157, 1205, 1290	C-O stretch
751, 772, 875, 976	753, 771, 799, 875, 939	Aromatic C-H bend

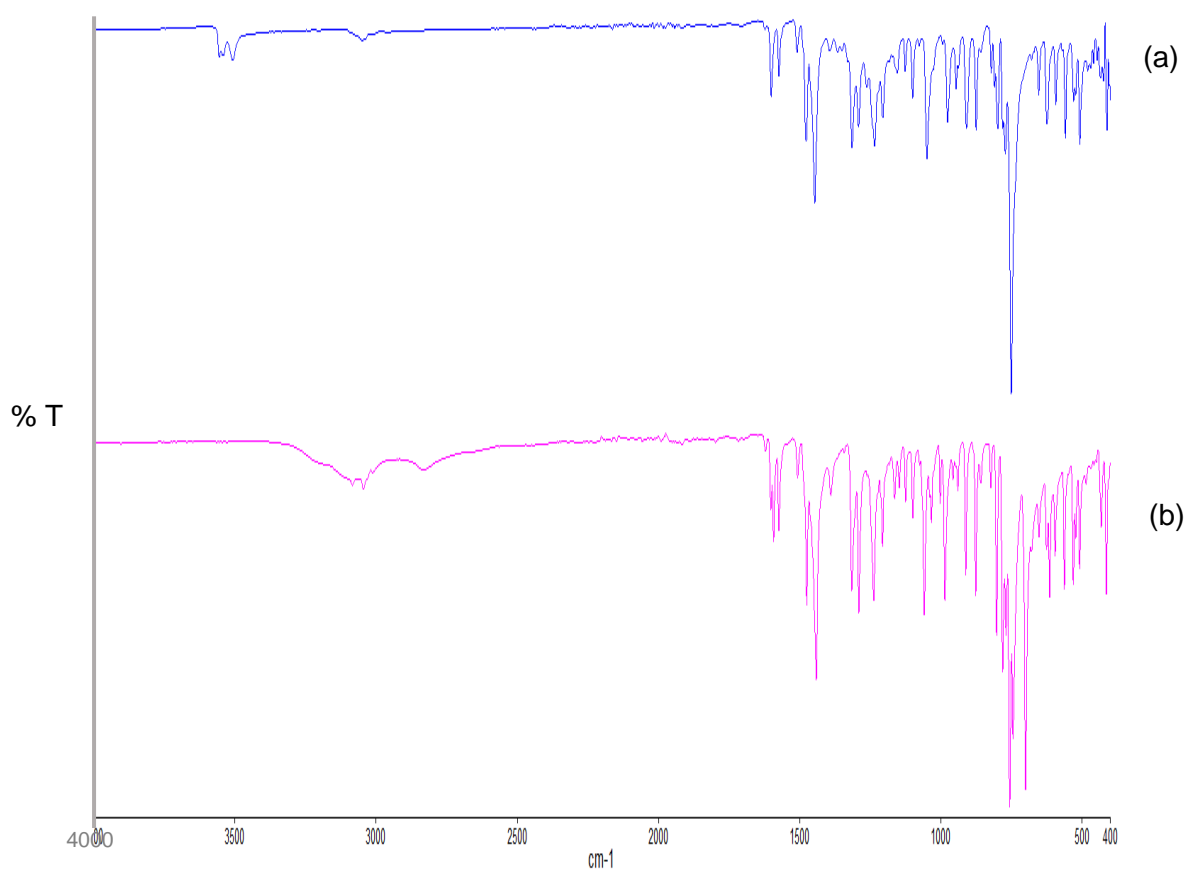


Figure 3.5: IR spectra of (a) H1 and (b) H1•PYR.

3.1.4 Powder X-ray diffraction (PXRD)

PXRD analysis was conducted to show that the compound **H1•PYR** can be obtained using a different technique (grinding). A mixture of **H1** and **PYR** was ground for 15 min and the PXRD pattern was then collected. The calculated PXRD pattern obtained from LAZYPULVERIX^[1] is similar to the PXRD pattern of the ground product (Figure 3.6). These two PXRD patterns differ from the PXRD pattern of **H1** (Figure 3.6).

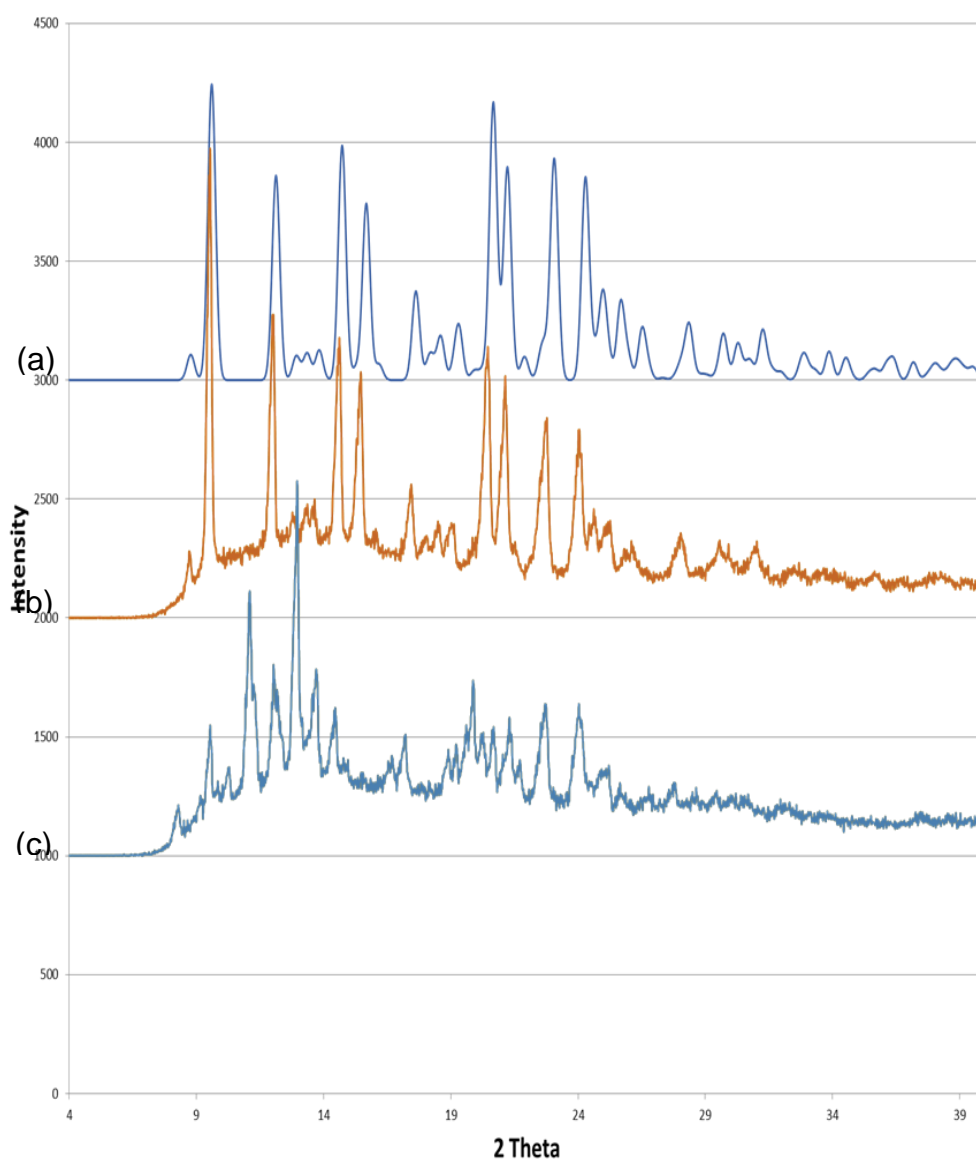


Figure 3.6: PXRD patterns of (a) H1•PYR calculated from LAZYPULVERIX, (b) H1•PYR ground product and (c) H1.

3.1.5 Crystal structure analysis

H1•PYR crystallised in the monoclinic space group $P2_1/c$ with $Z = 4$.^[2-3] The structure was solved using direct methods and refined by full-matrix least squares with SHELX-97,^[4] refining on F^2 . All non-hydrogen atoms were found in the difference electron density map. All of the hydrogens except the hydrogens involved in hydrogen bonding were placed with geometric constraints and allowed to refine isotropically. This approach was followed for all subsequent structures. The current structure refined to $R_1 = 0.0439$ with $wR_2 = 0.0968$. Crystal data and refinement parameters are summarised below in Table 3.3.

The asymmetric unit of **H1•PYR** observed in Figure 3.7 consists of one molecule of the host and one molecule of the guest. The H :G ratio was found to be 1:1 and this was confirmed by TG analysis (Table 3.1).

Table 3.3: Crystal data and refinement parameters of H1•PYR.

Compound	H1•PYR
Molecular formula	C ₂₈ H ₂₁ NO ₂
M _w (g mol ⁻¹)	403.5
Data collection temp (K)	173(2)
Crystal system	Monoclinic
Space group	<i>P2₁/c</i>
a (Å)	9.1932(18)
b (Å)	12.028(2)
c (Å)	18.489(4)
α (°)	90.00
β (°)	91.91(3)
γ (°)	90.00
Volume (Å ³)	2043.3 (7)
Z	4
μ (mm ⁻¹)	0.082
F (000)	848
No. of reflections collected	19309
No. of unique reflections	4902
No. of reflections with I>2σ(I)	3334
D _c , Calculated density (g cm ⁻³)	1.312
Index ranges	h: ± 12; k: ± 15; l: - 23, 24
Goodness of fit, S	1.015
Final R indices [I>2σ(I)]	R ₁ = 0.0439; wR ₂ = 0.0968
R indices (all data)	R ₁ = 0.0745; wR ₂ = 0.1102
Largest diff peak and hole (eÅ ⁻³)	0.231; -0.189

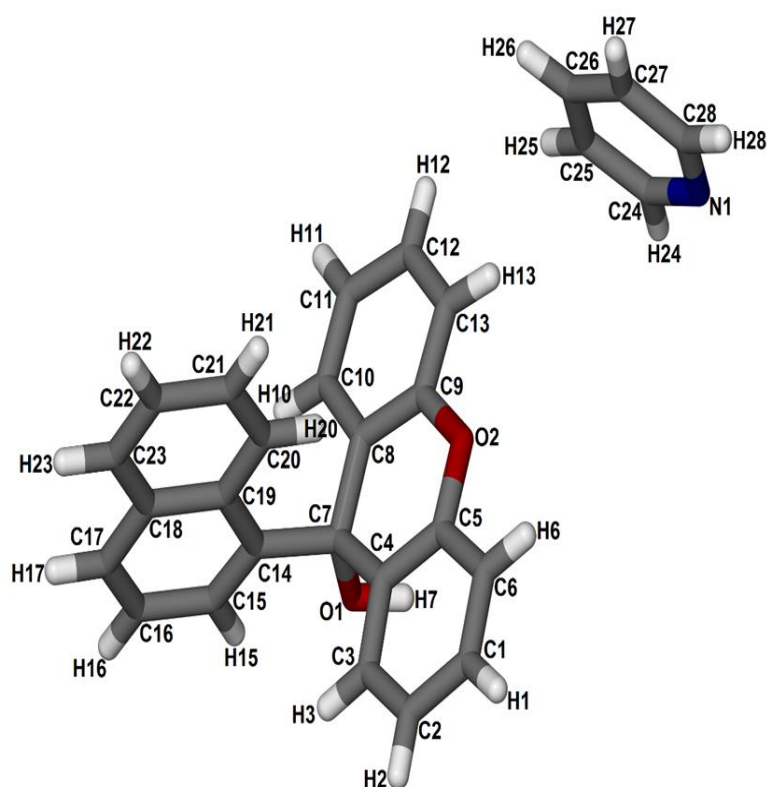


Figure 3.7: Asymmetric unit of H1•PYR.

H1 and PYR interact via (Host)OH...N(Guest) linkages where the OH group of the host is hydrogen bonded to the nitrogen atom of the pyridine (Figure 3.8). Only the hydrogens involved in hydrogen bonding are shown for clarity, this was adopted throughout the thesis. A similar situation was observed by Jacobs et al.^[5] For the inclusion compound of the host 9-(4-methoxyphenyl)-9*H*-xanthen-9-ol with the solid guest acridine. The structure is further stabilised by weak (Host)C-H...O(Host) hydrogen bonds, involving the hydroxyl oxygen.^[6]

C-H... π interactions are observed between the host aromatic rings (Figure 3.9). The shortest contacts of this type involve two of the host C-H bonds: C20... π (centroid): 3.095(1) Å, 136° and C1... π (centroid): 3.839(1) Å, 150°. The respective H... π distances are 2.989 Å and 2.342 Å.^[7] The hydrogen bonding details and the C-H... π parameters are shown in Table 3.4 and Table 3.5.

Table 3.4: Hydrogen bonding details of H1•PYR.

Donor (D)-H	Acceptor (A)	D...A (Å)	D-H (Å)	H...A (Å)	D-H...A (°)
O1-H7	N1	2.817(2)	0.94	1.88	173
C2-H2	O1 [-x,-y,-z]	3.338(2)	0.95	2.65	130

Table 3.5: C–H \cdots π parameters of H1•PYR.

C–H \cdots π	C \cdots π (Å)	H \cdots π (Å)	C–H– π (°)	Symmetry Operator
C1–H \cdots π	3.839 (1)	2.989	150	x, y, z
C20–H \cdots π	3.095 (1)	2.342	136	x, y, z

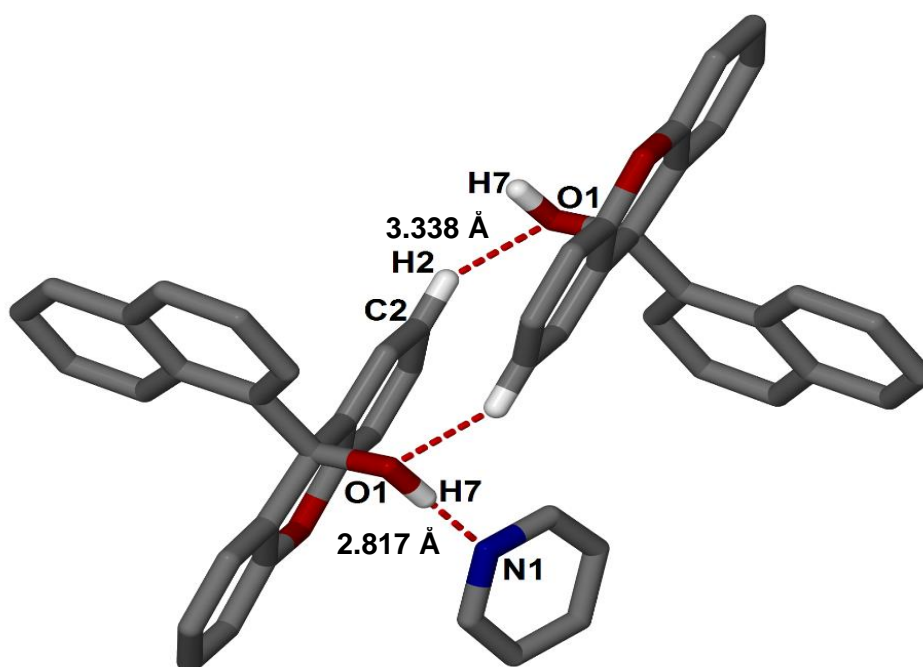


Figure 3.8: Hydrogen bonding in H1•PYR.

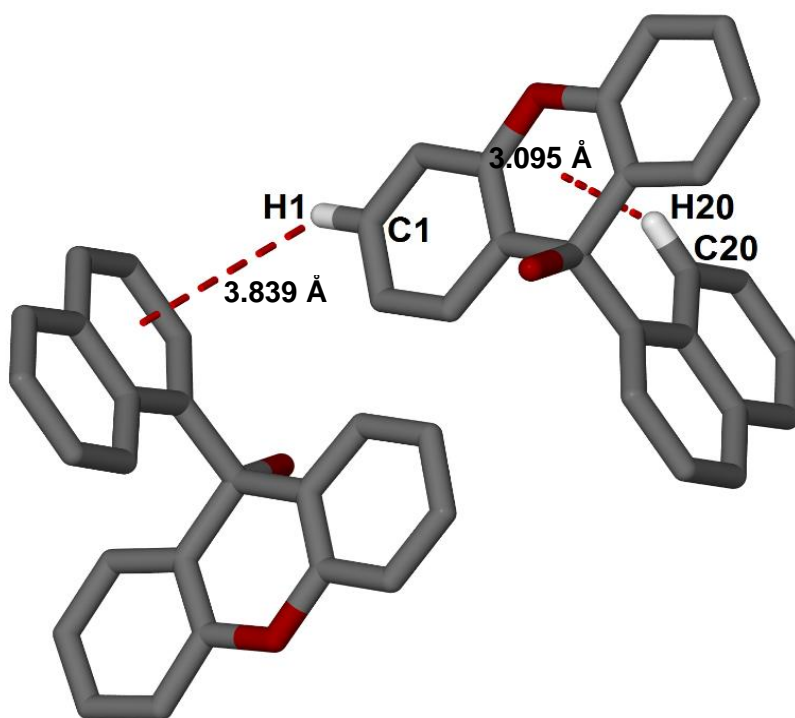


Figure 3.9: C–H••• π interactions in H1•PYR.

The packing diagram of **H1•PYR** viewed along [100] with hydrogen bonds is shown in Figure 3.10. The host molecules exhibit a wave-like arrangement. The **PYR** guests are located in channels along [010], which is shown using Mercury,^[8] Figure 3.11. A probe size of 1.2 Å was used in this and all plots generated with Mercury.

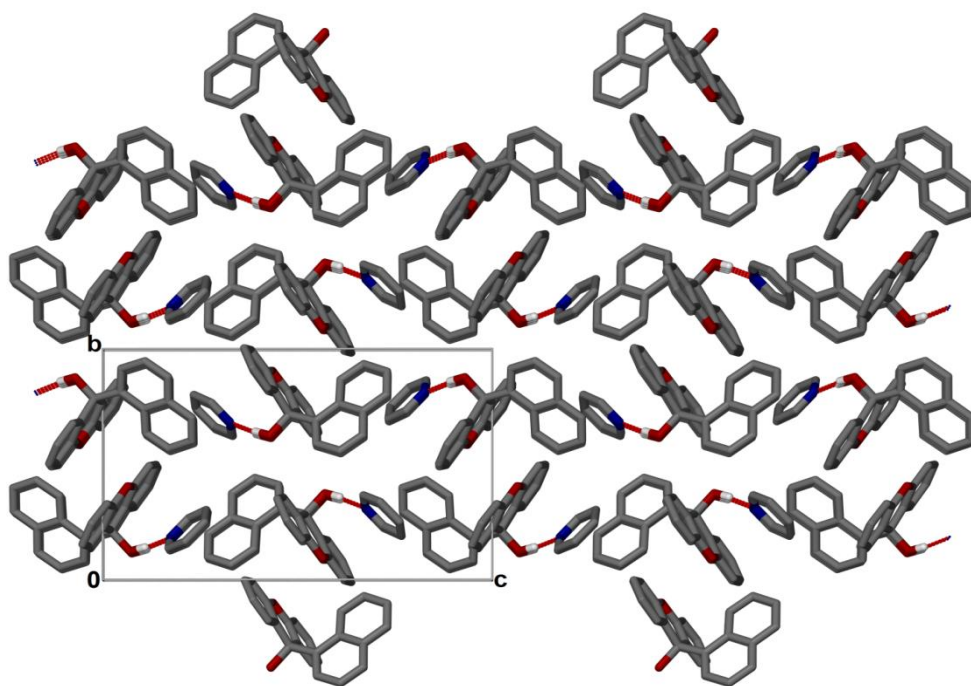


Figure 3.10: Packing diagram of H1•PYR viewed along [100], only the hydrogen atoms involved in hydrogen bonding are shown.

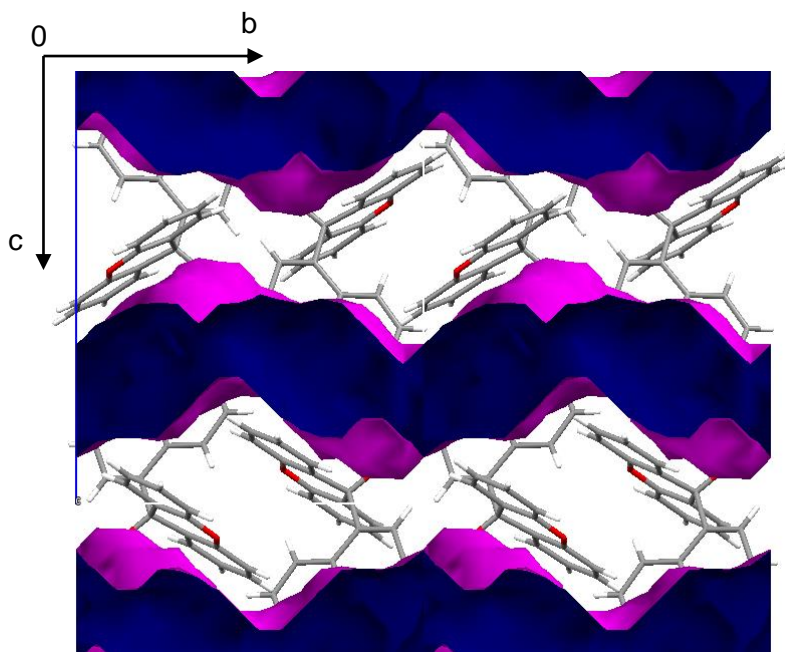


Figure 3.11: Channels in which PYR guests are located.

3.2 Inclusion compound of H1 and *N*-methyl-2-pyrrolidinone (H1•NMP)

3.2.1 Thermal analysis

The DSC and TG curves for **H1•NMP** are given in Figure 3.12. A single mass loss step of 23.3% was observed in the TG curve, and corresponds to the loss of one mole of **NMP**, confirming a host: guest ratio of 1: 1. The DSC curve for **H1•NMP** exhibits a single endotherm which occurs at a temperature of $T_{\text{onset}} = 398.3$ K and is due to the host dissolution in the hot **NMP**. A summary of the thermal data is given in Table 3.6.

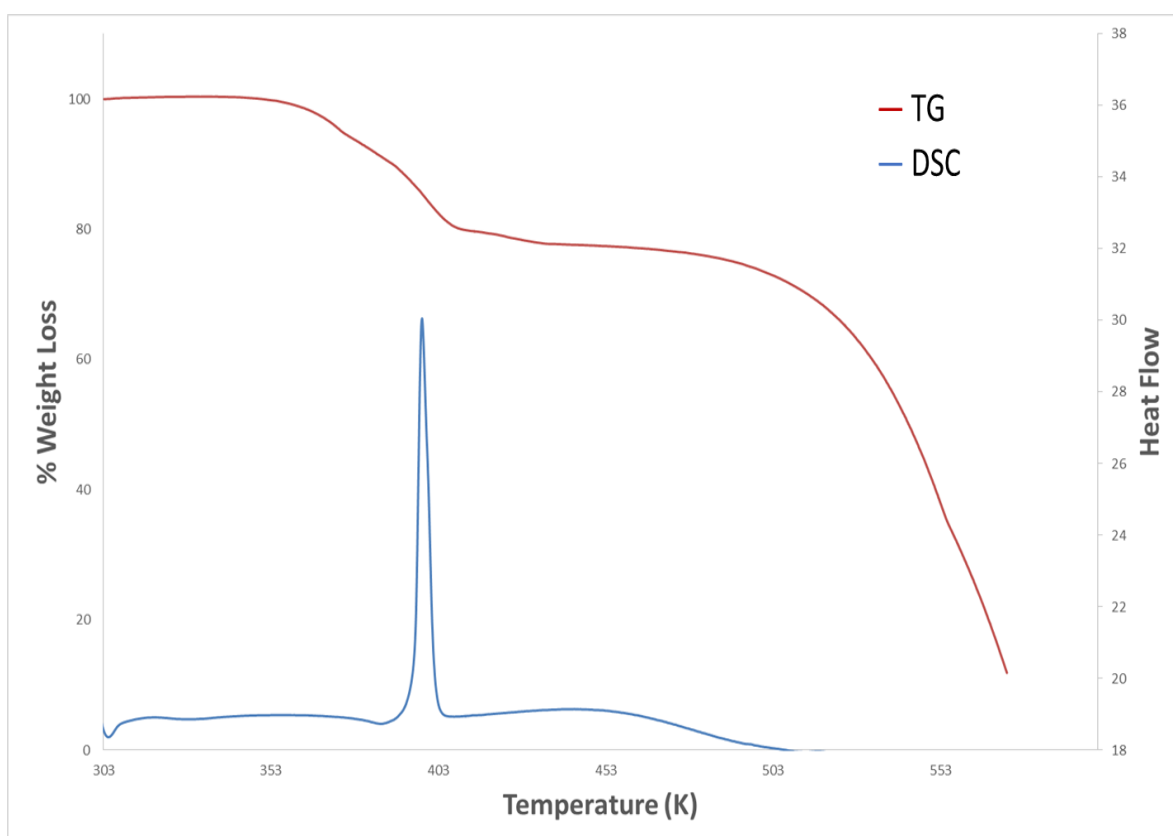


Figure 3.12: DSC and TG traces of H1•NMP.

Table 3.6: Thermal analysis results of H1•NMP.

Boiling Point of NMP (K)	477
Host : Guest ratio	1 : 1
TG calculated % weight loss	23.4
TG experimental % weight loss	23.3
DSC Endotherm 1 T_{onset} (K)	398.3

3.2.2 Hot stage microscopy (HSM)

The crystals were placed between two cover slips at room temperature and one drop of silicone oil was added. At 407 K bubbles start to form and the crystals started melting at 409.7 K. At 415.6 K a complete melt of the crystals was observed. The melting process of the crystal is shown in Figure 3.13.

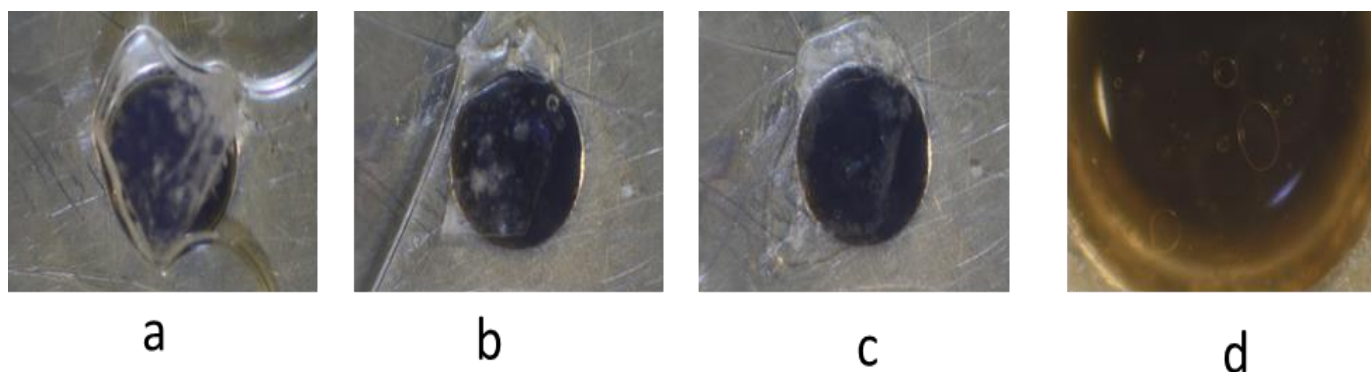


Figure 3.13: HSM photography of H1•NMP: (a) crystal immersed in silicone oil at 301 K, (b) bubbles start to form at 407 K, (c) crystals starts to melt at 409.7 K, (d) crystal completely melted at 415.6 K.

3.2.3 IR spectroscopy

The IR spectrum of **H1•NMP** shown in Figure 3.14 contains a broad peak at around 3321 cm^{-1} which does not appear in the spectrum of **H1**. This broad peak is due to the hydrogen bonded O-H present in the inclusion compound whereby the OH stretch in **H1** is observed at 3507 cm^{-1} and is smaller than the peak due to the hydrogen bonding. The spectrum also contains a small peak at around 2886 cm^{-1} which is due to the alkane (CH_3) present in **NMP**. IR positions and the assignment of peaks are given in Table 3.7.

Table 3.7: Positions and assignment of peaks in H1 and H1•NMP.

H1	H1•NMP	Assignment
3507	-	OH stretch
-	3321	Combination: OH and C-H stretch
-	2886	C-H Alkane stretch
-	1680	C=O stretch
1477, 1509, 1574, 1601	1474, 1507, 1573, 1600	Aromatic C=C stretch
1099, 1126, 1205, 1234, 1291	1156, 1171, 1204, 1238, 1288, 1308	C-O stretch
751, 772, 875, 976	752, 765, 779, 806, 857, 914	C-H Aromatic ring

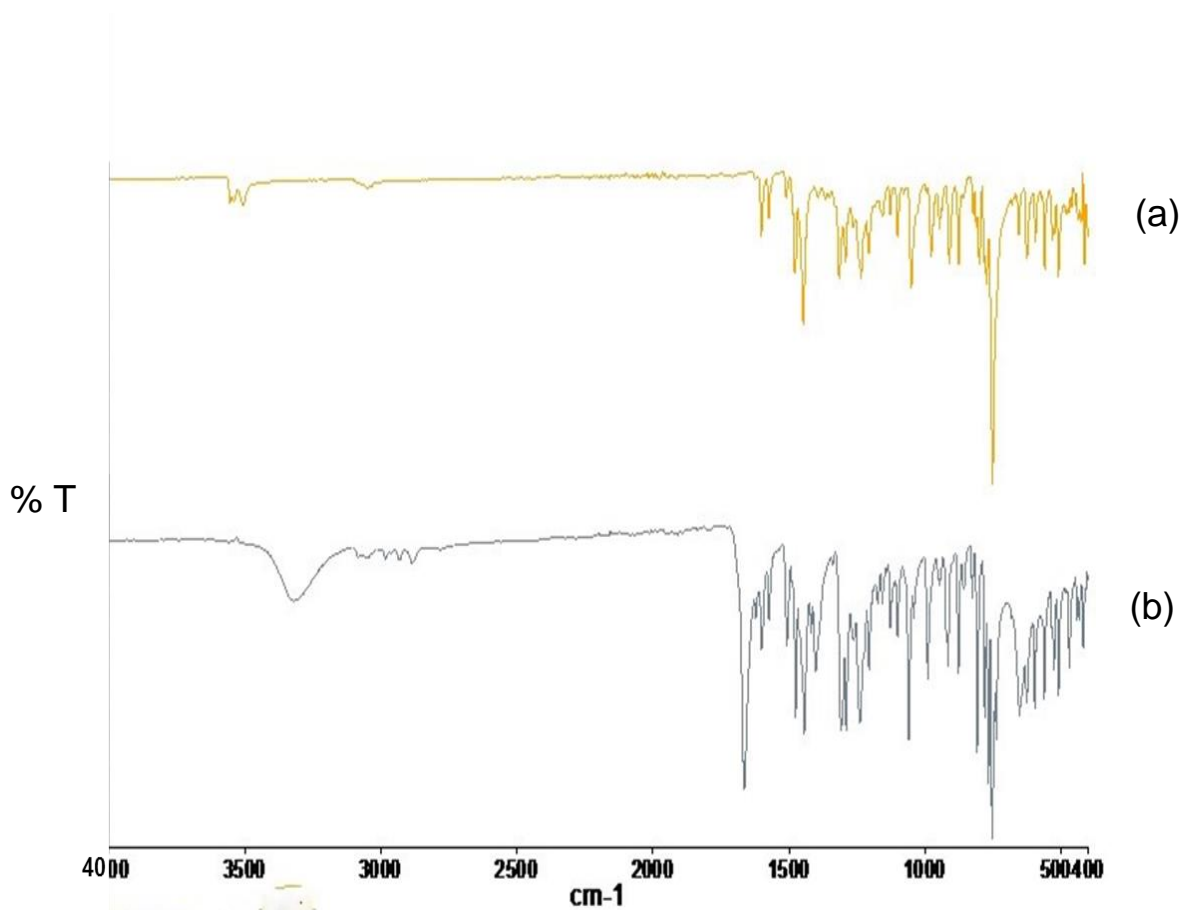


Figure 3.14: IR Spectra of (a) H1 and (b) H1•NMP.

3.2.4 Powder X-ray diffraction (PXRD)

Figure 3.15 shows the PXRD patterns of **H1•NMP** calculated from LAZYPULVERIX, ^[1] **H1•NMP** ground product and **H1**. There is an overall good match between the PXRD pattern of **H1•NMP** calculated from LAZYPULVERIX and that of the ground product, which differ from **H1**. Thus the PXRD patterns indicated that **H1•NMP** was successfully prepared through grinding.

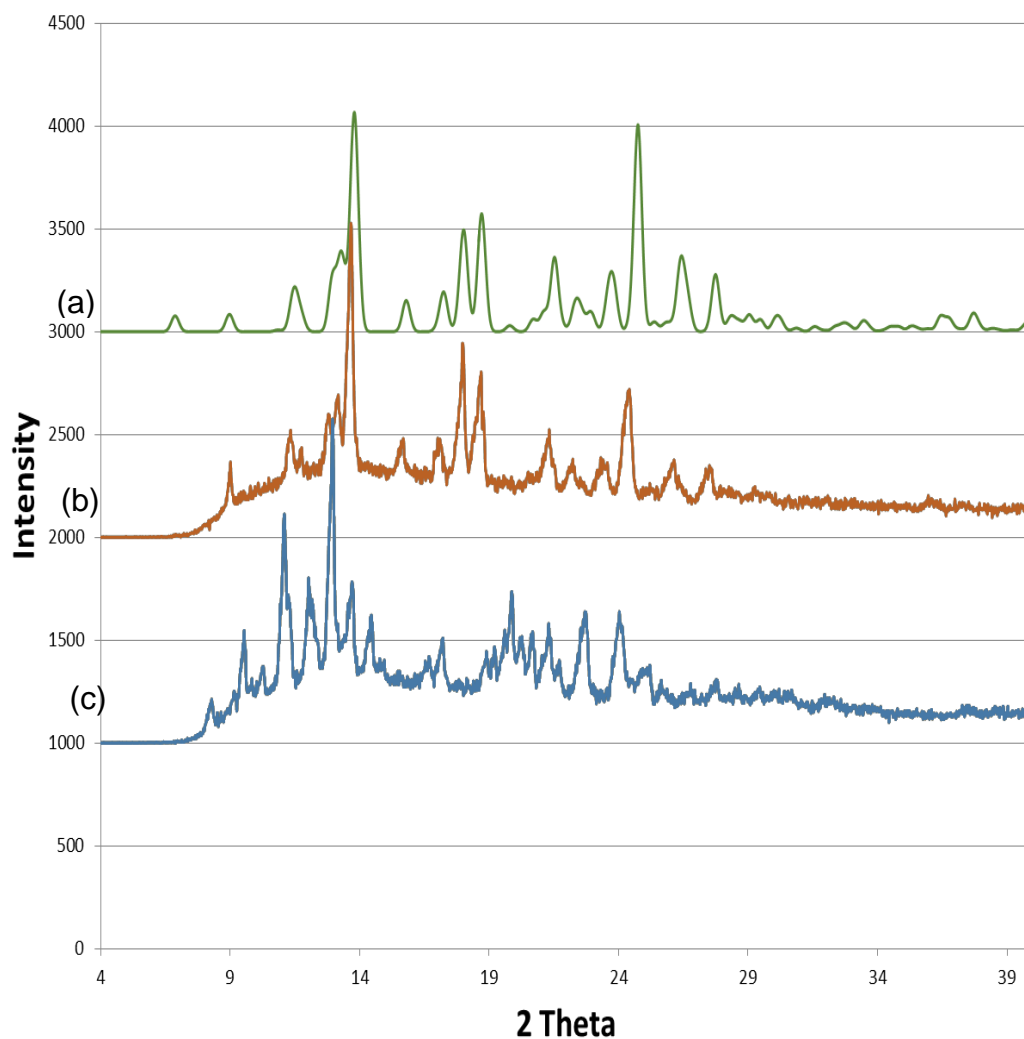


Figure 3.15: PXRD patterns of (a) H1•NMP calculated from LAZYPULVERIX, (b) H1•NMP ground product and (c) H1.

3.2.5 Crystal structure analysis

H1•NMP crystallized in the triclinic crystal system, space group $P\bar{1}$ with $Z=2$. The structure refined to $R_1= 0.0466$ and $wR_2= 0.1433$. Crystal data and refinement parameters are summarised below in Table 3.8.

The asymmetric unit shown in Figure 3.16 consists of one host molecule and one guest molecule. The TG curve confirmed the inclusion compound has a 1:1 host guest ratio.

Table 3.8: Crystal data and refinement parameters of H1•NMP.

Compound	H1•NMP
Molecular formula	$C_{28}H_{25}NO_3$
M_w (g mol ⁻¹)	423.5
Data collection temp (K)	173(2)
Crystal system	Triclinic
Space group	$P\bar{1}$
a (Å)	8.4187(17)
b (Å)	10.709(2)
c (Å)	12.933(3)
α (°)	84.64(3)
β (°)	87.43(3)
γ (°)	67.51(3)
Volume (Å ³)	1072.5(4)
Z	2
μ (mm ⁻¹)	0.085
F (000)	448
No. of reflections collected	12999
No. of unique reflections	5377
No. of reflections with $I > 2\sigma(I)$	4029
D_c , calculated density (g cm ⁻³)	1.311
Index ranges	h: -11, 5; k: -14,13; l: ± 17
Goodness of fit, S	1.057
Final R indices [$I > 2\sigma(I)$]	$R_1 = 0.0466$; $wR_2 = 0.1433$
R indices (all data)	$R_1 = 0.0645$; $wR_2 = 0.1605$
Largest peak and hole (eÅ ⁻³)	-0.231; 0.303

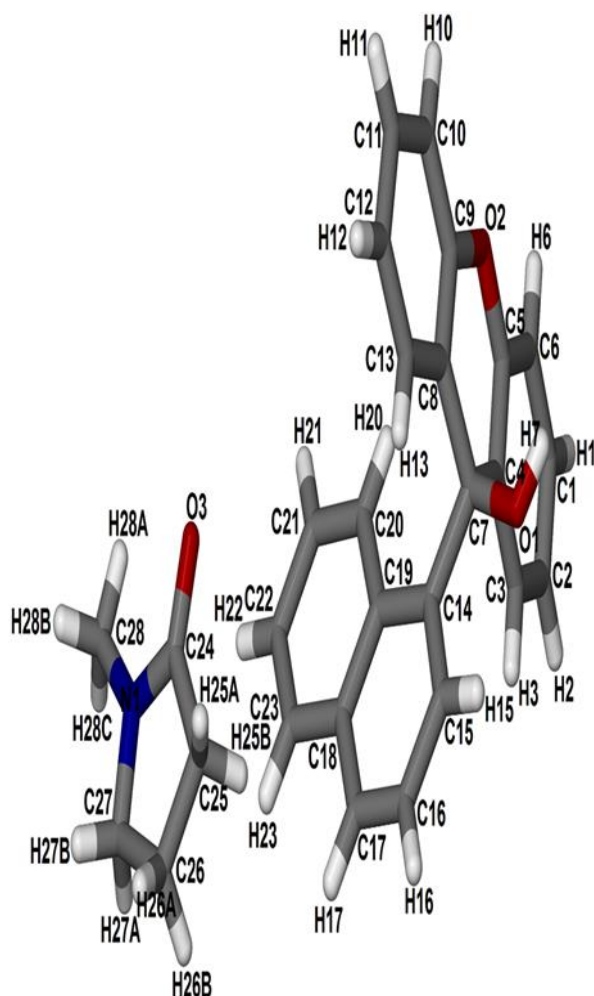


Figure 3.16: Asymmetric unit of **H1·NMP**.

The crystal structure of **H1·NMP** is stabilised via (Host) OH...O(Guest) interactions. Thus, hydrogen bonding was observed between the hydroxyl oxygen of the host and the oxygen of the guest (O1-H7...O3) (Figure 3.17). **H1** and **NMP** also interact via (Guest) C-H...O (Host) weak hydrogen bonds.^[9]

Two of the **NMP** C-H bonds and one of the **H1** C-H bonds are involved in C-H... π interactions with the naphthyl ring of the host (Figure 3.18).

The hydrogen bonding details and the C-H... π parameters are given in Table 3.9 and Table 3.10.

Table 3.9: Hydrogen bonding details of H1•NMP.

Donor (D)–H	Acceptor (A)	D···A (Å)	D–H (Å)	H···A (Å)	D–H···A (°)
O1–H7	O3	2.751 (2)	0.88	1.88	170
C25–H25B	O2	3.212 (2)	0.99	2.79	106

Table 3.10: C–H··· π parameters of H1•NMP.

C–H··· π	C··· π (Å)	H··· π (Å)	C–H– π (°)	Symmetry Operator
C1–H··· π	3.746	2.922	146	2-x, 2-y, 1-z
C26–H26A··· π	3.856	3.252	121	x, y, z
C26–H26B··· π	3.718	2.796	155	-x, 3-y, -z

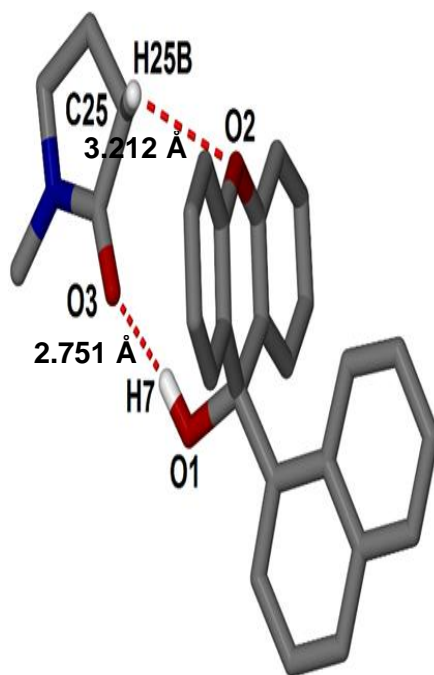


Figure 3.17: Hydrogen bonding in H1•NMP; for clarity the H atoms not involved in hydrogen bonding have been omitted.

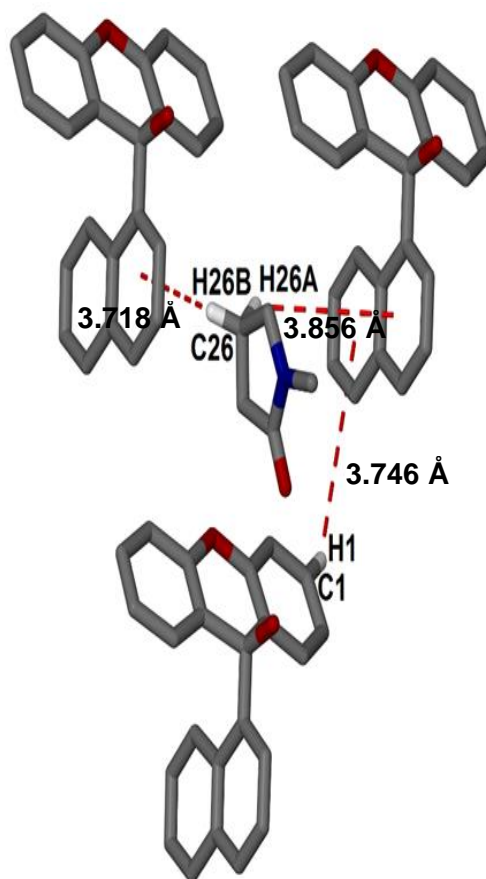


Figure 3.18: C–H··· π interactions in H1•NMP.

The packing diagram of **H1•NMP** viewed along [001] is shown in Figure 3.19. There are alternating columns of host and guest molecules, with the **NMP** guests located in cavities Figure 3.20.

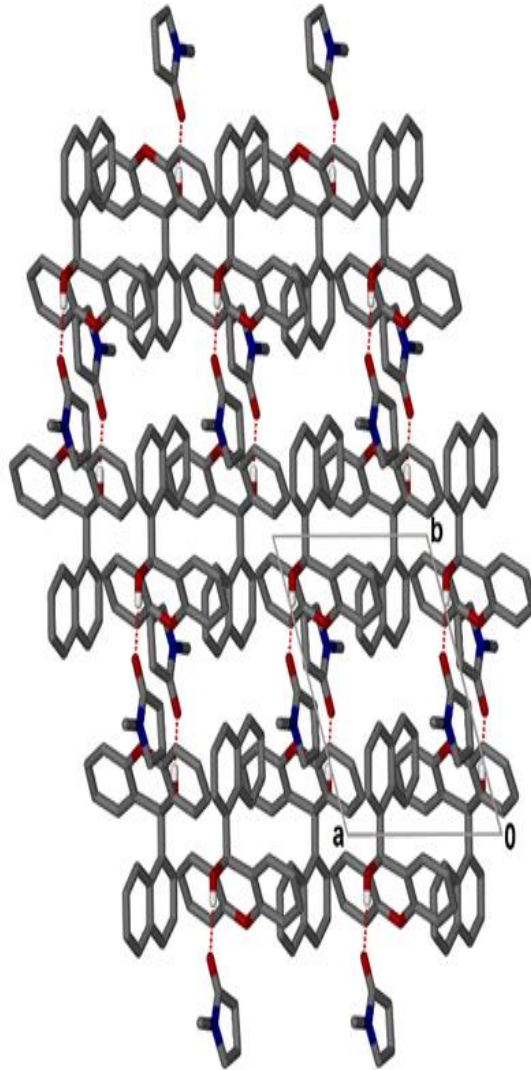


Figure 3.19: Packing diagram of H1•NMP viewed along [001].

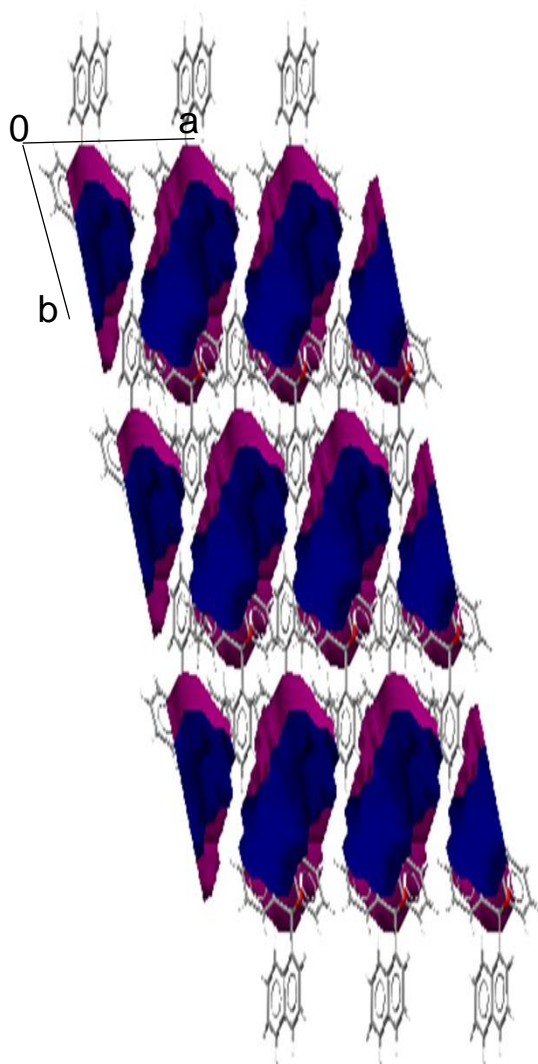


Figure 3.20: The cavities in which the NMP guests are located.

3.3 Inclusion compound of H1 and *N,N*-dimethylacetamide (H1•DMA)

3.3.1 Thermal analysis

The thermal analysis results for **H1•DMA** are listed in Table 3.11. A single mass loss step of 21.1% was observed in the TG curve which corresponds to the loss of one mole of **DMA** (calc: 21.2%), confirming a host: guest ratio of 1:1. The DSC curve shows two endotherms at $T_{\text{onset}} = 386.8$ K and $T_{\text{onset}} = 474.8$ K. The first endotherm is due to the release of the **DMA** guest and is followed by the melt of the host **H1**. The thermal analysis results are shown in Figure 3.21.

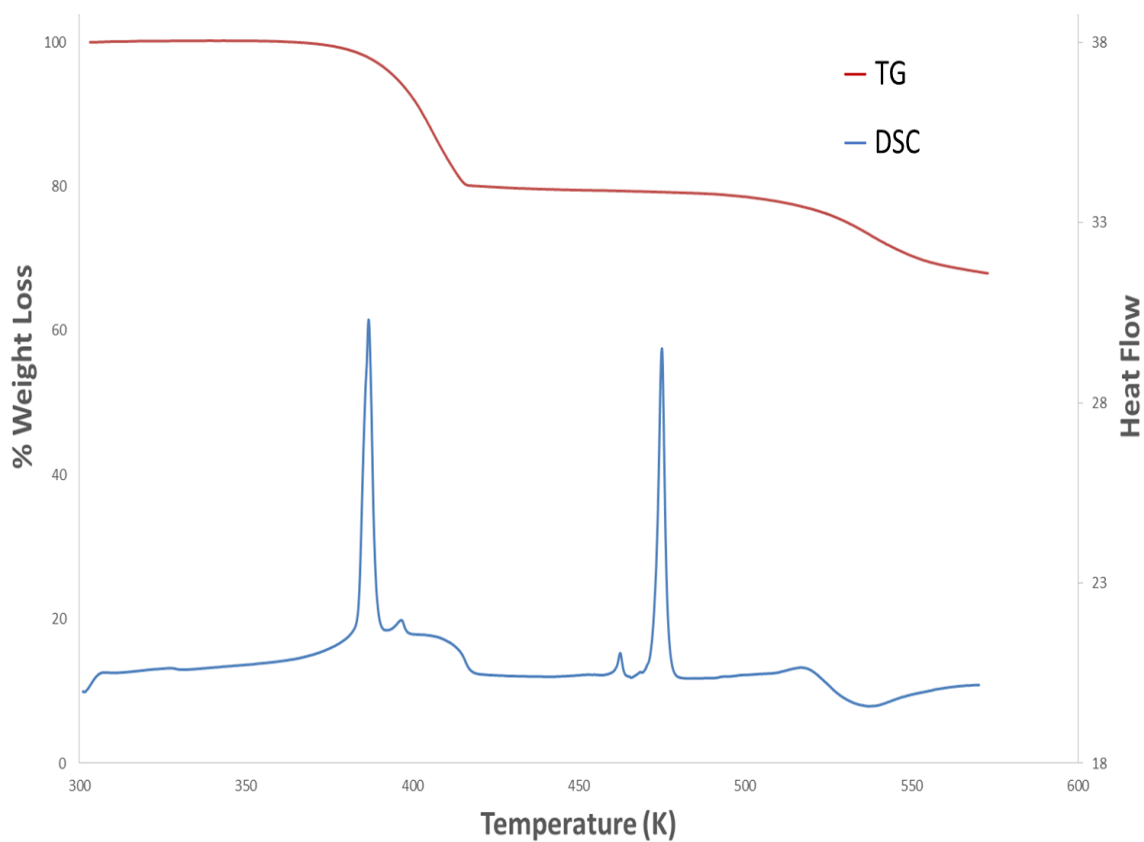


Figure 3.21: DSC and TG curves of H1•DMA.

Table 3.11: Thermal analysis results for H1•DMA.

Boiling Point of DMA (K)	438
Host : Guest ratio	1 : 1
TG calculated % weight loss	21.2
TG experimental % weight loss	21.1
DSC Endotherm 1 T_{onset} (K)	386.8
DSC Endotherm 2 T_{onset} (K)	474.8

3.3.2 Hot stage microscopy (HSM)

The crystals were immersed in silicone oil and placed on a hot stage microscope. The first step in the thermal decomposition was the opacity which was observed at 434 K. However, the crystal started melting at 484.6 K and the melt was completed at 488.6 K.

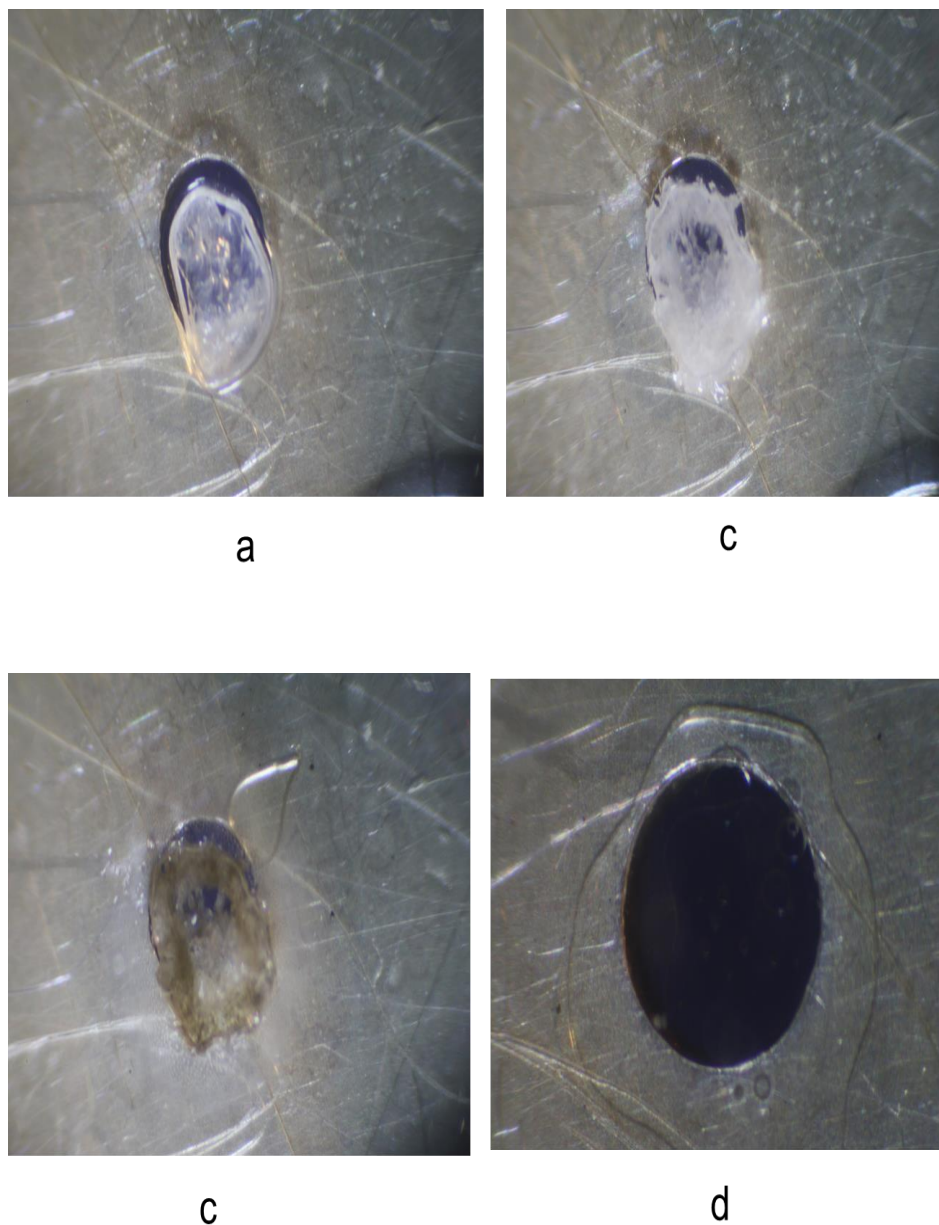


Figure 3.22: HSM photography of H1-DMA: (a) crystal immersed in silicone oil at 303 K, **(b)** crystal starts to become opaque at 434.6 K, **(c)** crystal starts melting at 484.6 K, **(d)** crystal completely melts at 488.6 K.

3.3.3 IR spectroscopy

The IR spectrum of **H1•DMA** (Figure 3.23) shows the formation of a new broad peak at 3267 cm^{-1} which is due to the hydrogen bonded OH present in the inclusion compound. This peak is observed at a lower frequency than the OH bond present in the IR spectrum of **H1** (3507 cm^{-1}). The band at 1680 cm^{-1} can be assigned to the C=O stretching vibration and the bands at 1204-1311 cm^{-1} can be assigned to the C-N stretching vibration. Since the **DMA** guest has two methyl groups attached to the amide nitrogen, this group then gives rise to a medium intensity band around 1508 cm^{-1} . This band is observed in the spectrum of **H1•DMA** and can also be assigned as a C-N stretch.^[109] The IR position and assignments are given below in Table 3.12.

Table 3.12: Positions and assignment of peaks in H1 and H1•DMA.

H1	H1•DMA	Assignment
3507	-	OH stretch
-	3267	Combination: OH and C-H stretch
-	1417, 1442, 1474	C-H Alkane stretch
-	1628, 1680	C=O stretch
1477, 1509, 1574, 1601	1474, 1573, 1601	Aromatic ring stretch
-	1204, 1239, 1289, 1311, 1508	C-N(CH ₃) ₂ stretch
751, 772, 875, 976	653, 765, 779, 804, 853, 915	C-H Aromatic ring

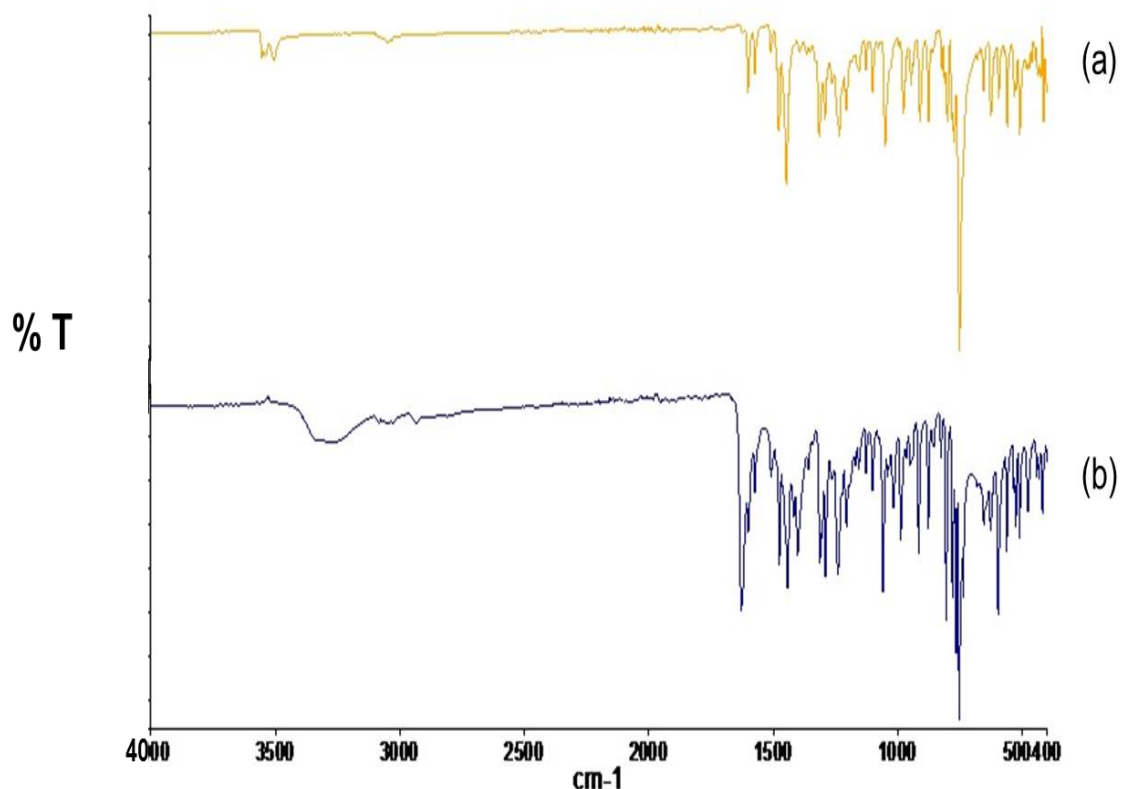


Figure 3.23: IR Spectra of (a) H1 and (b) H1•DMA.

3.3.4 Powder X-ray diffraction (PXRD)

A mixture of **H1** and 2-3 drops of **DMA** was ground for 15 min and the PXRD pattern of the resultant powder showed overall agreement with the calculated PXRD pattern obtained from LAZYPULVERIX.^[1] This result proved that **H1•DMA** was successfully prepared using the grinding experiment. PXRD patterns of **H1•DMA** calculated from LAZYPULVERIX, the ground product and **H1** are shown in Figure 3.24.

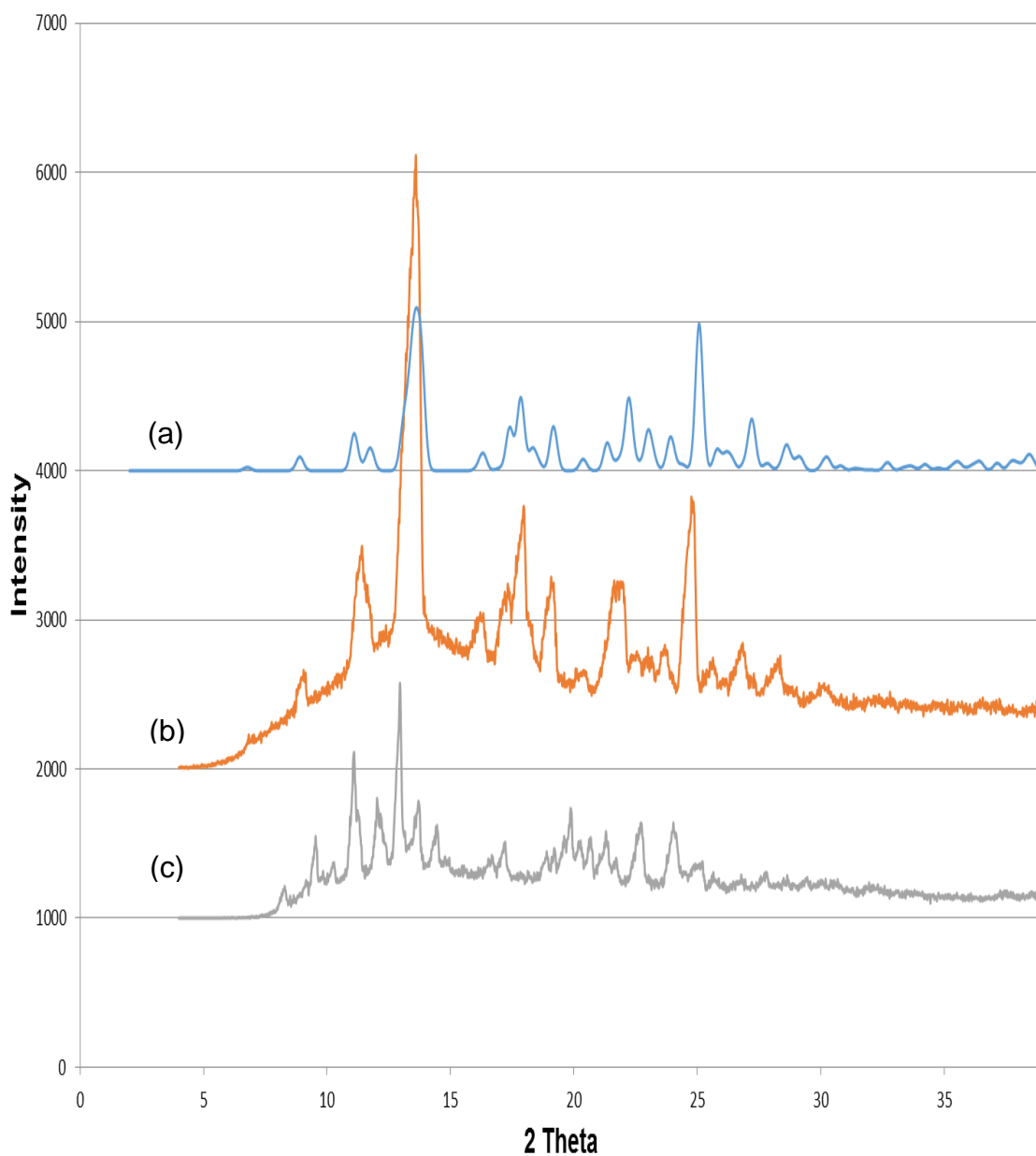


Figure 3.24: PXR D patterns of (a) H1•DMA calculated from LAZYPULVERIX, (b) ground product and (c) H1.

3.3.5 Crystal structure analysis

The structure was solved successfully in the triclinic space group $P\bar{1}$ with one host molecule and one **DMA** molecule in the asymmetric unit ($Z = 2$), Figure 3.25. The **DMA** is disordered over two positions, shown in Figure 3.26 and refined with site occupancy factors of 0.814 and 0.190 respectively. The suffixes A and B were used to distinguish between the

disordered fragments. The structure refined successfully with $R_1 = 0.0454$ with $wR_2 = 0.1150$. Crystal data and refinement parameters are given in Table 3.13.

Table 3.13: Crystal data and refinement parameters of H1•DMA.

Compound	H1•DMA
Molecular Formula	$C_{27}H_{25}NO_3$
M_w (g mol ⁻¹)	411.2
Data collection temp (K)	173(2)
Crystal system	Triclinic
Space group	$P\bar{1}$
a (Å)	8.2166 (16)
b (Å)	10.663(2)
c (Å)	13.085(3)
α (°)	89.68(3)
β (°)	87.22(3)
γ (°)	68.82(3)
Volume (Å ³)	1067.7
Z	2
μ (mm ⁻¹)	0.083
F(000)	436
No. of reflections collected	4858
No. of unique reflections	4858
No. of reflections with $I > 2\sigma(I)$	3692
D_c , calculated density (g cm ⁻³)	1.280
Index ranges	h: 0,10; k: -12,13; l: ± 16
Goodness of fit, S	1.040
Final R indices [$I > 2\sigma(I)$]	$R_1 = 0.0454$; $wR_2 = 0.1150$
R indices (all data)	$R_1 = 0.0646$; $wR_2 = 0.1303$
Largest peak and hole (eÅ ⁻³)	-0.252 ; 0.224

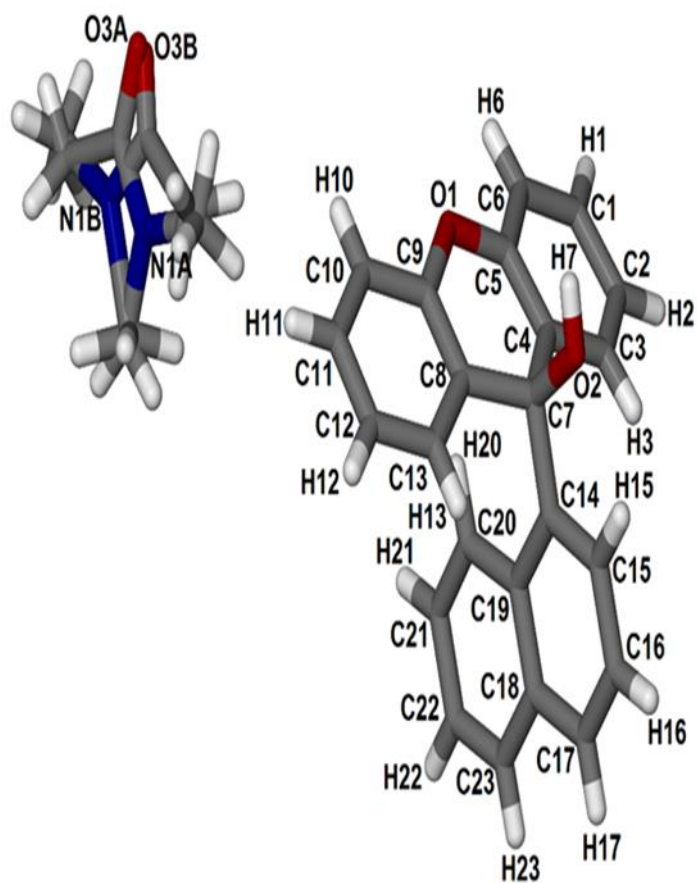


Figure 3.25: Asymmetric unit of H1•DMA.

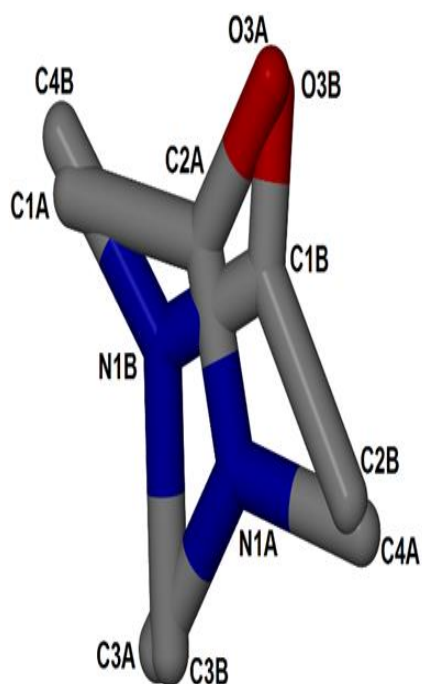


Figure 3.26: Disordered DMA guest with hydrogen atoms omitted.

The structure is stabilised by (Host)–OH \cdots O–(Guest) hydrogen bonds (Figure 3.27). The hydrogen bond parameters are given in Table 3.14. As was observed for the previous structures, a C–H \cdots π interaction was noted between adjacent host molecules (Figure 3.28) with a C \cdots π (centroid) distance of 3.720 Å and a C–H \cdots π angle of 149.1°.

Table 3.14: Hydrogen bonding details of H1•DMA.

Donor (D)–H	Acceptor (A)	D \cdots A (Å)	D–H (Å)	H \cdots A (Å)	D–H \cdots A (°)
O1–H7	O3A	2.637(11)	0.94	1.70	176
O1–H7	O3B	2.83(4)	0.94	1.89	175

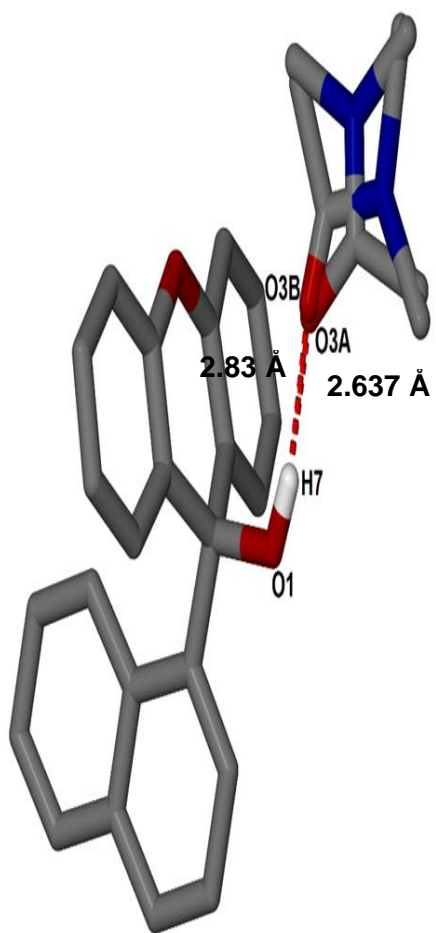


Figure 3.27: Hydrogen bonding in H1•DMA.

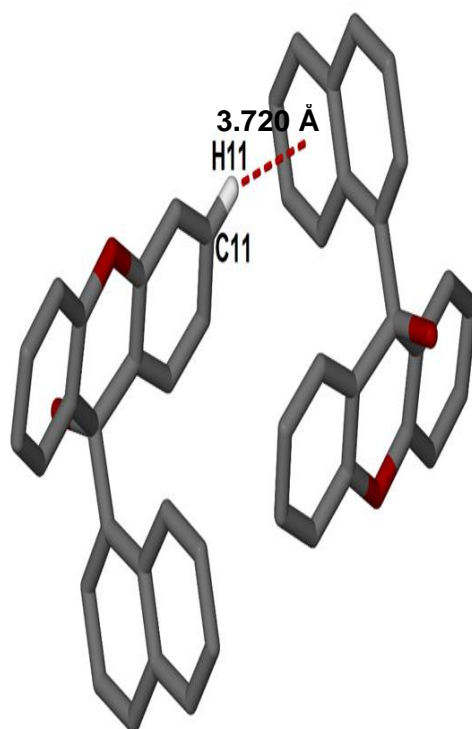


Figure 3.28: C–H... π interaction between host molecules.

The packing diagram of **H1•DMA** viewed along [010] with hydrogen bonds is shown in Figure 3.29. The **DMA** guests lie in cavities (Figure 3.30).

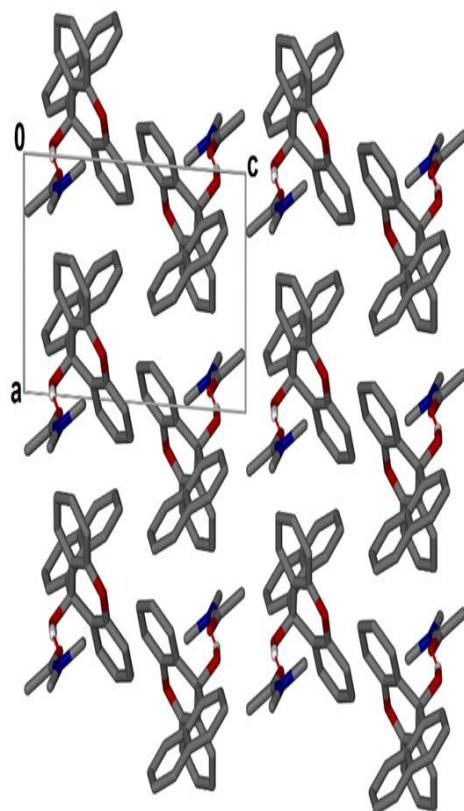


Figure 3.29: Packing diagram of H1•DMA along [010], only the major component of the disordered DMA guest is shown for clarity.

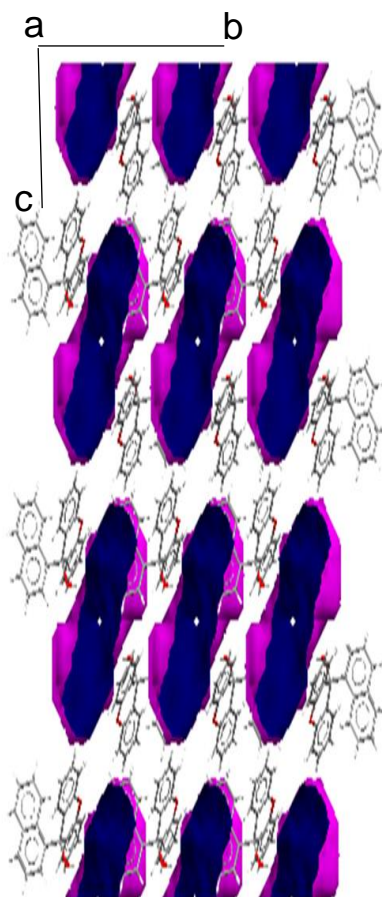


Figure 3.30: Cavities in which the DMA guests are located.

3.4 Inclusion compounds of H1 and morpholine (H1•MORP1 and H1•MORP2)

Two different inclusion compounds were obtained with **H1** and morpholine. A dilute solution of **H1** in morpholine gave crystals of **H1•MORP1**. The second inclusion compound **H1•MORP2** resulted from dissolution of **H1** in a 1:1 molar ratio of **MORP**: **DMA**. Both compounds crystallised in the space group $P\bar{1}$; however **H1•MORP1** demonstrated a host: guest ratio of $1:\frac{3}{2}$ whereas **H1•MORP2** was 1: 1.

3.4.1: H1•MORP1

3.4.1.1: Thermal analysis

The thermal analysis results for **H1•MORP1** are shown in Figure 3.31. The TG curve shows two mass loss steps of 8.8 and 19.4 % respectively, which gave a total mass loss of 28.2%. Thus the **H1•MORP1** host: guest ratio is $1:\frac{3}{2}$. The DSC curve shows three endotherms; the first two endotherms correspond to the loss of the **MORP** guest at $T_{\text{onset}} = 348.7$ K and $T_{\text{onset}} = 399.0$ K. The third one at $T_{\text{onset}} = 473.4$ K corresponds to the melt of the host. A summary of the thermal analysis data is given in Table 3.15.

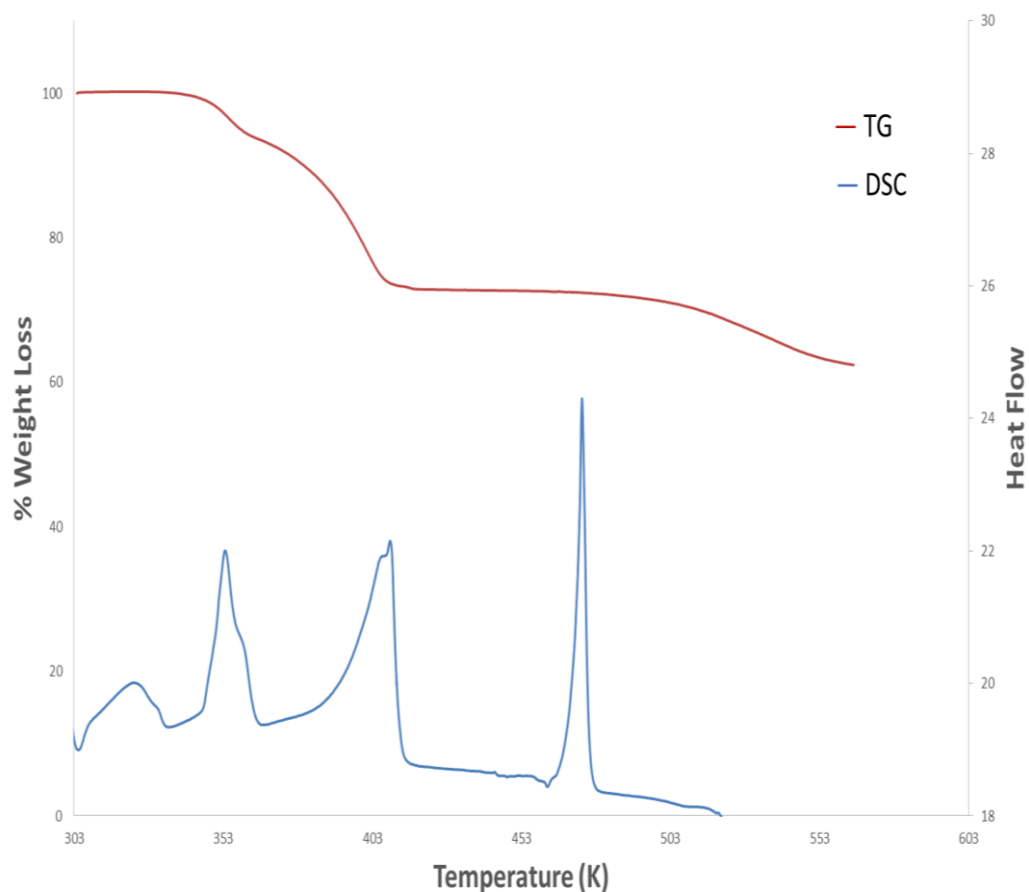


Figure 3.31: DSC and TG curves for H1•MORP1.

Table 3.15: Thermal analysis results of H1•MORP1.

Boiling point of MORP (K)	402
Host : Guest ratio	1: $\frac{3}{2}$
TG calculated % weight loss	28.8
TG experimental % weight loss	28.2
DSC Endotherm 1 T_{onset} (K)	348.7
DSC Endotherm 2 T_{onset} (K)	399.0
DSC Endotherm 3 T_{onset} (K)	473.4

3.4.1.2 Hot stage microscopy (HSM)

A crystal immersed in silicone oil was placed on a hot stage microscope and was observed over a temperature range starting at 300 K. The results are shown in Figure 3.32.

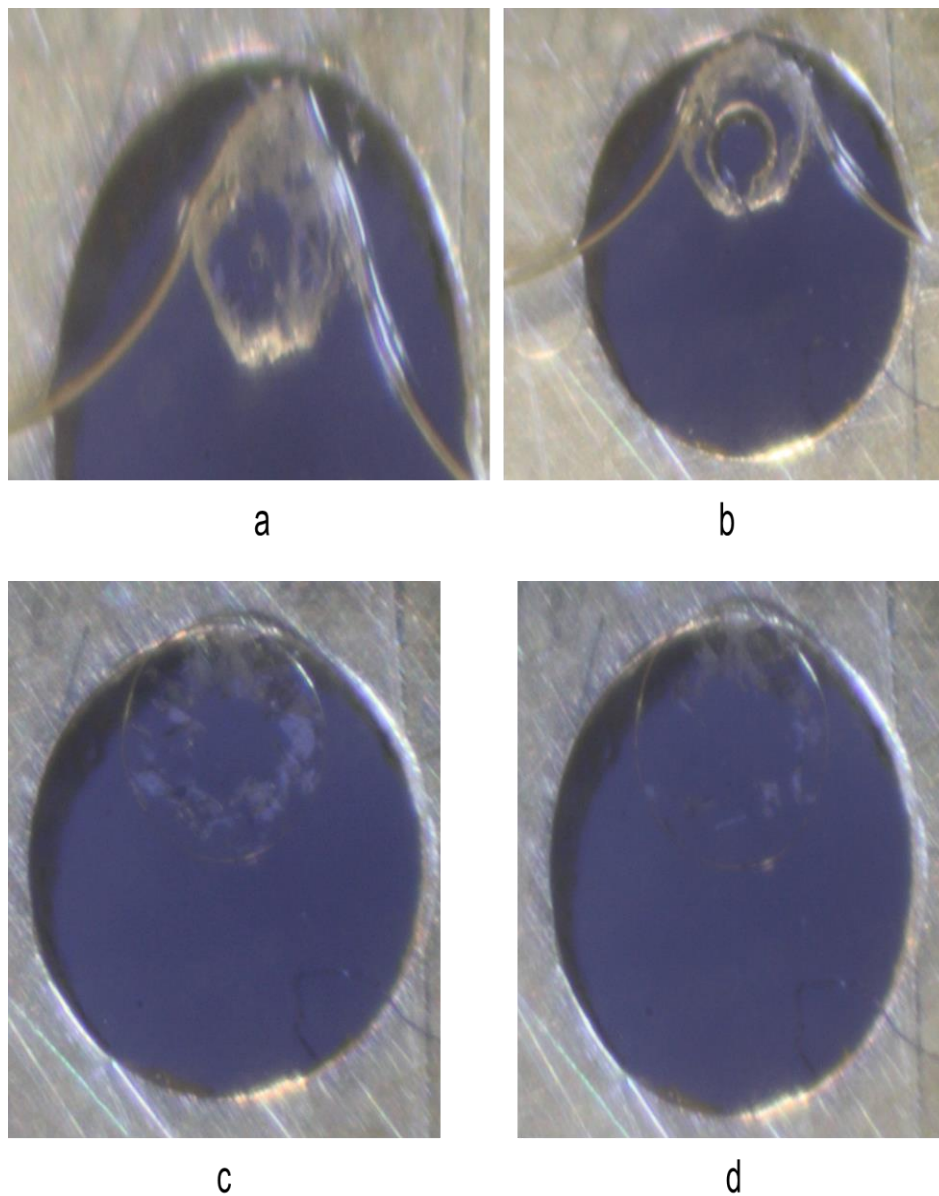


Figure 3.32: HSM photography of H1•MORP1: (a) crystal immersed in silicone oil at 300 K, **(b)** bubbles form and crystal starts melting at 456 K, **(c)** crystal continues to melt at 463 K, **(d)** crystal completely melts at 466 K.

3.4.1.3 IR spectroscopy

The IR spectra of **H1** and **H1•MORP1** are shown below in Figure 3.33. IR positions and the assignment of peaks are given in Table 3.16. The IR spectrum of **H1•MORP1** demonstrates the formation of an inclusion compound by the presence of new peaks around 2823 and 2989 cm^{-1} . These bands are due to the hydrogen bonded OH present in the inclusion compound. These peaks are observed at a lower frequency than the OH stretch present in the IR spectrum of **H1** (3507 cm^{-1}).

Table 3.16: Positions and assignment of peaks in H1 and H1•MORP1.

H1	H1•MORP1	Assignment
3507	-	OH stretch
-	2823, 2866, 2989	Combination: OH and N stretch
1477, 1509, 1574, 1601	1460, 1537, 1633	Aromatic ring stretch
1099, 1126, 1205, 1234, 1291	1072, 1101, 1260, 1307, 1363, 1396	C-O stretch
751, 772, 875, 976	666, 815, 849, 880, 995	C-H Aromatic ring

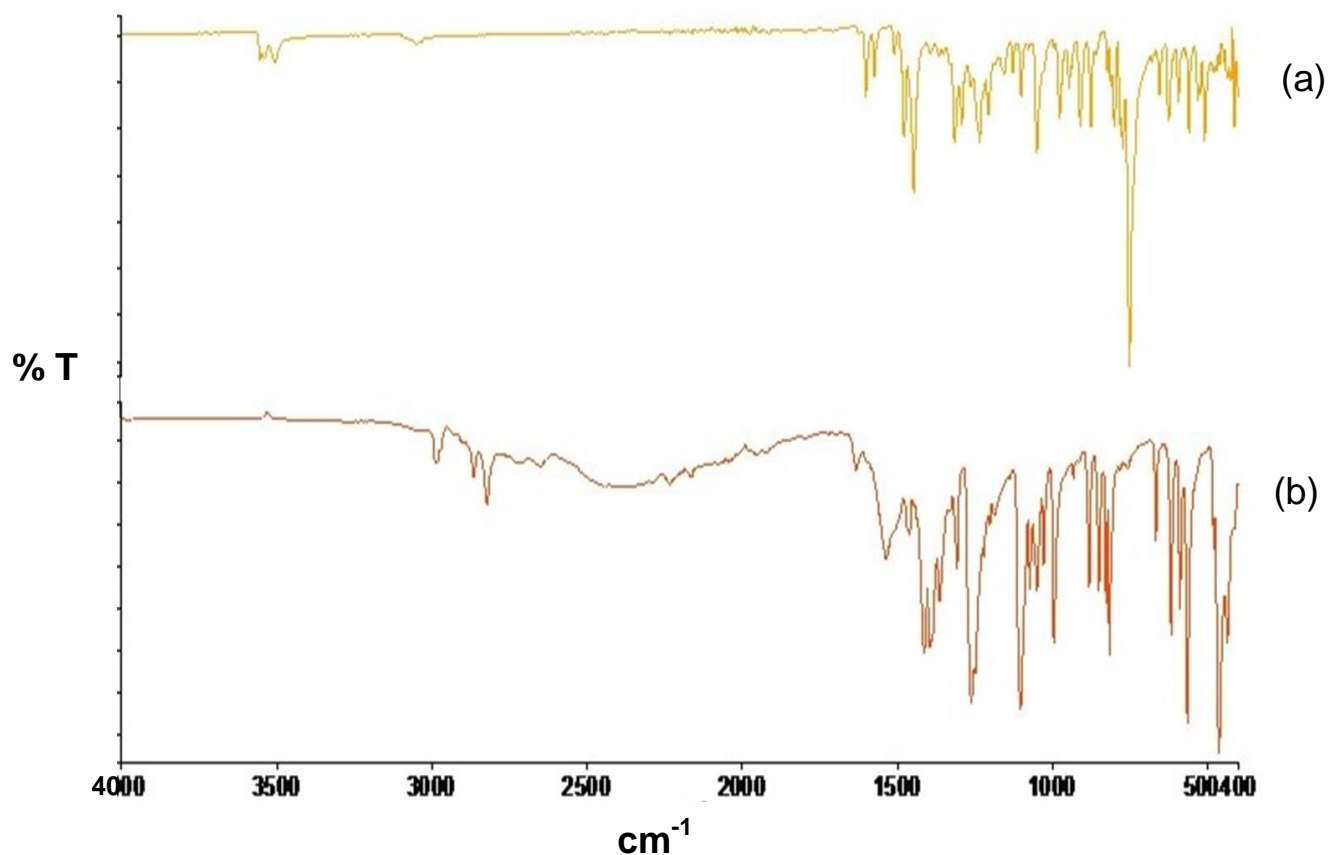


Figure 3.33: IR Spectra of (a) H1 and (b) H1•MORP1.

3.4.1.4 Powder X-ray diffraction (PXRD)

A mixture of **H1** and **MORP** was ground for 15 min and the PXRD pattern of the resultant powder is similar to the calculated PXRD pattern obtained from LAZYPULVERIX.^[1] PXRD patterns of **H1•MORP1** calculated from LAZYPULVERIX, the ground product and **H1** are shown below in Figure 3.34.

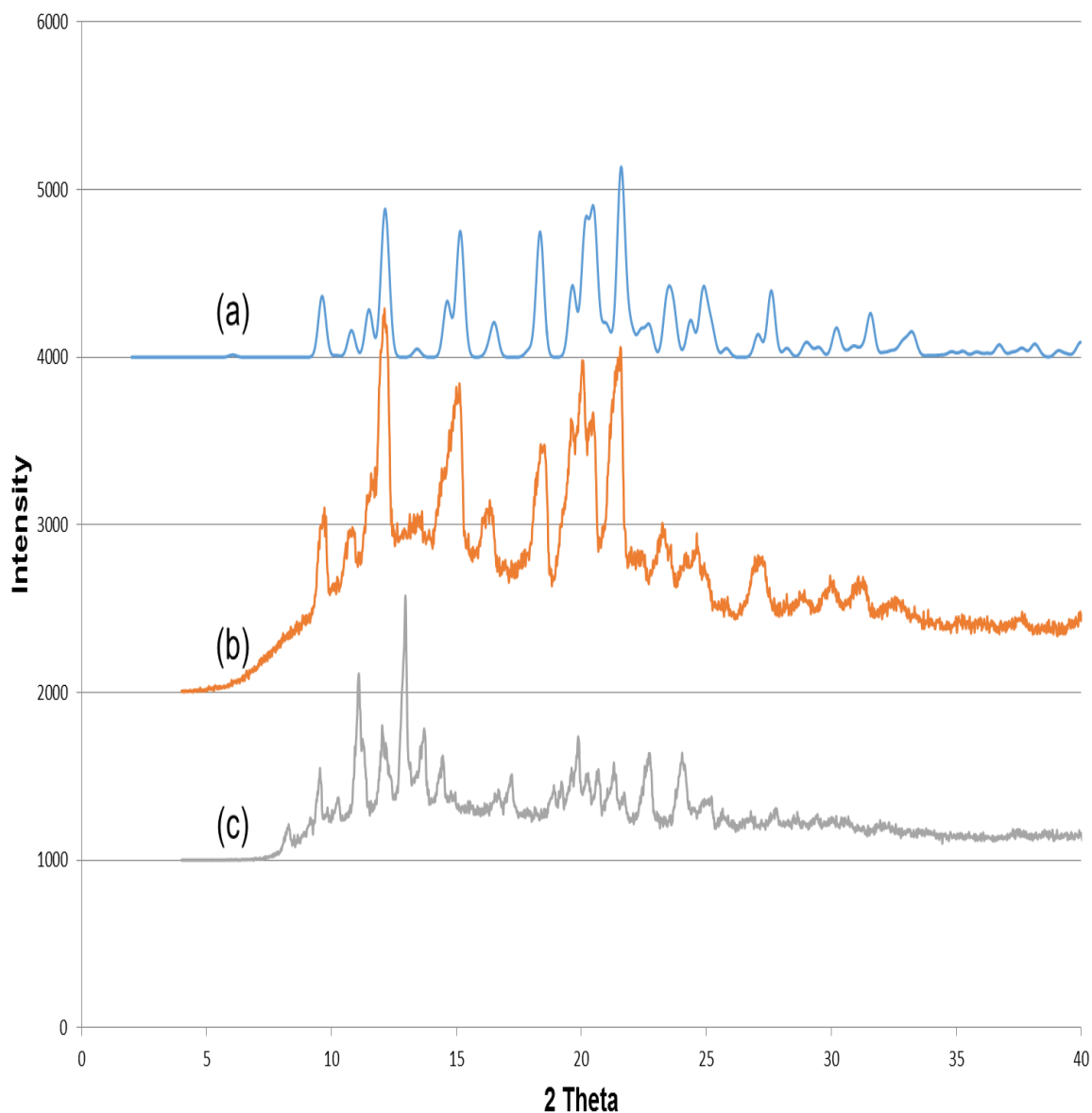


Figure 3.34: PXRD patterns of H1•MORP1 calculated from (a) LAZYPULVERIX, (b) ground product and (c) H1.

3.4.1.5 Crystal structure analysis

H1•MORP1 crystallised in the triclinic system space group $P\bar{1}$ with one host molecule and $\frac{3}{2}$ **MORP** molecules in the asymmetric unit ($Z = 2$), Figure 3.35. The crystallographically independent half of the morpholine molecule is disordered and refined with site occupancy factors of 0.722 and 0.278 respectively. The structure refined with $R_1 = 0.0487$ and $wR_2 = 0.1199$. The crystal data and refinement parameters are given in Table 3.17 below. The asymmetric unit of **H1•MORP1** is shown in Figure 3.35.

Table 3.17: Crystal data and refinement parameters of H1•MORP1.

Compound	H1•MORP1
Molecular Formula	$C_{29}H_{30}N_2O_3$
M_w (g mol ⁻¹)	454.87
Data collection temp (K)	173(2)
Crystal system	Triclinic
Space group	$P\bar{1}$
a (Å)	8.7130(17)
b (Å)	9.2721(19)
c (°)	14.732(3)
α (°)	96.00(3)
β (°)	93.46(3)
γ (°)	94.47(3)
Volume (Å ³)	1177.2(4)
Z	2
μ (mm ⁻¹)	0.084
F(000)	484
No. of reflections collected	15401
No. of unique reflections	5908
No. of reflections with $I > 2\sigma(I)$	4528
D_c , calculated density (g cm ⁻³)	1.283
Index ranges	h: ± 11 ; k: ± 12 ; l: ± 19
Goodness of fit, S	1.055
Final R indices [$I > 2\sigma(I)$]	$R_1 = 0.0487$; $wR_2 = 0.1199$
R indices (all data)	$R_1 = 0.0645$; $wR_2 = 0.1303$
Largest difference peak and hole (e Å ³)	-0.284; 0.279

Table 3.18: Hydrogen bonding details of H1•MORP1.

Donor (D)–H	Acceptor (A)	D...A (Å)	D–H (Å)	H...A (Å)	D–H...A (°)
O1–H7	N1MA	2.700 (2)	0.88	1.92	170
N1MA–H1MA	O3B	3.266 (1)	0.87	2.45	157

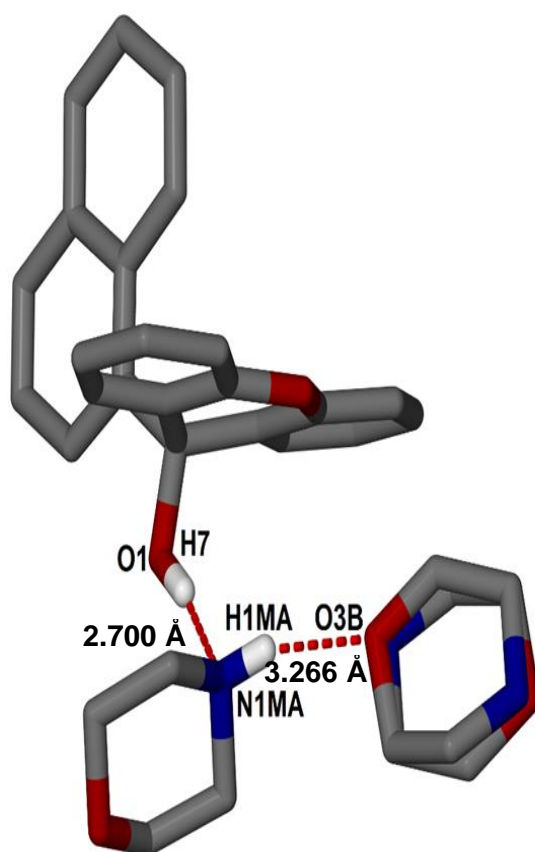


Figure 3.36: Hydrogen bonding in H1•MORP1.

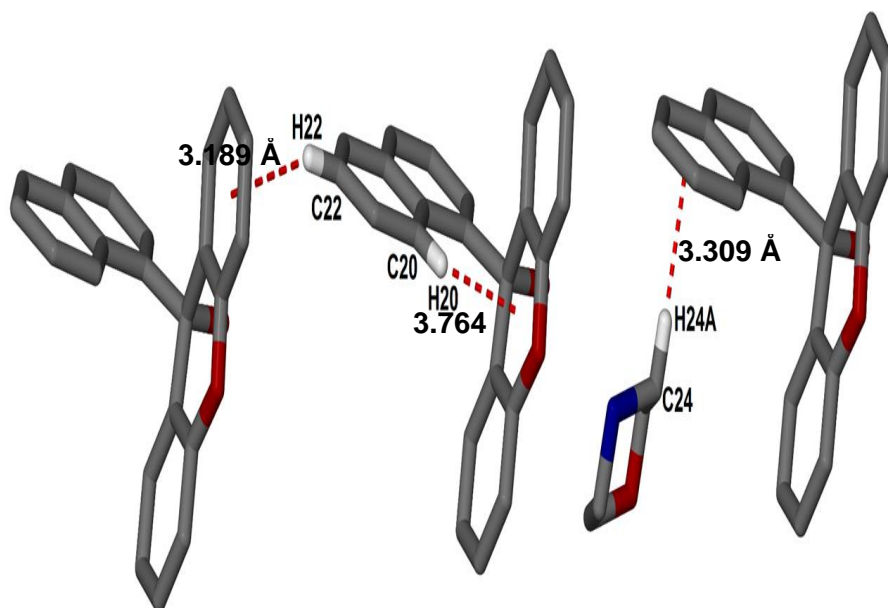


Figure 3.37: C–H... π interactions in H1•MORP1.

The packing diagram of **H1•MORP1** viewed along [001] with hydrogen bonds is shown below in Figure 3.38. Columns of host molecules are interleaved between columns of **MORP** molecules with the **MORP** molecules occupying channels along [001], Figure 3.39. Figure 3.40 shows the space filling diagram along [001] with the guests omitted.

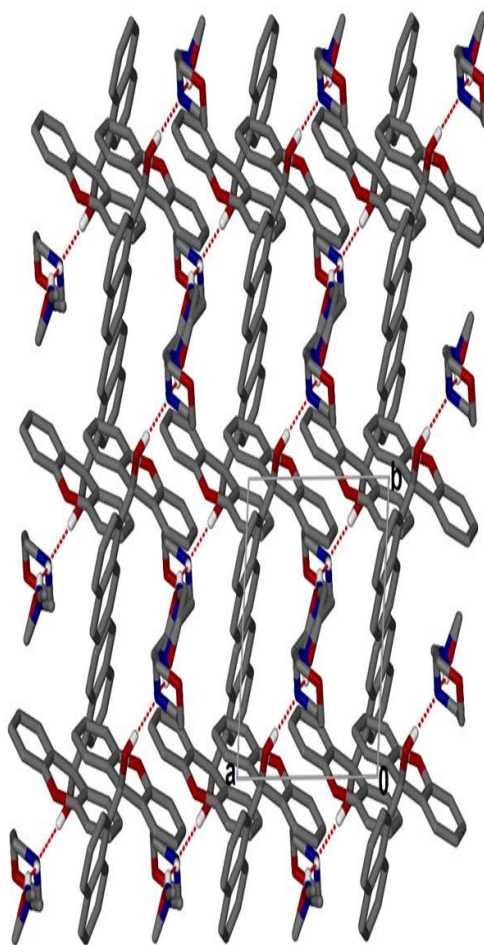


Figure 3.38: Packing diagram of H1•MORP1 viewed along [001].

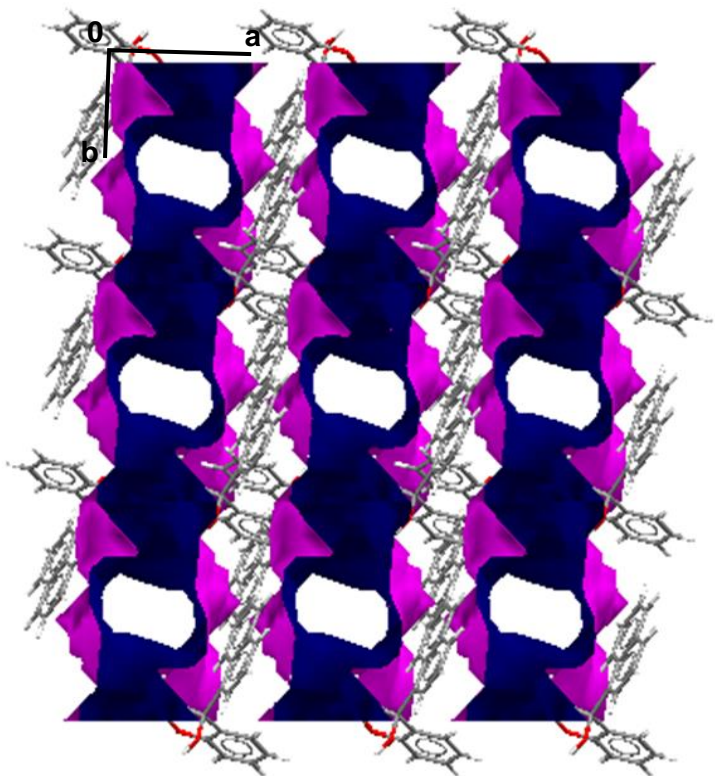


Figure 3.39: Channels in which the MORP guests are located.

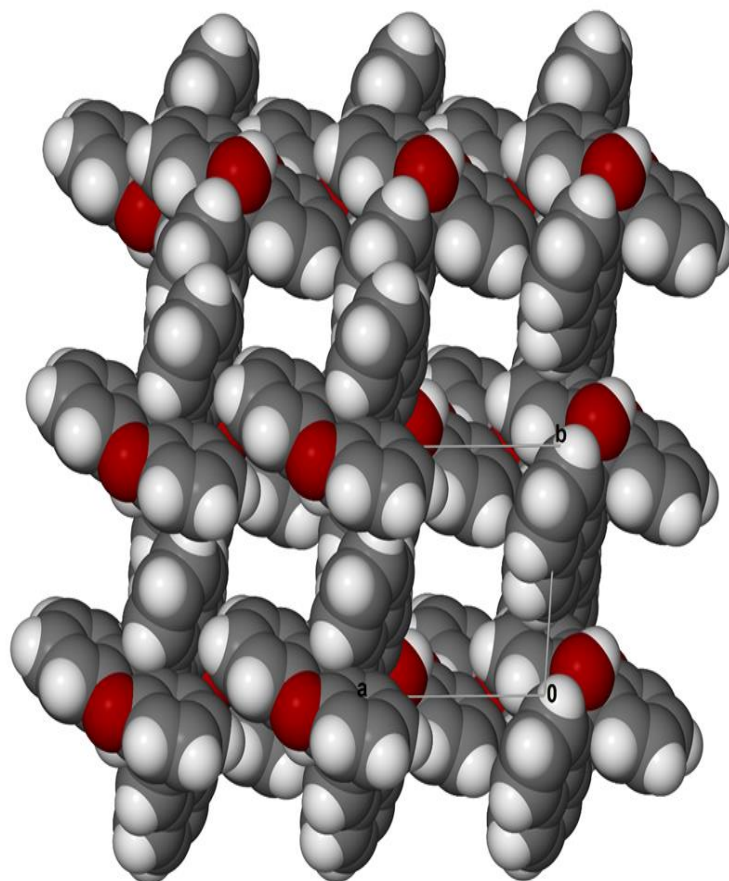


Figure 3.40: Space filling diagram along [001] with the MORP guests omitted.

3.5 H1•MORP2

3.5.1 Thermal analysis

The TG and DSC curves of **H1•MORP2** are shown in Figure 3.41. The TG curve shows one mass loss step of 20.1%. Thus the **H1•MORP2** host: guest ratio is 1:1. The DSC curve shows two endotherms; the first endotherm corresponds to the loss of the **MORP** guest at $T_{\text{onset}} = 398.0$ K and the second one at $T_{\text{onset}} = 474.7$ K corresponds to the melt of the host. A summary of the thermal analysis data is given in Table 3.19.

Table 3.19: Thermal analysis results of H1•MORP2.

Boiling point of MORP (K)	402
Host : Guest ratio	1 : 1
TG calculated % weight loss	21.2
TG experimental % weight loss	20.1
DSC Endotherm 1 T _{onset} (K)	398.0
DSC Endotherm 2 T _{onset} (K)	474.7

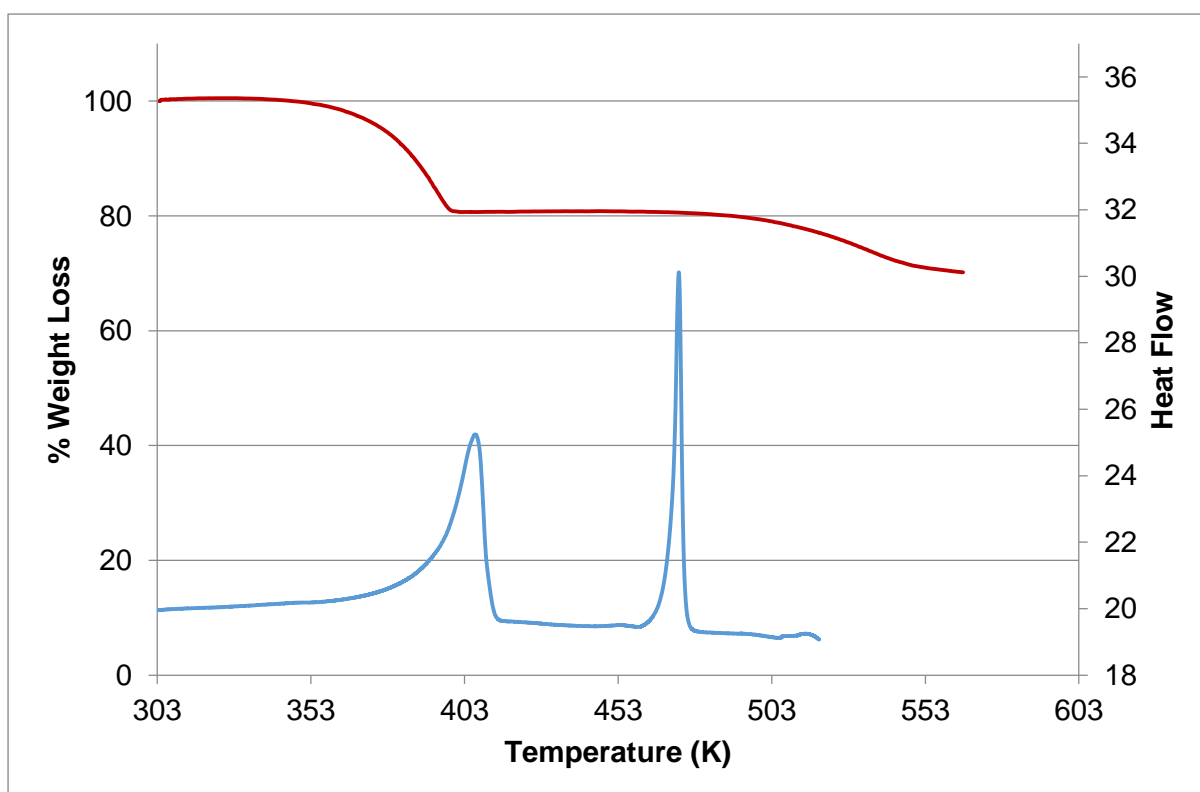
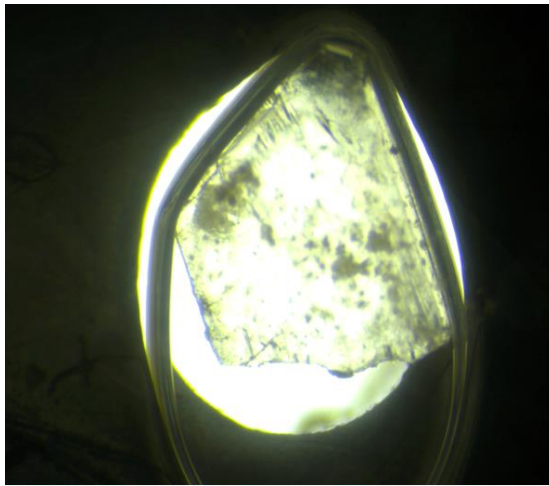


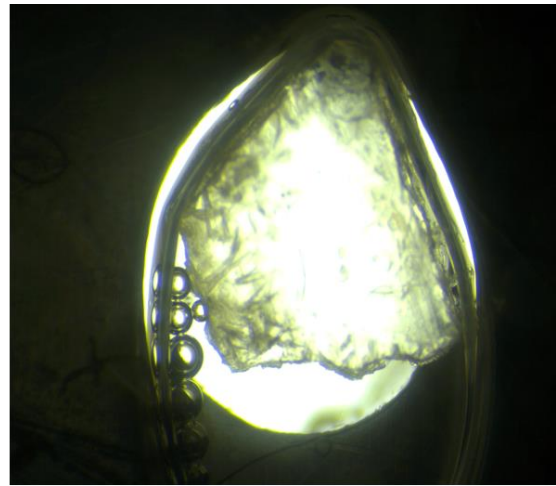
Figure 3.41: TG and DSC curves of H1•MORP2.

3.5.2 Hot stage microscopy

The crystals immersed in silicone oil were placed between two cover slips on a hot stage microscope. The melting process of the crystals is shown in Figure 3.42.



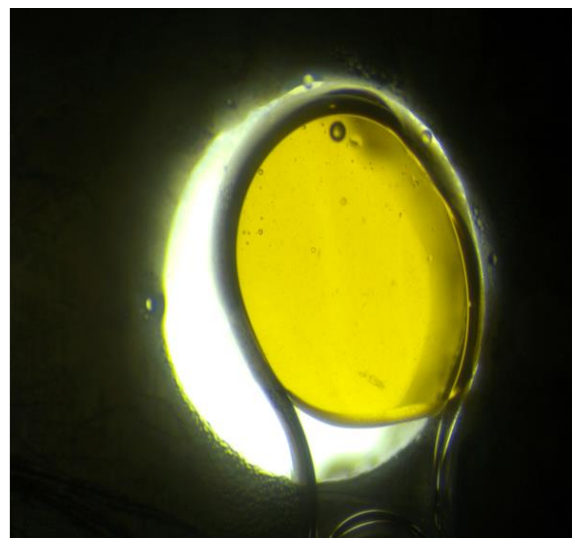
a



b



c



d

Figure 3.42: HSM photography of H1•MORP2: (a) crystal immersed in silicone oil at 300 K, **(b)** bubbles form and crystal starts melting at 410 K, **(c)** crystal continues to melt at 470 K, **(d)** crystal completely melts at 480 K.

3.5.3 IR spectroscopy

The IR spectra of **H1** and **H1•MORP2** are shown below in Figure 3.43. IR positions and the assignment of peaks are given in Table 3.20. In the IR spectrum of **H1•MORP2**, there is the presence of new peaks around 3053 cm^{-1} and 2856 cm^{-1} . These peaks demonstrate the formation of an inclusion compound and are due to the hydrogen bonded OH present in the inclusion compound. These peaks are observed at a lower frequency than the OH stretch present in the IR spectrum of **H1** (3507 cm^{-1}).

Table 3.20: Positions and assignments of peaks in H1 and H1•MORP2.

H1	H1•MORP2	Assignment
3507	-	OH stretch
-	2856, 3053	Combination: OH and N stretch
1477, 1502, 1574, 1601	1475, 1509, 1573, 1599, 1631	Aromatic ring stretch
1099, 1126, 1205, 1234, 1291	1060, 1173, 1241, 1289	C–O stretch
751, 772, 875, 976	750, 767, 811, 953	C–H Aromatic ring

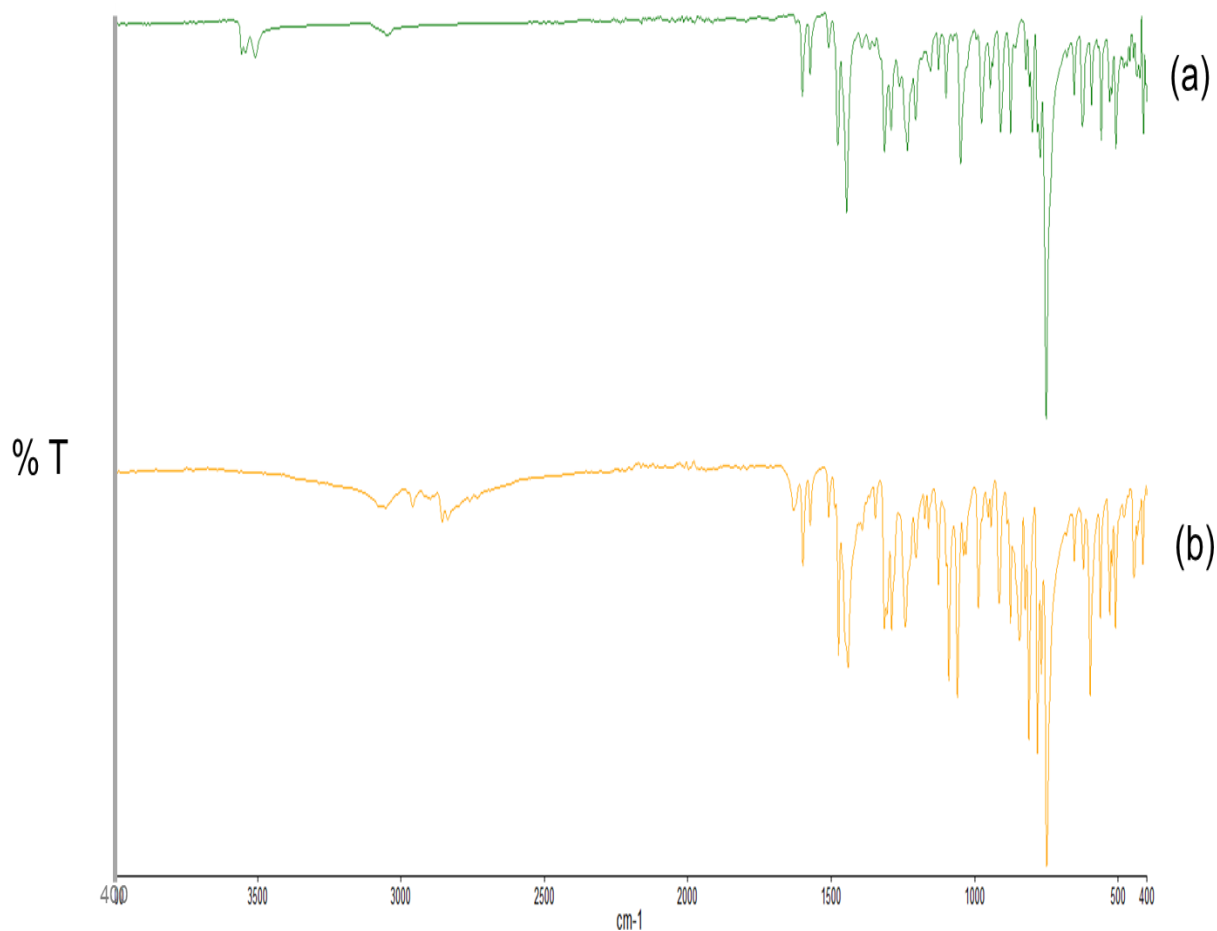


Figure 3.43: IR spectra of (a) H1 and (b) H1•MORP2.

3.5.4 Crystal structure analysis

H1•MORP2 solved in the triclinic space group $P\bar{1}$ with one host molecule and one **MORP** molecule in the asymmetric unit ($Z = 2$), Figure 3.44 and gave a 1: 1 host: guest ratio. The morpholine molecule is disordered and refined with site occupancy factors of 0.267 and 0.733 respectively. The structure refined to $R_1 = 0.0455$ and $wR_2 = 0.1120$. Crystal data and refinement parameters are summarised in Table 3.21.

Table 3.21: Crystal data and refinement parameters of H1•MORP2.

Compound	H1•MORP2
Molecular formula	C ₂₇ H ₂₅ NO ₃
M _w (g.mol ⁻¹)	411.48
Data collection temp (K)	173(2)
Crystal system	Triclinic
Space group	$P\bar{1}$
a(Å)	8.7465(17)
b(Å)	9.1918(18)
c(Å)	14.210(3)
α(°)	72.97(3)
β(°)	75.57(3)
γ(°)	85.24(3)
Volume (Å ³)	1057.8(4)
Z	2
μ (mm ⁻¹)	0.084
F(000)	436
No. of reflection collected	16204
No. of unique reflection	5077
No. of reflection with I>2σ(I)	3910
D _c , calculated density (g.cm ⁻³)	1.292
Index ranges	h: ± 11; k: ± 12; l: ± 18
Goodness of fit, S	1.025
Final R indices I>2σ(I)	R ₁ = 0.0455; wR ₂ = 0.1120
R indices (all data)	R ₁ = 0.0605; wR ₂ = 0.1223
Largest diff peak and hole (eÅ ⁻³)	0.298; -0.244

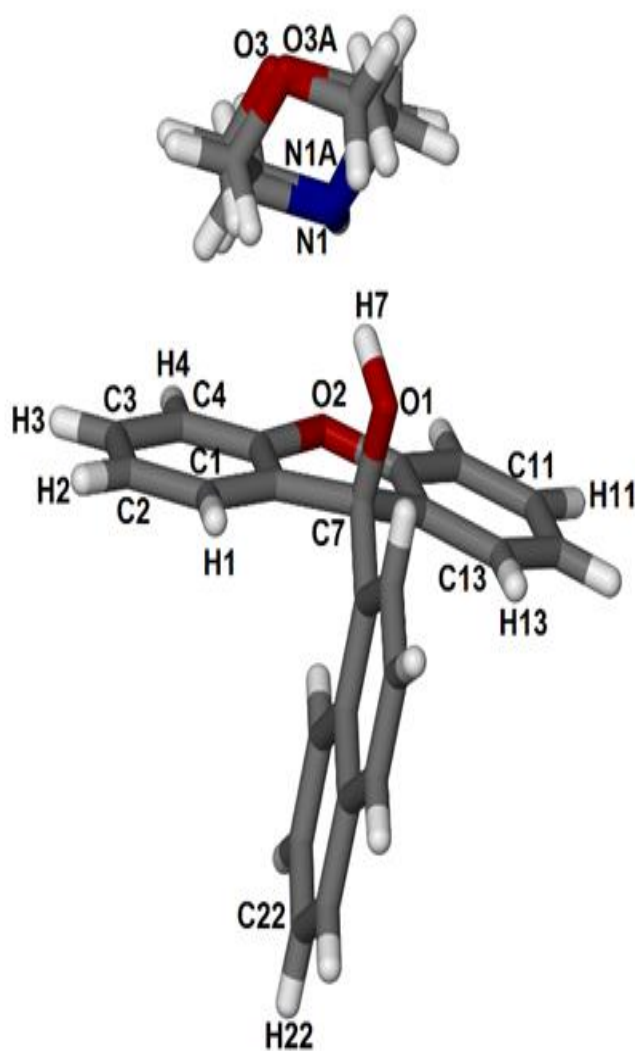


Figure 3.44: Asymmetric unit of H1•MORP2.

The host molecule is hydrogen bonded to the **MORP** molecule via (Host)-OH•••N (**MORP**) hydrogen bonds. The host molecule interacts also via weak hydrogen bonds (Figure 3.45). The hydrogen bond details are given in Table 3.22. A C-H••• π contact is observed between the host aromatic rings (Figure 3.46) with a C••• π (centroid) distance of 3.252 Å; and C-H••• π angle of 135°. There is also a C-H••• π interaction observed between host and guest molecules with a C••• π (centroid) distance of 3.621 Å and C-H••• π angle of 149°.

Table 3.22: Hydrogen bonding in H1•MORP2.

Donor (D)-H	Acceptor (Å)	D...A (Å)	D-H (Å)	H...A (Å)	D-H...A (°)
C15-H15	O1	2.627(2)	0.95	2.21	105
O1-H7	N1	2.839(13)	1.00	1.85	170
O1-H7	N1A	2.823(10)	1.00	1.83	174

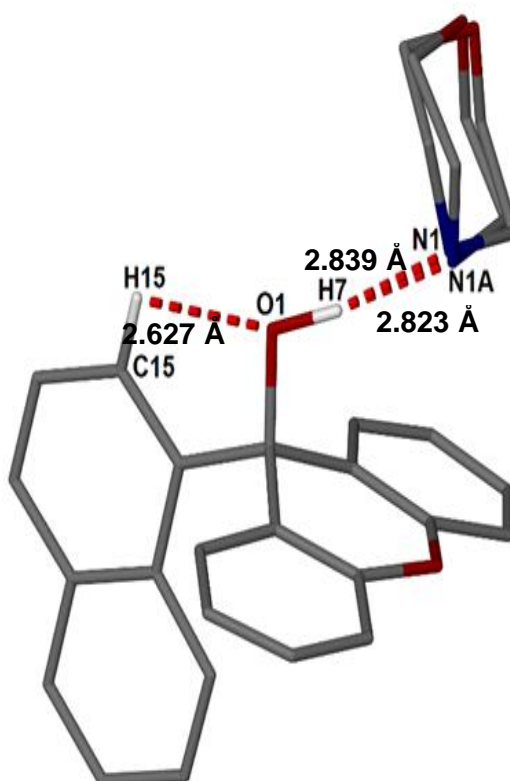


Figure 3.45: Hydrogen bonding in H1•MORP2.

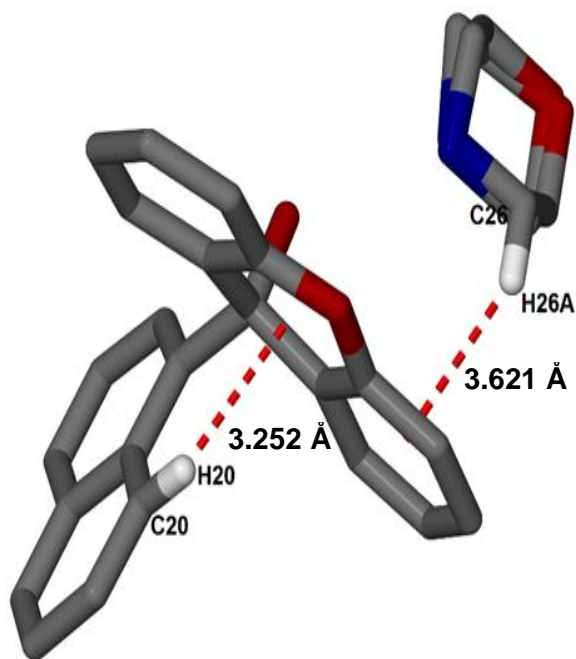


Figure 3.46: C-H... π interactions in H1•MORP2.

The packing diagram of **H1•MORP2** viewed along [001] with hydrogen bonds is shown below in Figure 3.47. The host molecules are interleaved between **MORP** molecules with the guests occupying channels along [010], Figure 3.48.

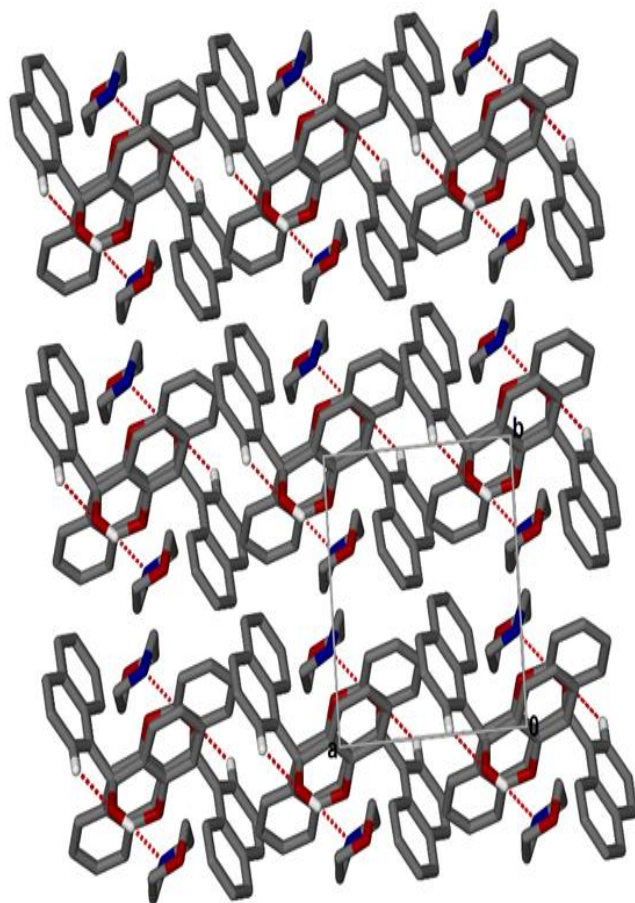


Figure 3.47: Packing diagram of H1•MORP2 along [001], only the major component of the disordered MORP guest is shown for clarity.

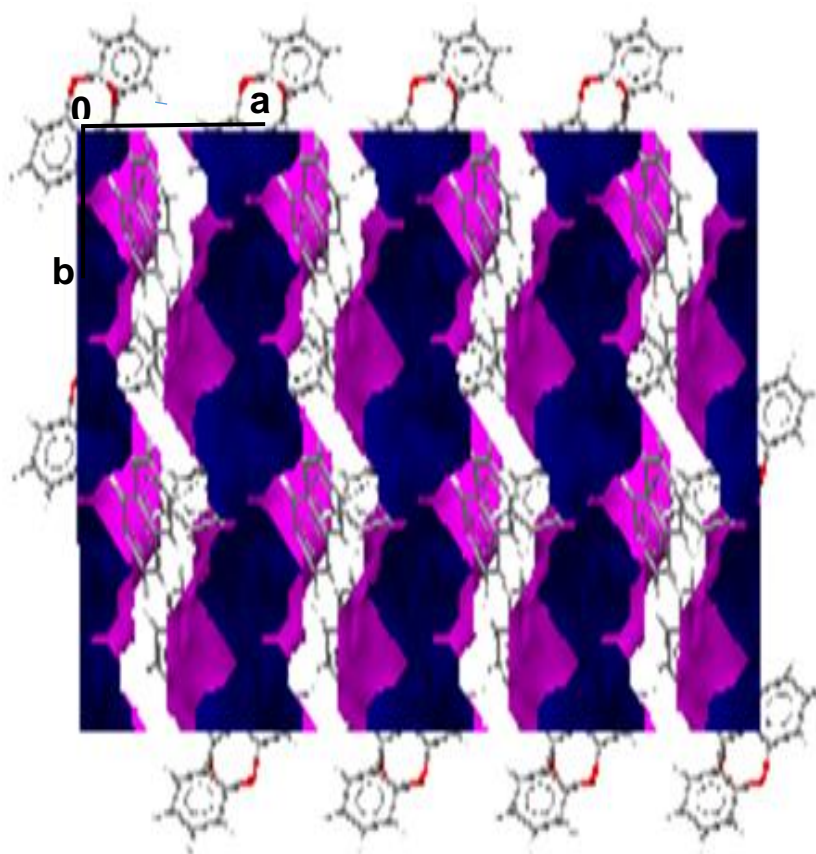


Figure 3.48: Channels in which the MORP guests are located.

Comparison of the packing diagrams of **H1•MORP1** and **H1•MORP2** (Figure 3.49) show the similarity in the host packing for the two compounds. The extra guest has resulted in interconnected channels. The T_{on} values found in the DSC for the release of the morpholine guest is higher for **H1•MORP2** (398 K) than for **H1•MORP1** (348.7 K) which is consistent with the different types of channels found in the two structures.

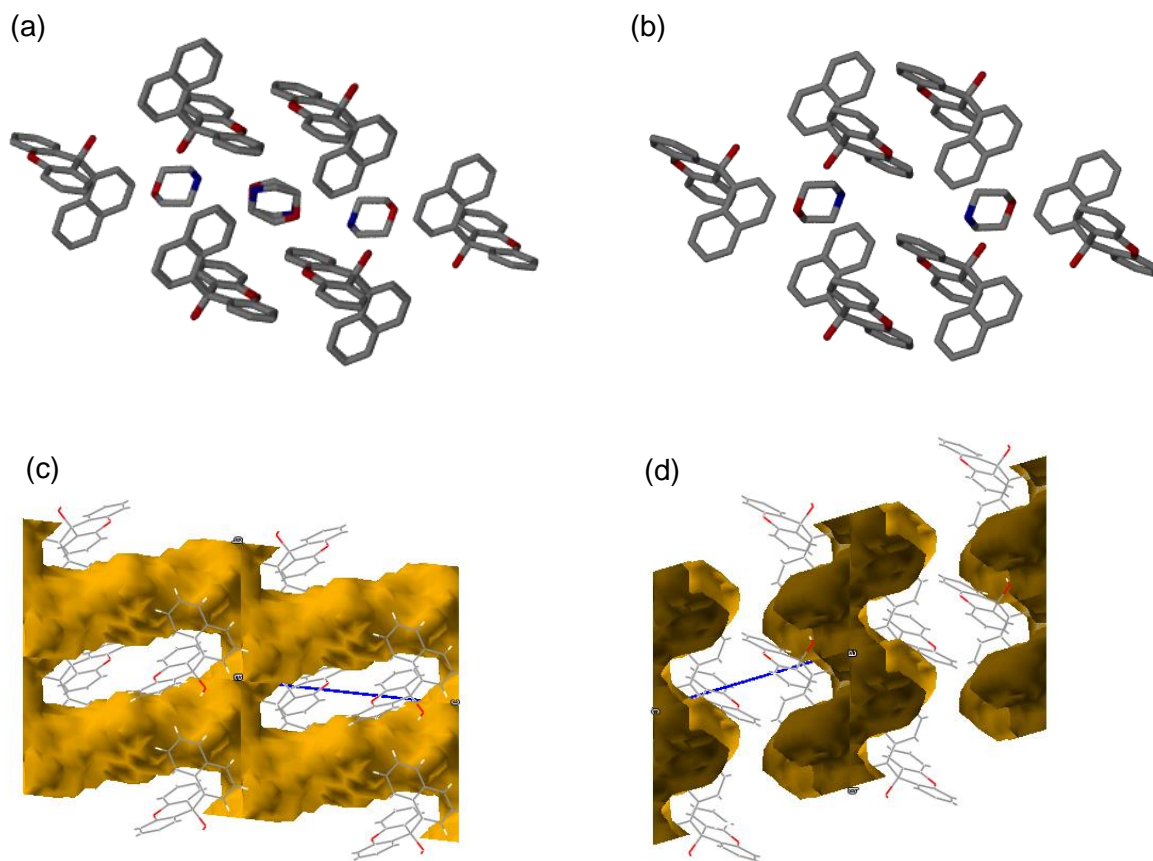


Figure 3.49: Packing diagrams of (a) H1•MORP1 and (b) H1•MORP2. Channels of (c) H1•MORP1 and (d) H1•MORP2 along [100] with the guests omitted.

3.6: Summary of thermal analysis results of H1 and its inclusion compounds

A summary of the thermal analysis results of **H1** and its inclusion compounds are shown below in Table 3.23.

Table 3.23: Summary of thermal analysis results of H1 and its inclusion compounds.

Compound	H1	H1•PYR	H1•NMP	H1•DMA	H1•MORP1	H1•MORP2
H:G ratio	-	1:1	1:1	1:1	1: $\frac{3}{2}$	1:1
TG (Calc % mass loss)	-	19.6	23.4	21.2	28.8	21.2
TG (Exp % mass loss)	-	18.8	23.3	21.1	26.2	20.1
DSC Endotherm (T_{on}/K)						
Peak 1	464.7	375.9	398.3	386.8	348.7	398.0
Peak 2		469.9		474.8	399.0	474.7
Peak 3					473.4	
Normal boiling point of pure guest (T_b/ K)	-	388	477	438	402	402
$(T_{on}-T_b)/K$	-	-12.3	-78.7	-51.2	-53.3	-4

For all the inclusion compounds of **H1**, the guest is released at a lower boiling point than the normal boiling point of the pure liquid guest. Interestingly **H1•NMP** is the only compound which gave one endotherm in the DSC. It was found that T_{on} , the temperature at which the guest is released is a consistent measure of thermal stability. However, T_b , the normal boiling point of the guest is also very important. A useful measure of the relative stability of an inclusion compound is the difference between the two values, $(T_{on}-T_b)$.^[11] The values in the table suggest that the order of thermal stability is **H1•MORP2** > **H1•PYR** > **H1•DMA** > **H1•MORP1** > **H1•NMP**. However it is important to note that there is a large boiling point difference between the guests, with **NMP** having the highest boiling point of 477 K compared to the lowest boiling point for **PYR** (388 K). In addition **H1•NMP** is the only inclusion

compound with a single DSC endotherm. All of the other inclusion compounds have at least two DSC endotherms and this can make comparisons of the thermal stability difficult.^[12]

3.7: Selectivity experiments

A quantitative measure of the selectivity of a given host compound for a given guest in a mixture can be obtained by competition experiments.^[11] Competition experiments were performed to determine the selectivity of the host compound **H1** towards mixtures of two guests. These were done for 1: 1 molar ratios of **PYR: NMP**, **PYR: MORP**, **MORP: NMP**, **DMA: NMP**, **DMA: PYR** and **DMA: MORP**. The total guest: host ratio was approximately 20: 1. The resultant crystals were analysed using TG or DSC. The DSC experimental results are shown in Appendix A1-A13). In each case only one product was found and the results are summarised in Table 3.24. In all experiments involving **NMP**, the **NMP** was selectively enclathrated.

Table 3.24: Summary of the selectivity experiments.

Guest Mixture	Resultant inclusion compound
PYR: NMP	H1•NMP
PYR: MORP	H1•MORP2
MORP: NMP	H1•NMP
DMA : PYR	H1•DMA
DMA : NMP	H1•NMP
DMA : MORP	H1•MORP2

Thus the selectivity trend is **NMP > MORP > DMA > PYR**. There is no correlation between the selectivity results and the relative thermal stability of the inclusion compounds as suggested by the ($T_{on} - T_b$) values. A similar result was observed by Barton et al. in a study on bis(9-amino-9-aryl-9*H*-thioxanthenes), where a poor correlation was found between the ($T_{on} - T_b$) values and the competition experiments.^[13]

3.8: Torsion angles for the host molecule H1

The torsion angles involving the xanthene and the naphthyl rings of the host molecule (Figure 3.50) are summarised in Table 3.25. The torsion angles between the xanthene and the naphthalene moieties of the host (τ_1 (C4-C7-C14-C19) and τ_3 (C10-C8-C7-C14)) is principally the cause of the scissor shape observed. For all the structures the hydroxyl group of the host is aligned with the naphthyl group as seen by the values for τ_2 (O1-C7-C14-C15). The dihedral angle between the least squares planes of the xanthene rings A and B was also determined. The values (1.4°-12.3°) show that the xanthene moiety is not flat with the smallest deviation from planarity observed for the host molecule in **H1•PYR**.

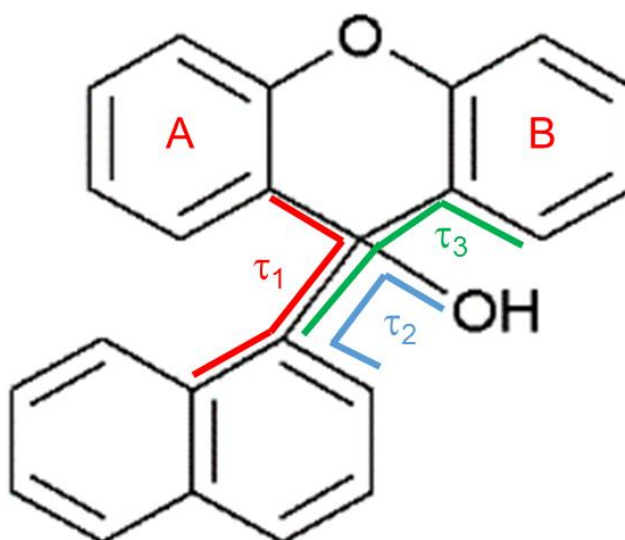


Figure 3.50: Torsion angles (τ_1 , τ_2 and τ_3) analysed for the host molecule (H1).

Table 3.25: Selected geometrical parameters of the host molecule H1.

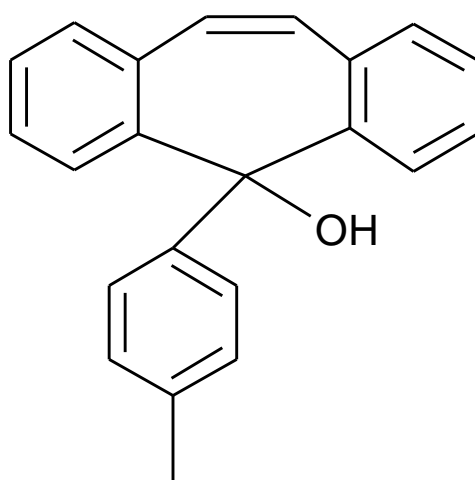
Torsion angle	H1•PYR	H1•NMP	H1•DMA	H1•MORP1	H1•MORP2
τ_1 (°)	61.7	61.5	62.2	-61.9	60.5
τ_2 (°)	0.04	0.52	-0.69	-0.33	-0.13
τ_3 (°)	-51.6	-44.3	-41.1	44.9	-39.8
Dihedral angle between rings A and B	1.4	9.7	12.3	9.7	12.2

References

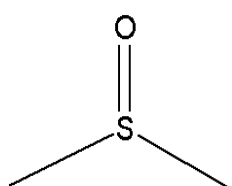
1. Yvon, K., Jeitschko, W. & Parth, E (1977) *Appl. Crystallogr.*, 10: 73-74.
2. Jacobs, A., Nassimbeni, L.R. & Taljaard, J.H. (2006) *Acta Cryst.*, E62, o825-o827.
3. Jacobs, A., Nassimbeni, L.R. & Taljaard, B. (2004) *Acta Cryst.*, C60, 0668-0670.
4. Sheldrick, G.M. (1997) SHELX-97, program for crystal structure refinement. University of Göttingen, Germany.
5. Jacobs, A., Nassimbeni, L.R., Nohako, K.L., Ramon, G. & Taljaard, J.H. (2005) *New J. Chem.*, 33:1960-1964.
6. Nassimbeni, L.R., Su, H., Davies, K. & Weber, E. (2013) *Supramol. Chem.*, 25: 310-314.
7. Desiraju, G.R. (2011) *Cryst. Growth & Des.*, 11: 896-898.
8. Macrae, C.F., Edgington, P.R., McCabe, P., Pidcock, E., Shields, G.P., Taylor, R., Towler, M. & van de Streek, J. (2006) *J. Appl. Cryst.*, 39: 453-457.
9. Desiraju, G.R. & Steiner, T. (1999) The weak hydrogen bond in structural and biology. Vole 9. IUCR Monographs on Crystallography, Oxford.
10. Smith, B.C. (1998) *Infrared Spectral Interpretation: A systematic approach.*
11. Nassimbeni, L.R. (2003) *Acc. Chem. Res.*, 36:631-637.
12. Jacobs, A., Bathori, N.B., Nassimbeni, L.R. & Silwana, N. (2011) *CrystEngComm.*, 13: 7014-7018.
13. Barton, B., McClelland, C.W. & Taljaard, B.(2002) *S.Afr.J.Chem.*, 55:144-148.

4. CHAPTER 4- H2 AND ITS INCLUSION COMPOUNDS

The host 5-(4-methylphenyl)-5*H*-dibenzo[*a,b*]cyclohepten-5-ol (**H2**) forms inclusion compounds with morpholine (**MORP**), dimethylsulfoxide (**DMSO**) and *N*-methyl-2-pyrrolidinone (**NMP**). The numbering scheme for **H2** is shown in Figure 4.1 and the DSC curve (Figure 4.2) gives one endotherm that corresponds to the melt of the host compound at $T_{on} = 409.8$ K.

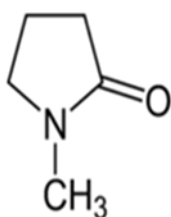


5-(4-methylphenyl)-5*H*-dibenzo[*a,d*]cyclohepten-5-ol (**H2**)



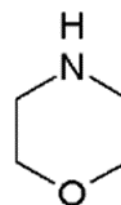
Dimethylsulfoxide

(DMSO)



N-methyl-2-pyrrolidinone

(NMP)



Morpholine

(MORP)

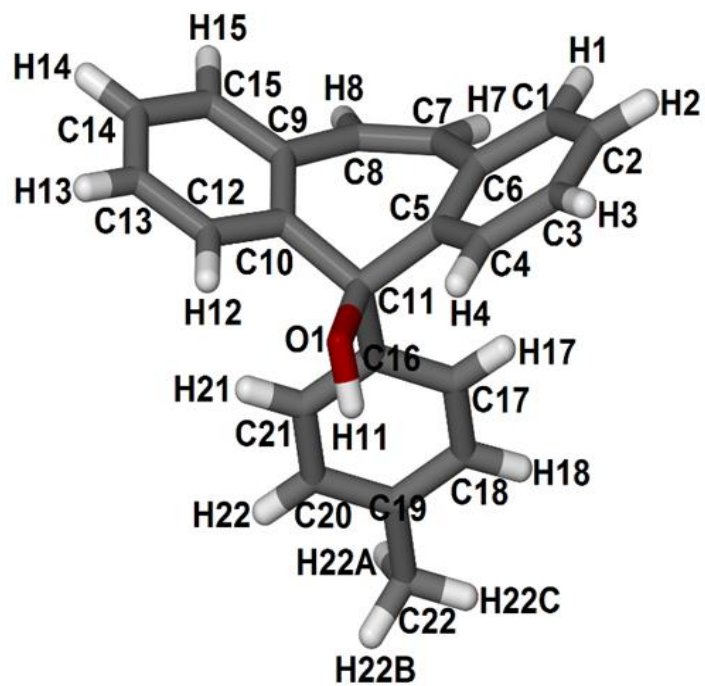


Figure 4.1: Numbering scheme of H2.

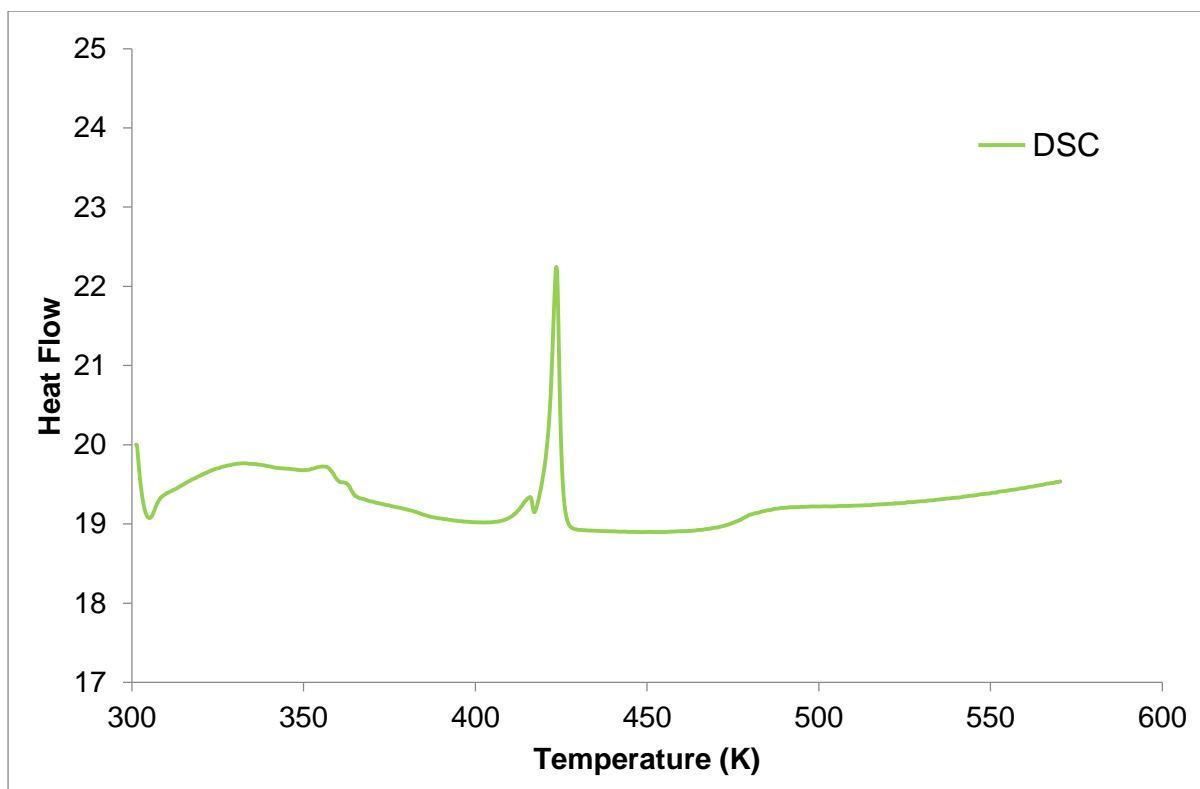


Figure 4.2: DSC curve of the host compound H2.

4.1 Inclusion compound of H2 and dimethylsulfoxide (H2•DMSO)

4.1.1: Thermal analysis

TGA was used to confirm the host: guest ratio of 1: 1 for the inclusion compound (Table 4.1). The TG and DSC curves for **H2•DMSO** are given in Figure 4.3. The DSC curve shows two peaks, which is due to the release of the guest, followed by the host melt. The broad endotherm at 303 K is due to the loss of surface solvent. Furthermore the TGA curve shows a single mass loss step of 20.0% which corresponds to the loss of one mole of **DMSO** (calc. 20.7%), confirming a host: guest ratio of 1:1.

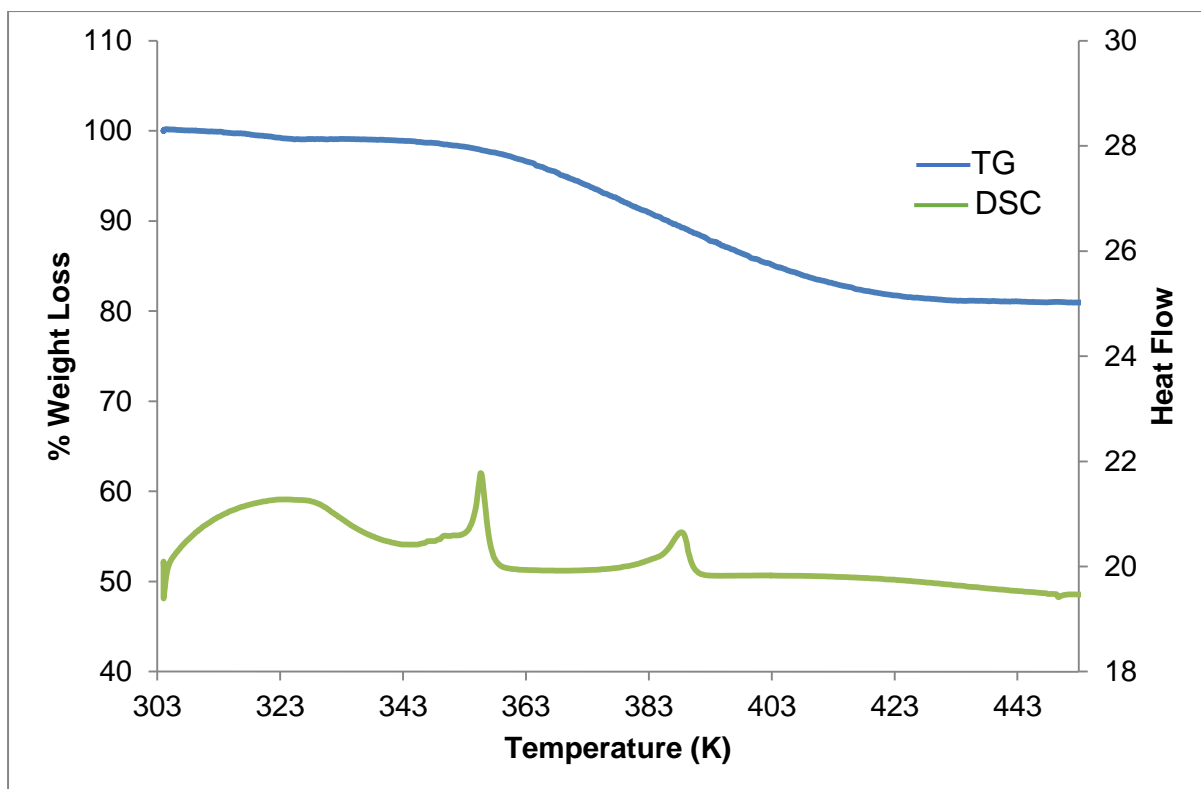


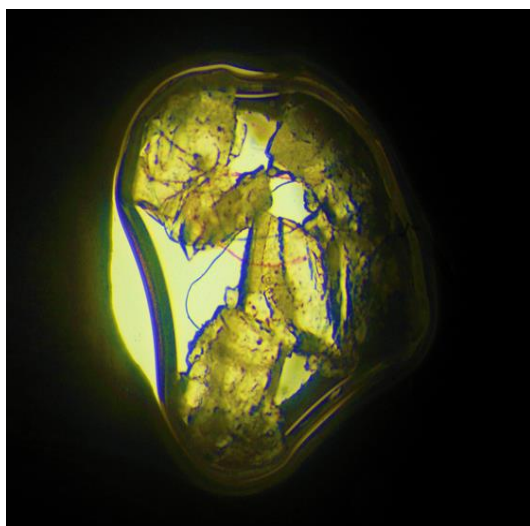
Figure 4.3: TG and DSC curves of H2•DMSO.

Table 4.1: Thermal analysis results of H2•DMSO.

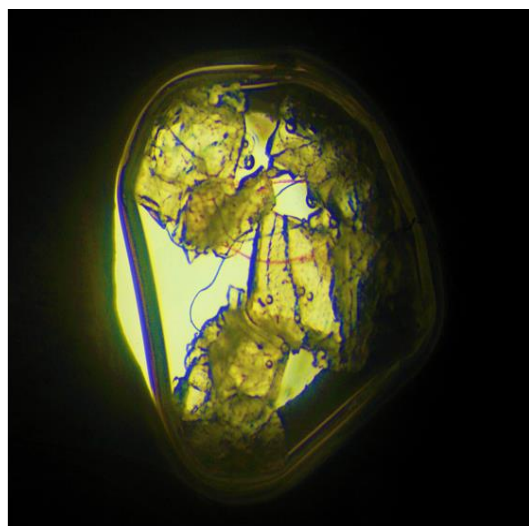
Boiling Point of DMSO (K)	462.2
Host-Guest ratio	1 : 1
TG calculated % weight loss	20.7
TG experiment	20.0
DSC Endotherm 1 T_{onset} (K)	363.7
DSC Endotherm 2 T_{onset} (K)	393.1

4.1.2 Hot stage microscopy

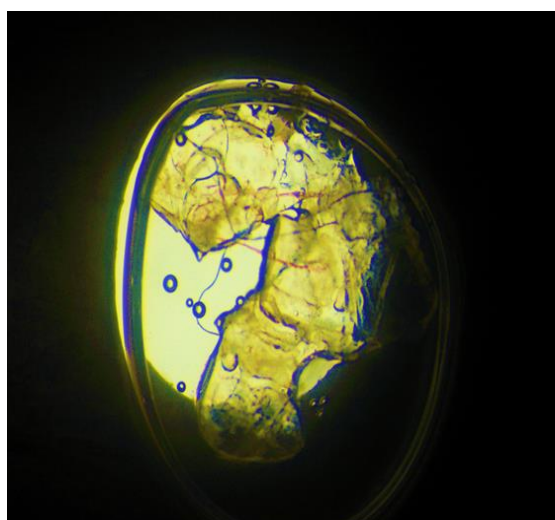
The crystals were immersed in silicone oil and were monitored over a temperature range starting at 300 K. The results are shown in Figure 4.4.



a



b



c



d

Figure 4.4: HSM photography of H₂•DMSO: (a) crystal immersed in silicone oil at 300 K, **(b)** bubbles starts to form at 388 K, **(c)** crystal starts to melt at 460 K, **(d)** crystal completely melts at 468 K.

4.1.3 IR spectroscopy

The IR spectrum of **H2•DMSO** (Figure 4.5) shows a broad peak at around 3225 cm^{-1} which is due to the hydrogen bonded OH present in the inclusion compound. The band at 1030-1049 cm^{-1} can be assigned to the S = O stretching vibration. The IR positions and assignments of peaks are given in Table 4.2.

Table 4.2: Positions and assignments of peaks in H2 and H2•DMSO.

H2	H2•DMSO	Proposed Assignment
3019	-	OH stretch
-	3225	Hydrogen bonded OH
2858	-	C-H Alkane stretch
1482, 1508, 1661	1482, 1509, 1662	Aromatic ring stretch
755, 772, 796, 804	751, 770, 795, 805, 887	C-H aromatic ring
-	1039, 1049	S = O stretch

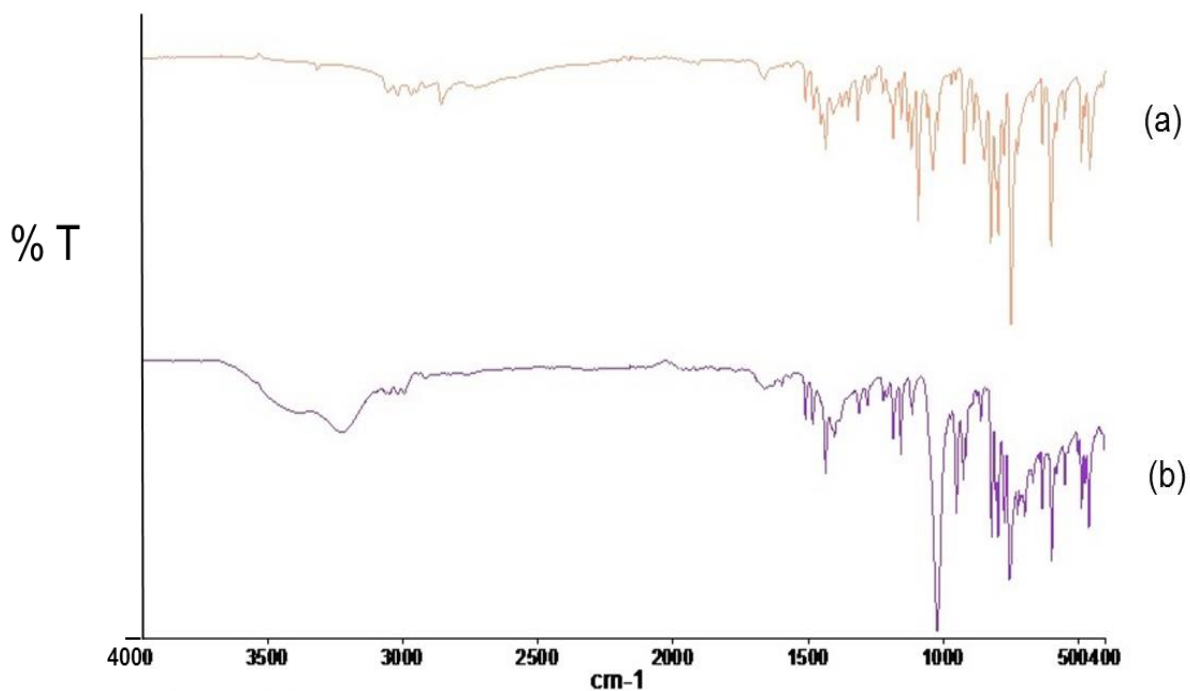


Figure 4.5: IR spectra of (a) H2 and (b) H2•DMSO.

4.1.4 Powder X-ray diffraction (PXRD)

A mixture of **H2** and **DMSO** was ground for 15 min and the resulting PXRD pattern of the ground product was compared to the calculated pattern of **H2•DMSO** obtained from LAZYPULVERIX.^[1] There is an overall agreement between the PXRD patterns of the ground product and that obtained from LAZYPULVERIX. This result proved that the **H2•DMSO** crystal was successfully prepared using the grinding experiment. PXRD patterns are shown in Figure 4.6.

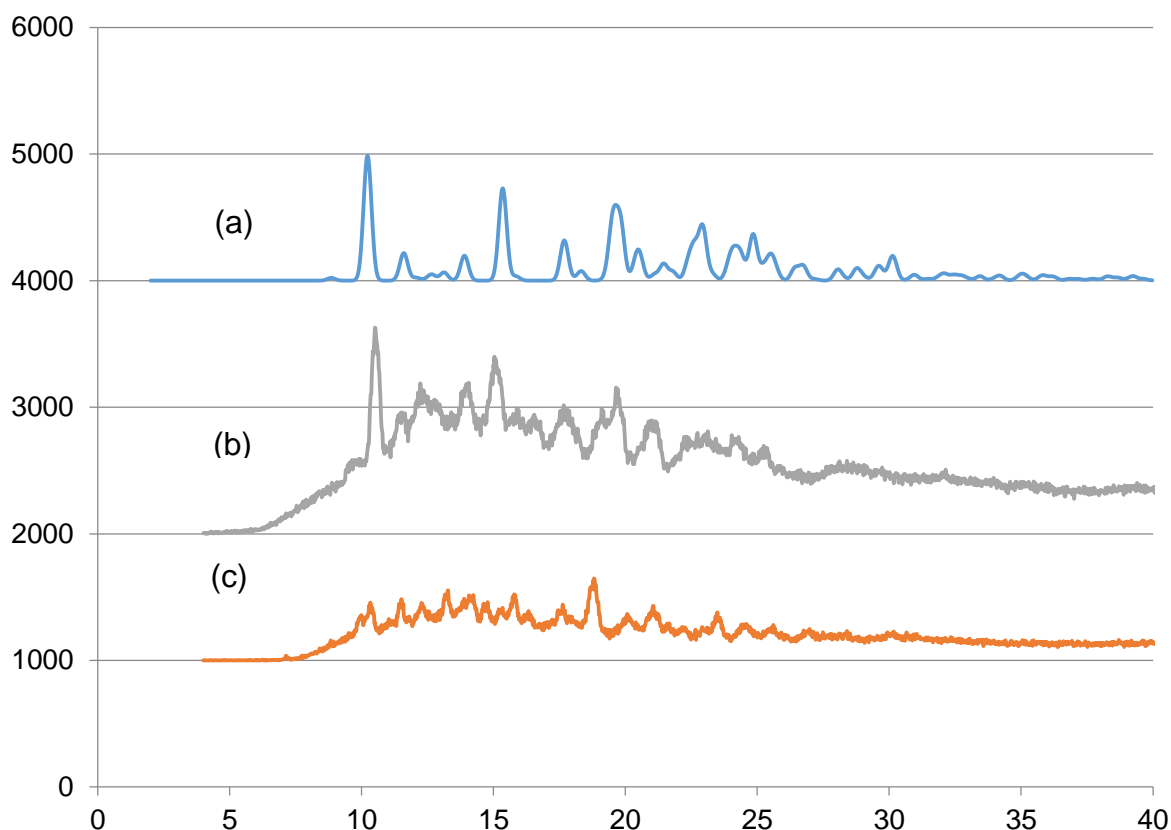


Figure 4.6: PXR D patterns of (a) H₂•DMSO calculated from LAZYPULVERIX, (b) ground product and (c) H₂.

4.1.5 Crystal structure analysis

The crystal structure of **H₂•DMSO** solved in the monoclinic space group $P2_1/n$ with one host molecule and one **DMSO** molecule in the asymmetric unit ($Z = 4$).^[2] Unit cell parameters were determined from intensity data measured on a Kappa CCD diffractometer.^[3] The structure was solved using direct methods and refined by full-matrix least squares with SHELX-97,^[4] refining on F^2 . Xseed^[5] was used as a graphical interface. All non-hydrogen atoms were found in the difference electron density map. All of the hydrogens except the OH hydrogen were placed with geometric constraints and allowed to refine isotropically. The structure refined to $R_1 = 0.0443$ and $wR_2 = 0.0997$. Crystal data and refinement parameters are summarised in Table 4.3 and the asymmetric unit of **H₂•DMSO** is shown in Figure 4.7.

Table 4.3: Crystal data of H2•DMSO.

Compound	H2•DMSO
Structural Formula	$C_{24}H_{24}O_2S$
M_w (g mol ⁻¹)	376.49
Temperature (K)	173(2)
Crystal system	Monoclinic
Space group	$P2_1/n$
a (Å)	9.4447(19)
b (Å)	17.289(4)
c (Å)	12.261(3)
α (°)	90.00
β (°)	92.42(3)
γ (°)	90.00
Volume (Å ³)	2000.3(7)
Z	4
μ (mm ⁻¹)	0.178
F(000)	800
Index ranges	h: ± 12 ; k: ± 22 ; l: ± 15
Goodness of fit, S	1.027
No. of reflections collected	46767
No. of unique reflections	4574
Calculated density (g cm ³)	1.250
Final R indices [$I > 2\sigma(I)$]	$R_1 = 0.0443$, $wR_2 = 0.0997$
R indices (all data)	$R_1 = 0.0785$, $wR_2 = 0.1157$
Largest difference peak and hole (e Å ⁻³)	0.201 and -0.327

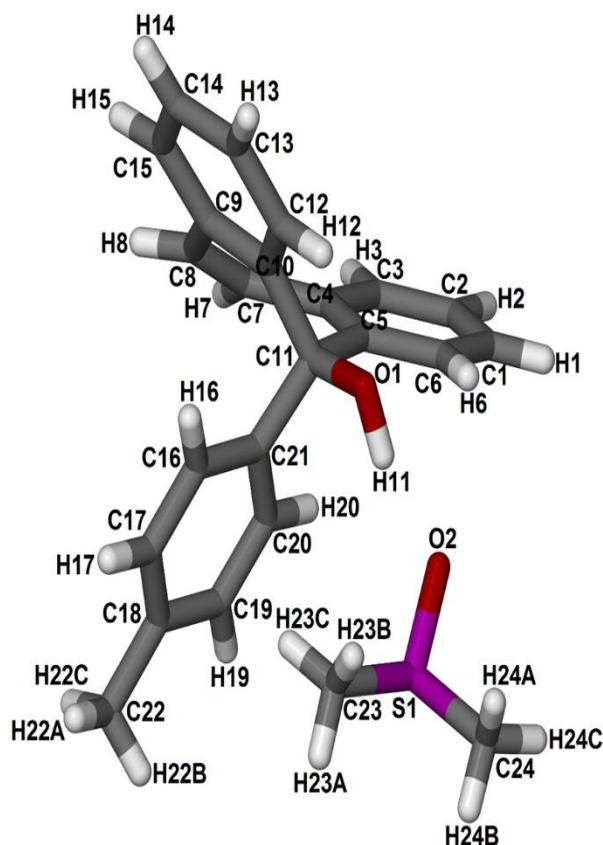


Figure 4.7: Asymmetric unit of H2•DMSO.

The structure of **H2•DMSO** is stabilised by (Host)–OH•••O–(Guest) hydrogen bonds. (Figure 4.8). The OH group of the host is hydrogen bonded to the oxygen atom of the **DMSO**. The hydrogen bond data are summarised in Table 4.4. Two of the **DMSO** C–H bonds are involved in C–H••• π interactions (Table 4.5) with neighbouring host aromatic rings (Figure 4.7); C23••• π (centroid): 3.696(1) Å, 154° and C24••• π (centroid): 3.666(1) Å, 150°. [6, 7]

Table 4.4: Hydrogen bonding details of H2•DMSO.

Donor (D)	Acceptor (A)	D•••A (Å)	D–H (Å)	H•••A (Å)	D–H•••A (°)
O1	O2	2.727(2)	0.97	1.78	165

Table 4.5: C–H··· π parameters of H2•DMSO.

C–H··· π	C··· π (Å)	H··· π (Å)	C–H– π (°)	Symmetry Operator
C23–H23C··· π	3.696(1)	2.79	154	x, y, z
C24–H24C··· π	3.666(1)	2.78	150	x, y, z

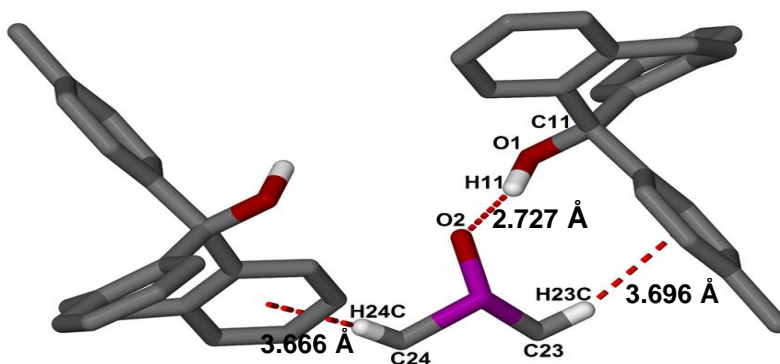


Figure 4.8: Hydrogen bonding and C–H··· π in H2•DMSO.

The packing diagram of **H2•DMSO** along [010] is shown in Figure 4.9. The **DMSO** guests lie in constricted channels along [010] shown in Figure 4.10. These constricted channels are effectively cavities as can be seen in Figure 4.11, generated using Mercury^[8] with a probe size of 1.2 Å

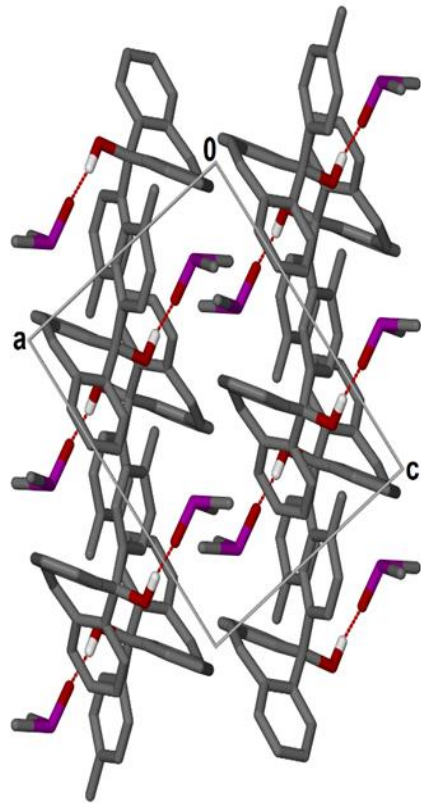


Figure 4.9: Packing diagram of H₂·DMSO viewed along [010].

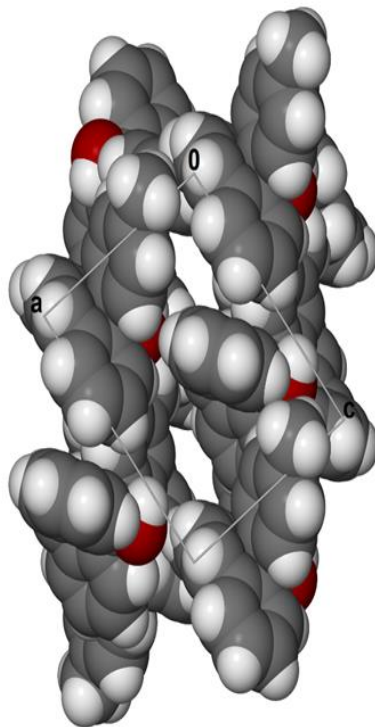


Figure 4.10: Space filling diagram along [010] with the DMSO guests omitted.

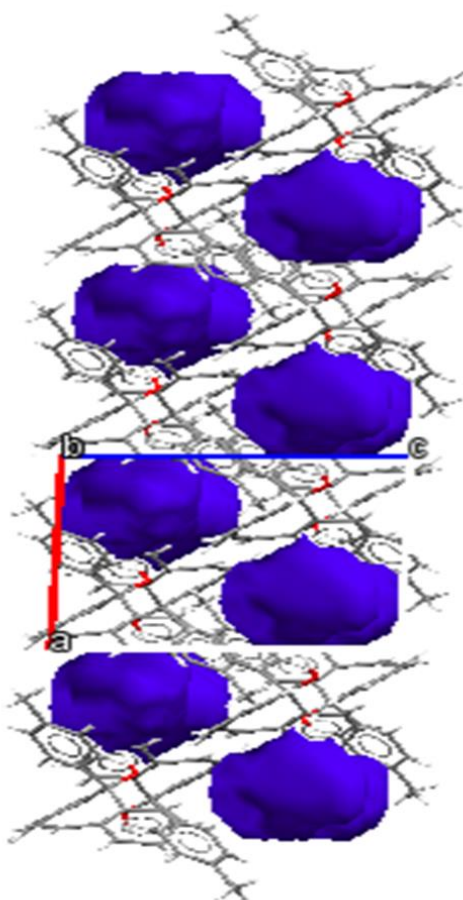


Figure 4.11: Voids (blue) occupied by DMSO guests in H2•DMSO.

4.2 Inclusion compound of H2 and *N*-methyl-2-pyrrolidinone (H2•NMP)

4.2.1: Thermal analysis

The TG curve for **H2•NMP** shows a single mass loss step which corresponds to the loss of the guest. One endotherm is observed in the DSC curve. This single endotherm is due to the melt of the host in the hot **NMP**. The TG and DSC curves are shown in Figure 4.12. A summary of the thermal data is shown in Table 4.6.

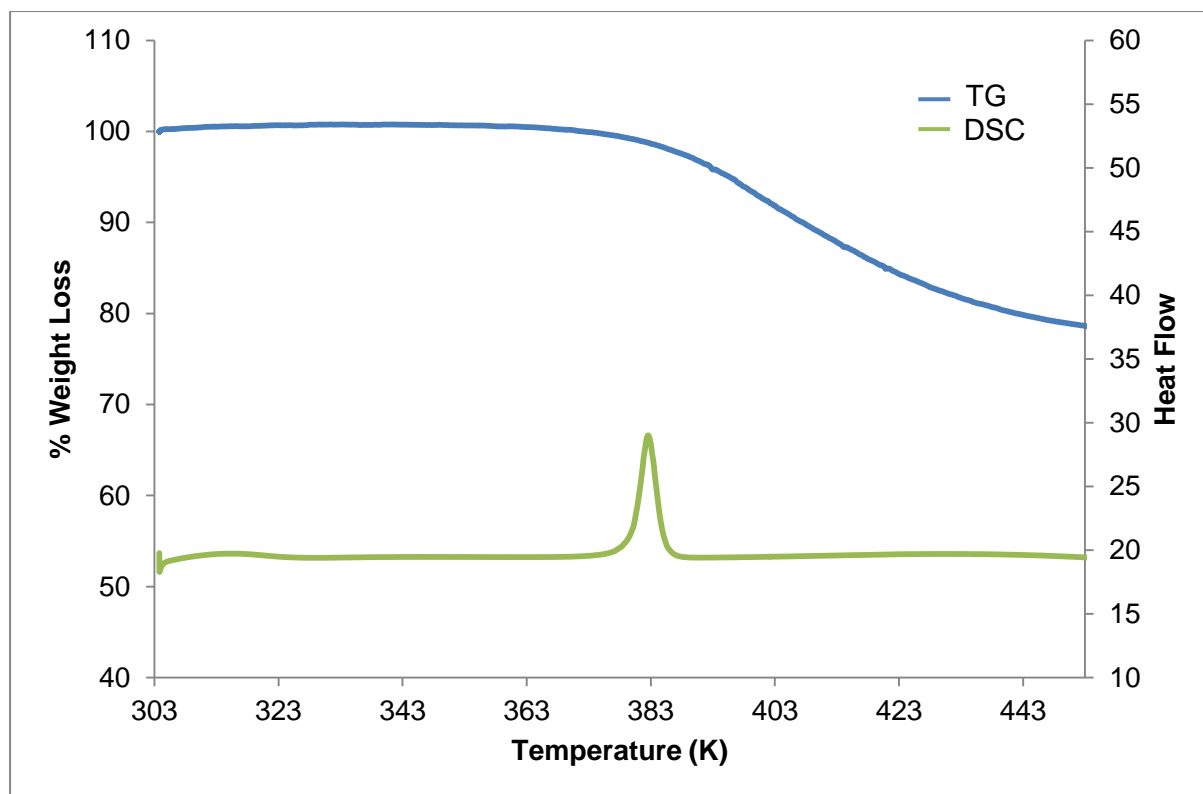


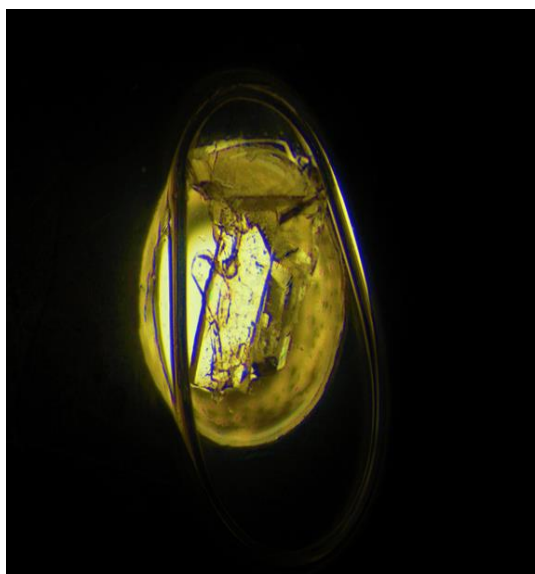
Figure 4.12: TG and DSC curves of H₂•NMP.

Table 4.6: Thermal analysis results of H₂•NMP.

Boiling Point of NMP (K)	475.0
Host-Guest ratio	1 : 1
TG calculated % weight loss	24.9
TG experiment % weight loss	24.2
DSC Endotherm 1 T_{onset} (K)	389.4

4.2.2 Hot stage microscopy (HSM)

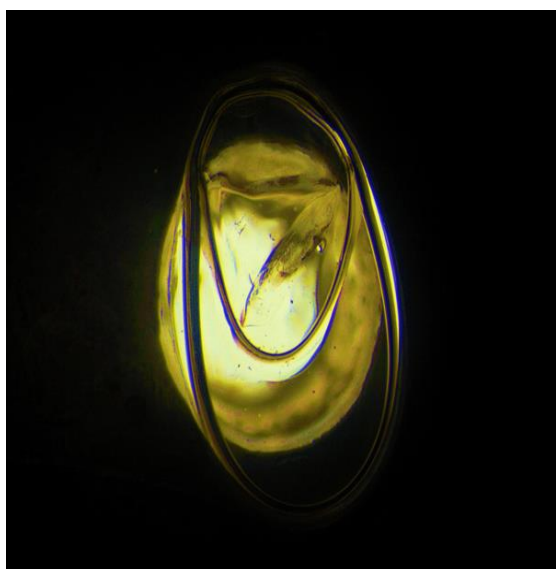
The crystals were placed between two cover slips and one drop of silicone oil was added. On a hot stage microscope, the crystals were observed over a temperature range starting at 299 K. The thermal decomposition is shown in Figure 4.13.



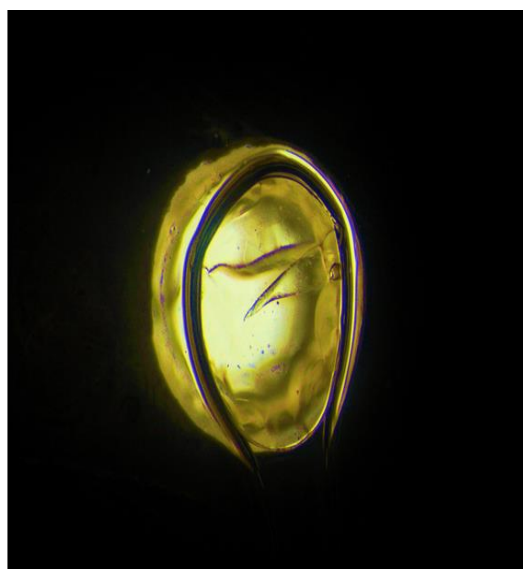
a



b



c



d

Figure 4.13: HSM photography of H1•NMP: (a) crystal immersed in silicone oil at 299 K, **(b)** crystal starts melting at 359 K, **(c)** melting of the crystal at 373 K, **(d)** crystal completely melts at 392 K.

4.2.3 IR spectroscopy

The IR spectrum of **H2•NMP** shown in Figure 4.14 contains a broad peak at around 3245 cm^{-1} which does not appear in the spectrum of **H2**. This broad peak is due to the hydrogen bonded OH present in the inclusion compound, which shows the formation of a new compound. This peak is observed at a higher frequency than the OH stretch present in the IR spectrum of **H2** (3019 cm^{-1}). Both spectra contain peaks at 2858 cm^{-1} (**H2**) and at 2870 cm^{-1} (**H2•NMP**) which can be assigned to the alkane (CH_3) present in **H2** and in the inclusion compound. IR positions and the assignment of peaks are given in Table 4.7.

Table 4.7: Positions and assignments of peaks of H2 and H2•NMP.

H2	H2•NMP	Proposed Assignment
3019	-	OH stretch
-	3245	Hydrogen bonded OH
2858	2870	C-H Alkane stretch
-	1656	C = O stretch
1482, 1508, 1661	1479, 1505	Aromatic ring stretch
755, 772, 796, 804	752, 772, 795, 824	C-H aromatic ring

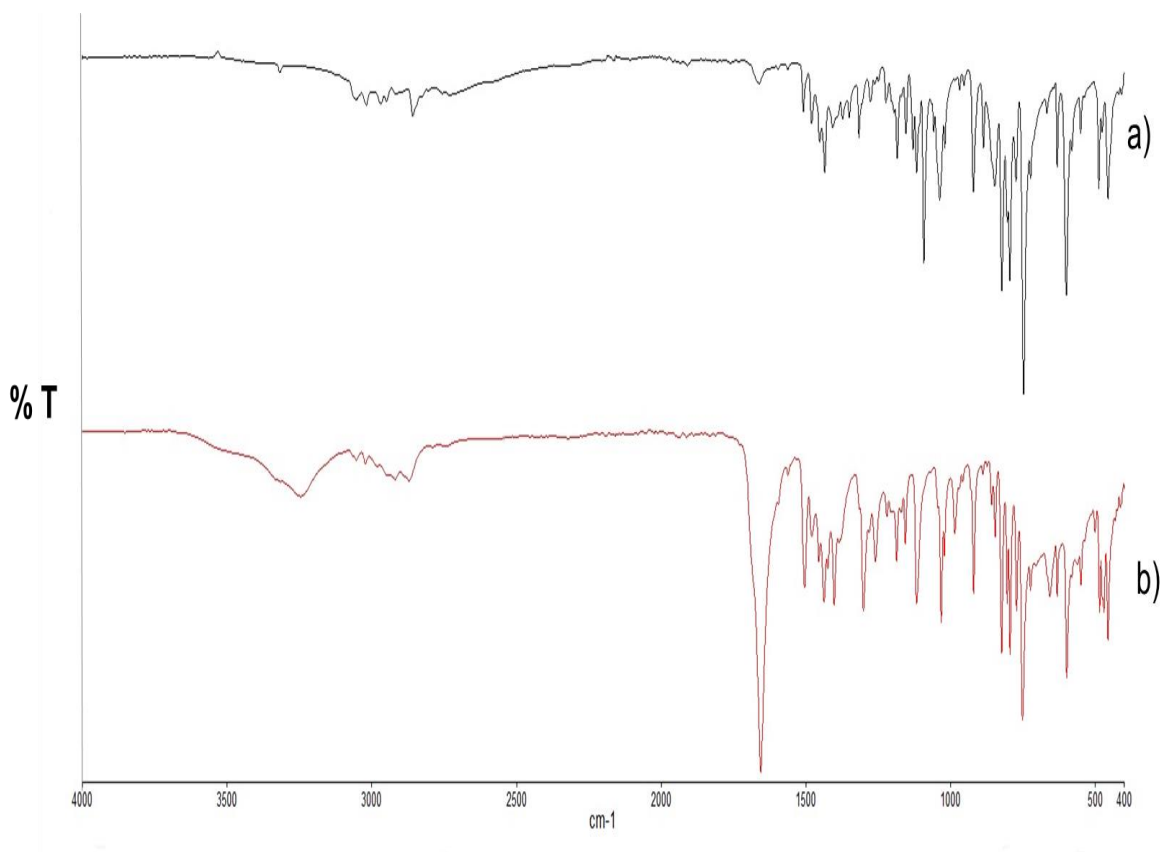


Figure 4.14: IR spectra of (a) H2 and (b) H2•NMP.

4.2.4 Powder X-ray diffraction (PXRD)

A mixture of **H2** and **NMP** was ground for 15 min. The resultant PXRD pattern of the ground product was collected and compared to the PXRD pattern of **H2•NMP** calculated from LAZYPULVERIX. ^[1] There is overall agreement between the PXRD pattern of **H2•NMP** calculated from LAZYPULVERIX and the ground product. (Figure 4.15).

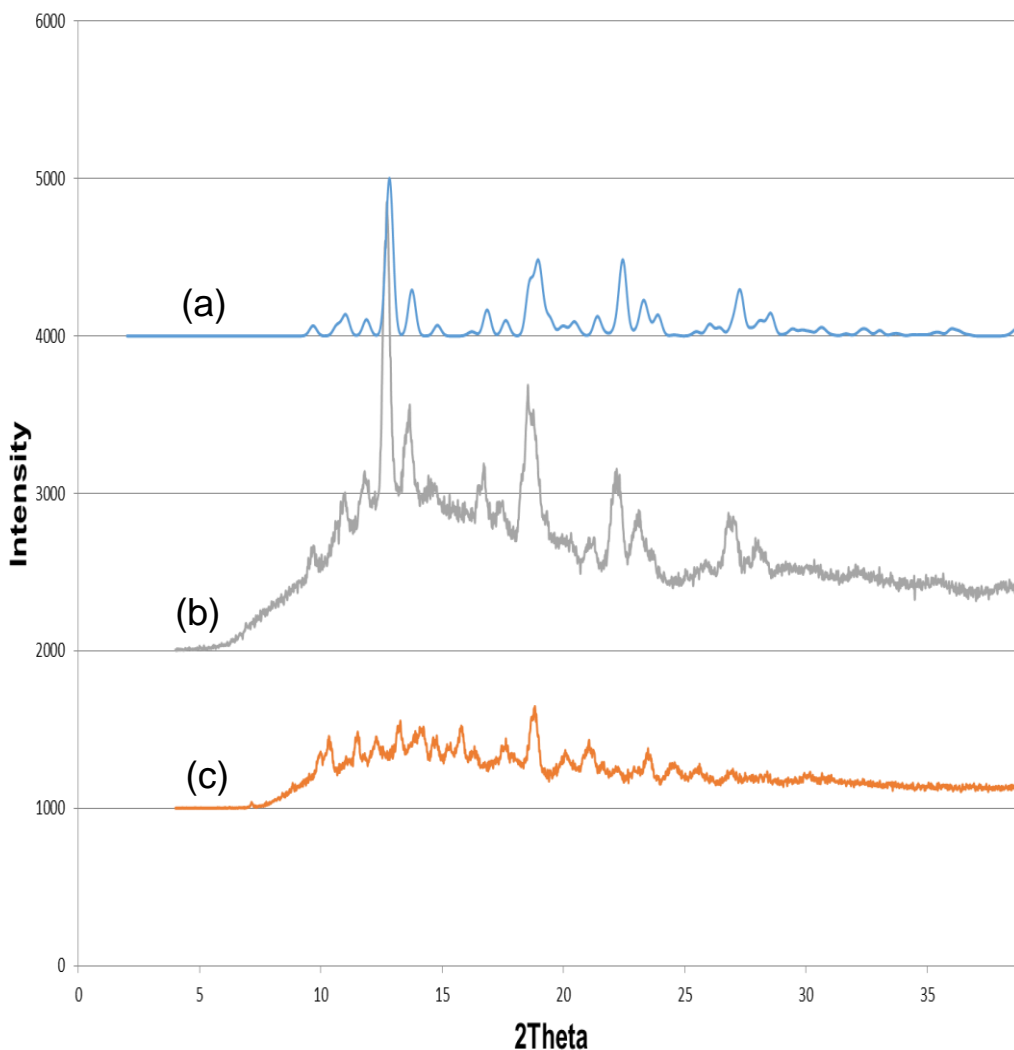


Figure 4.15: PXRD patterns of (a) H₂•NMP calculated from LAZYPULVERIX, (b) ground product and (c) H₂.

4.2.5 Crystal structure analysis

H₂•NMP crystallised in the monoclinic space group $P2_1/n$, with one host molecule and one **NMP** molecule in the asymmetric unit. The crystal structure was solved using direct methods and was refined by full-matrix least squares with SHELX-97,^[4] refining on F^2 . The structure refined with $R_1 = 0.0493$ and $wR_2 = 0.1256$. Crystal data and refinement parameters are summarised below in Table 4.8. All non-hydrogen atoms were found in the difference electron density map. All of the hydrogens except the OH and NH hydrogens were placed with geometric constraints and allowed to refine isotropically. The asymmetric unit is shown below in Figure 4.16.

Table 4.8: Crystal data of H2•NMP.

Compound	H2•NMP
Structural Formula	$C_{27}H_{27}NO_2$
M_w (g mol ⁻¹)	397.50
Temperature (K)	173(2)
Crystal system	Monoclinic
Space group	$P2_1/n$
a (Å)	10.322(2)
b (Å)	12.873(3)
c (Å)	16.444(3)
α (°)	90.00
β (°)	95.97(3)
γ (°)	90.00
Volume (Å ³)	2173(8)
Z	4
μ (mm ⁻¹)	0.076
F(000)	848
Index ranges	h: ± 13 ; k: ± 17 ; l: ± 21
Goodness of fit, S	1.039
No. of reflections collected	19128
No. of unique reflections	5373
Calculated density (g cm ⁻³)	1.215
Final R indices [$I > 2\sigma(I)$]	$R_1 = 0.0493$, $wR_2 = 0.1256$
R indices (all data)	$R_1 = 0.0675$, $wR_2 = 0.1373$
Largest difference peak and hole (e Å ⁻³)	0.396 and -0.228

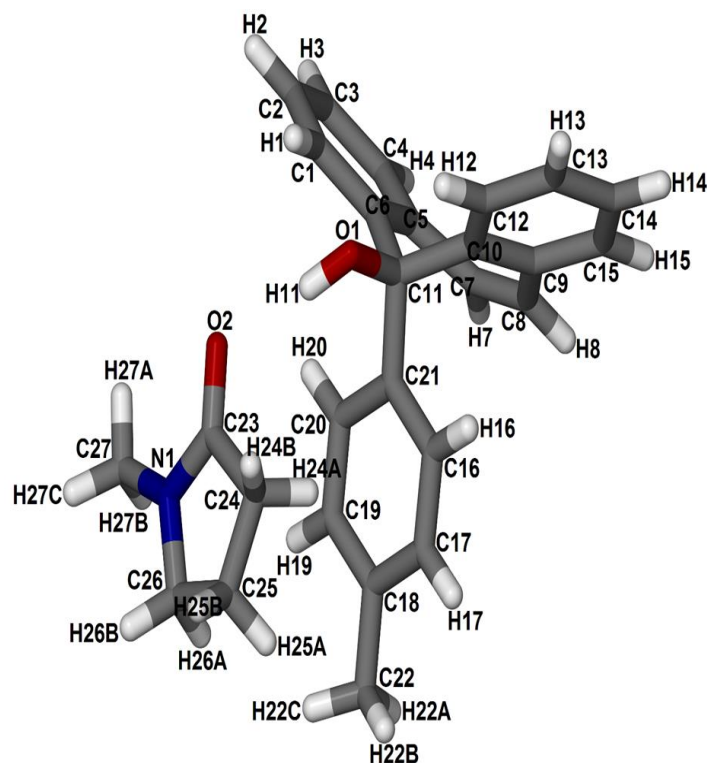


Figure 4.16: Asymmetric unit of **H2•NMP**.

The crystal structure of **H2•NMP** is stabilised via (Host)–OH–(Guest) hydrogen bonds. (Figure 4.17). The hydroxyl group of the host is hydrogen bonded to the oxygen of the **NMP**. The shortest interaction for **H2•NMP** between ring centroids, 3.735 (1) Å, occurs between the *p*-tolyl moiety of the host and the five membered ring of the guest. Thus the **NMP** guests interact with the host aromatic system via C–H••• π contacts: C24••• π (centroid): 3.499(1) Å, 135°; C25••• π (centroid): 3.584(1) Å, 121° and C26••• π (centroid): 3.462(1) Å, 130° (Figure 4.17).

Table 4.9: Hydrogen bonding details of **H2•NMP**.

Donor (D)–H	Acceptor (A)	D•••A (Å)	D–H (Å)	H•••A(Å)	D–H•••A (°)
O1	O2	2.782 (2)	0.89	1.90	171

Table 4.10: C–H... π parameters of H2•NMP.

C–H... π	C... π (Å)	H... π (Å)	C–H– π (°)	Symmetry Operator
C24–H24A... π	3.499(1)	2.73	135	x, y, z
C25–H25B... π	3.584(1)	2.97	121	-1 + x, y, z
C26–H26B... π	3.462(1)	2.74	130	-1+ x, y, z

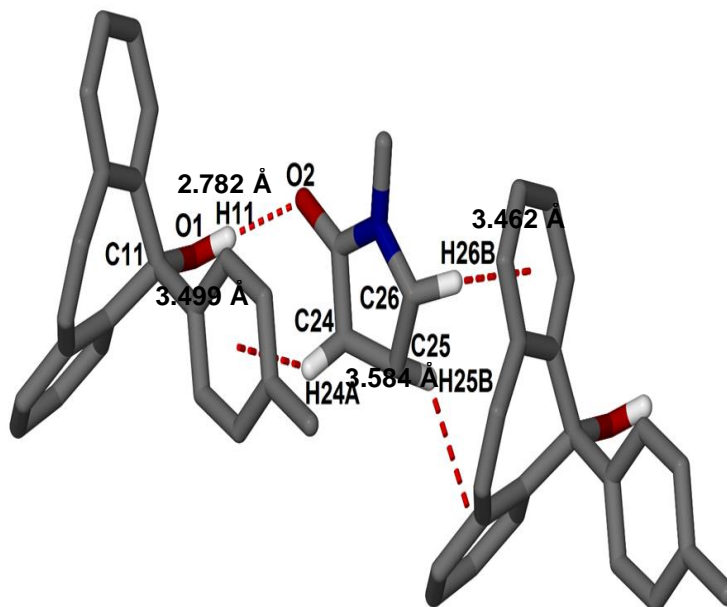


Figure 4.17: Hydrogen bonding and C–H... π interactions in H2•NMP.

The packing diagram of **H2•NMP** along [010] is shown in Figure 4.18. The **NMP** guests are located in cavities down [010] Figure 4.19.

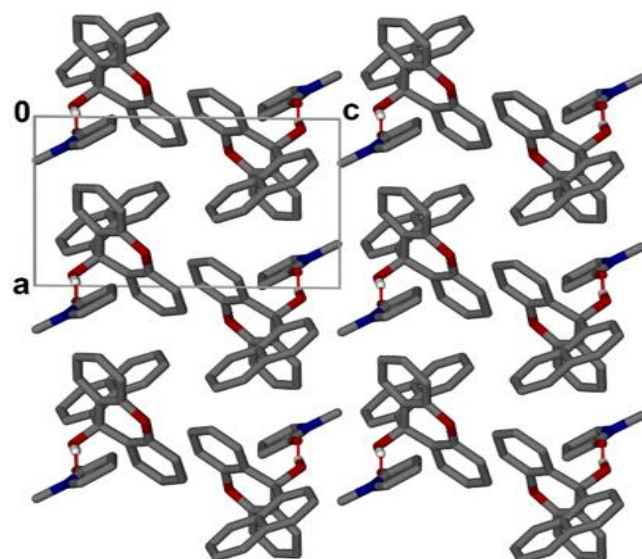


Figure 4.18: Packing diagram of H₂•NMP viewed along [010].

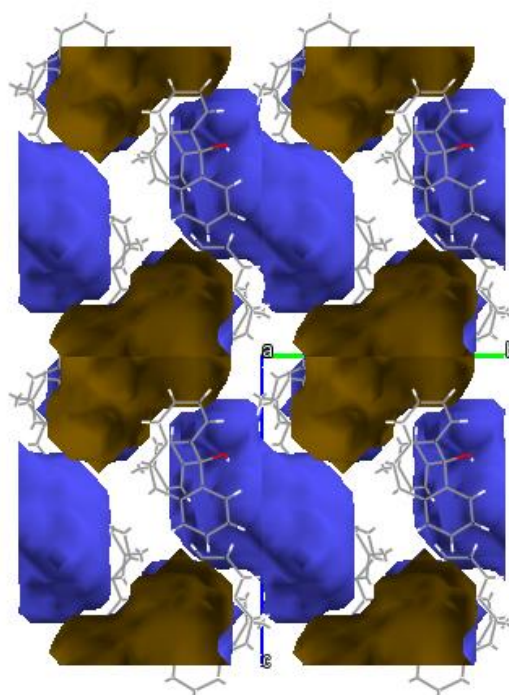


Figure 4.19: Cavities in which the NMP guests are located.

4.3 Inclusion compound of H₂ and morpholine (H₂•MORP)

4.3.1 Thermal analysis

The TG and DSC curves for **H₂•MORP** are shown below in Figure 4.20. The TG shows a single mass loss step of 21.0% (calc. 22.6 %). The DSC exhibits a single endotherm due to the host melt in the hot **MORP**. Table 4.11 summarises the thermal data.

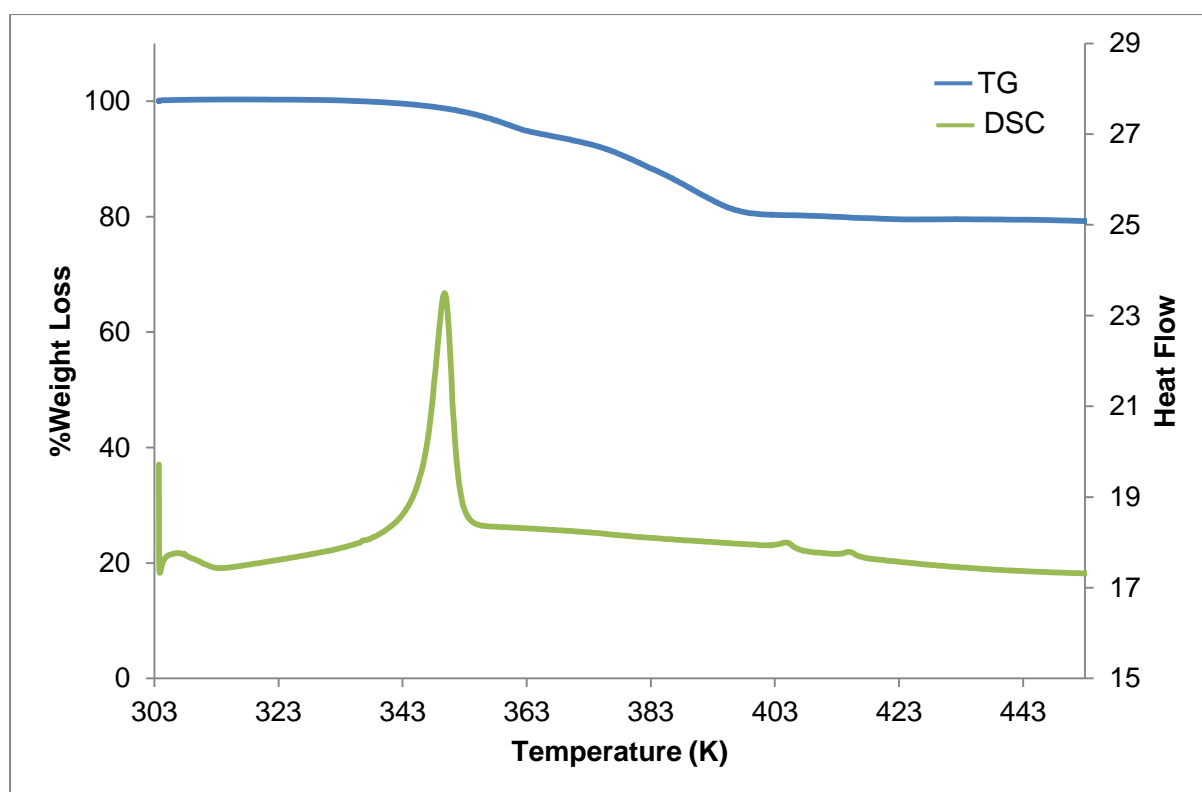


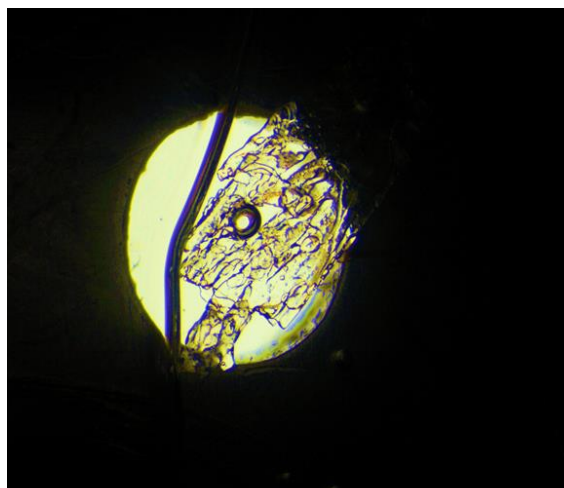
Figure 4.20: TG and DSC curves of H₂•MORP.

Table 4.11: Thermal analysis results of H₂•MORP.

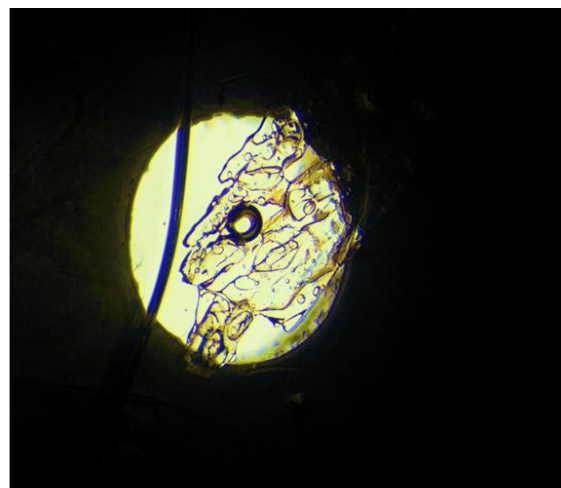
Boiling Point of MORP (K)	401.2
Host-Guest ratio	1 : 1
TG calculated % weight loss	22.6
TG experimental % weight loss	21.0
DSC Endotherm1 T _{onset} (K)	355.7

4.3.2 Hot stage microscopy

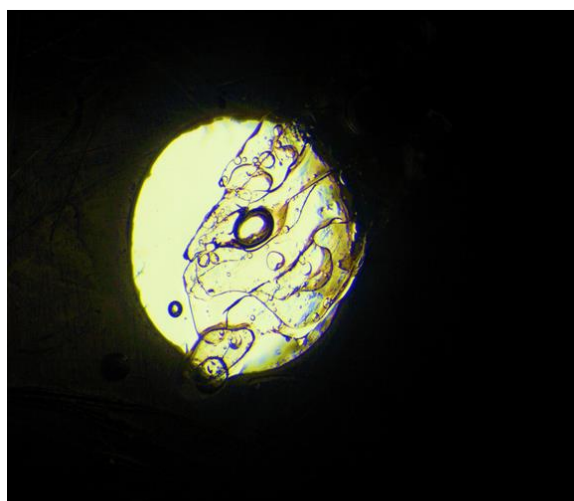
The crystals immersed in silicone oil were placed on a hot stage microscope and observed over a temperature range starting at 303 K.



a



b



c



d

Figure 4.21: HSM photography of H₂•MORP: (a) crystal immersed in silicone oil at 303 K, (b) bubbles form and crystal starts melting at 394 K, (c) crystal continues to melt at 462 K, (d) crystal completely melts at 478.

4.3.3 IR spectroscopy

The IR spectra of **H2** and **H2•MORP** are shown in Figure 4.22. IR positions and the assignments of peaks are given in Table 4.12. The peak at 2857 cm^{-1} in the spectrum of **H2•MORP** is due to the hydrogen bonded OH present in the inclusion compound. This peak indicates the formation of a new compound.

Table 4.12: Positions and assignments of peaks in H2 and H2•MORP.

H2	H2•MORP	Proposed Assignment
3019	-	OH stretch
-	2858, 2966	Hydrogen bonded OH
2858	-	C-H Alkane stretch
1482, 1508, 1661	1509	Aromatic ring stretch
755, 772, 796,804	773, 847, 823, 886	C-H aromatic ring

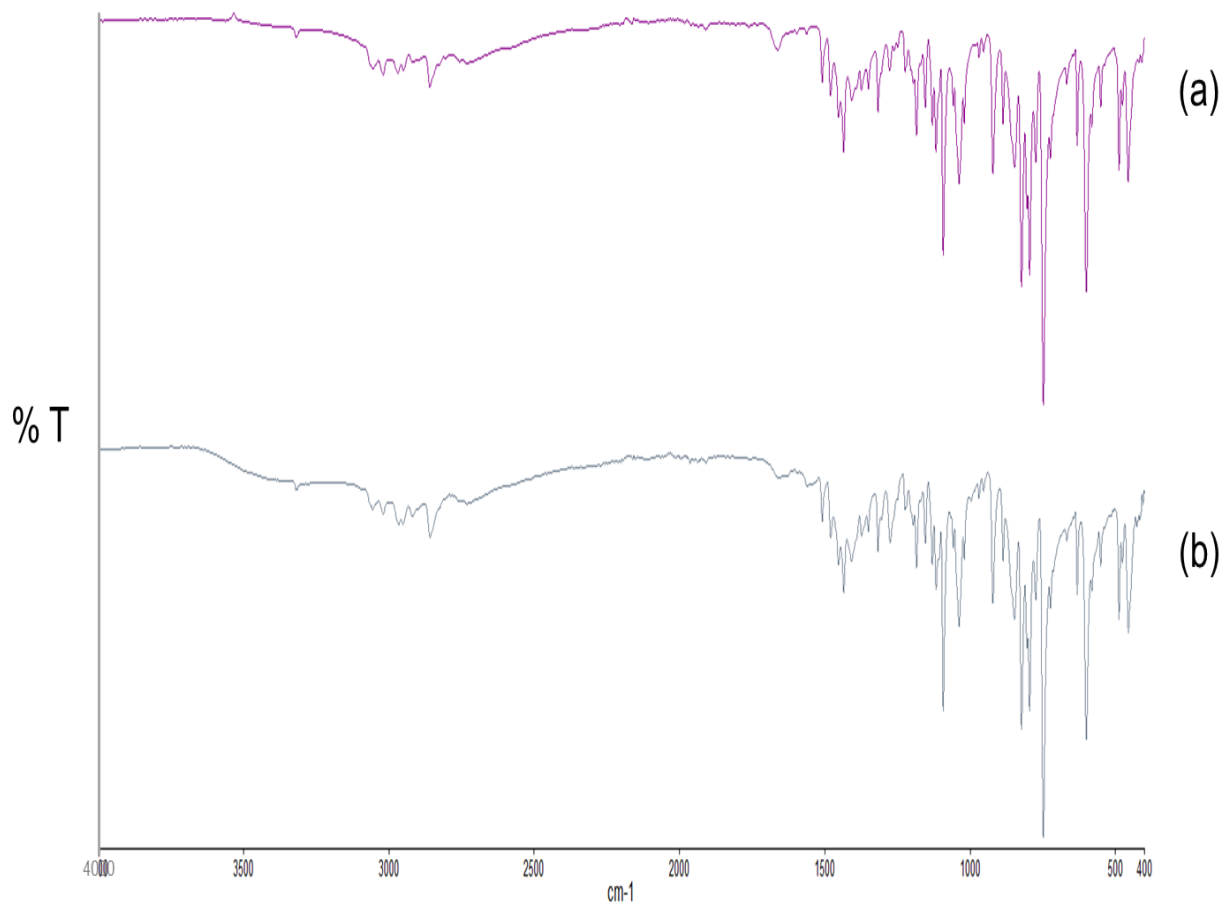


Figure 4.22: IR spectra of (a) H2 and (b) H2•MORP.

4.3.4 Powder X-ray diffraction (PXRD)

A mixture of **H2** and **MORP** was ground for 15 min and the resulting PXRD pattern of the ground product showed overall agreement with the calculated PXRD pattern obtained from LAZYPULVERIX. ^[1] PXRD patterns of **H2•MORP** calculated from LAZYPULVERIX, the ground product and **H2** are shown in Figure 4.23.

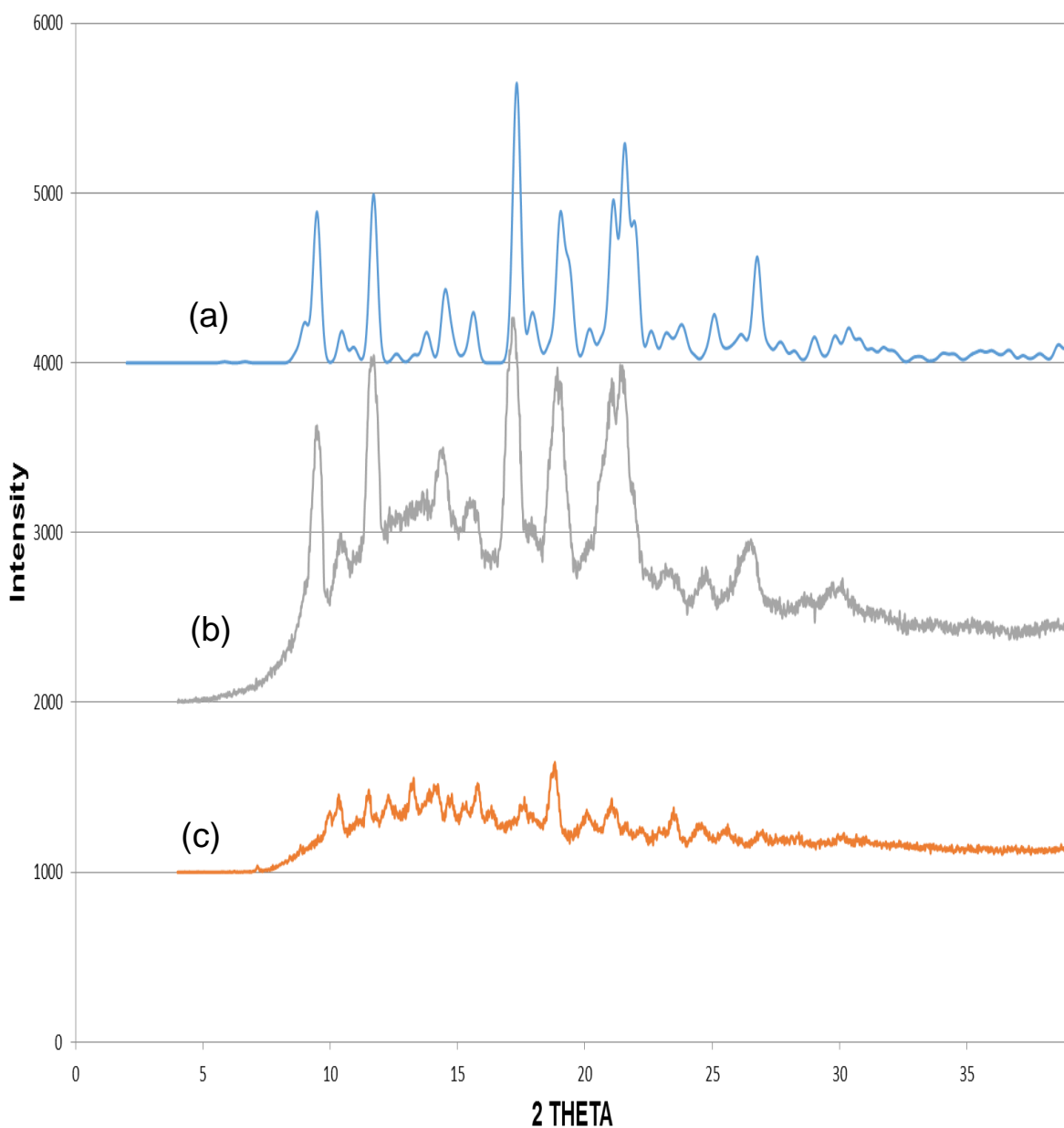


Figure 4.23: PXR D patterns of (a) H₂•MORP calculated from LAZYPULVERIX, (b) ground product and (c) H₂.

4.3.5 Crystal structure analysis

The crystal structure of **H₂•MORP** was solved in the triclinic space group *P*1 with two host molecules and two **MORP** molecules in the asymmetric unit (*Z* = 4). One of the morpholine guests is disordered and refined with site occupancy factors of 0.811 and 0.199 respectively. All the hydrogens except the NH hydrogens were geometrically constrained. The structure

refined with $R_1 = 0.0621$ and $wR_2 = 0.1519$. The asymmetric unit is shown in Figure 4.24. Crystal data and refinement parameters are summarised in Table 4.13.

Table 4.13: Crystal data of H2•MORP.

Compound	H2•MORP
Molecular Formula	$C_{26}H_{27}NO_2$
M_w (g mol ⁻¹)	385.59
Temperature (K)	173(2)
Crystal system	Triclinic
Space group	$P\bar{1}$
a (Å)	10.353(2)
b (Å)	13.924(3)
c (Å)	15.182(3)
α (°)	86.51(3)
β (°)	86.38(3)
γ (°)	73.07(3)
Volume (Å ³)	2087.5(7)
Z	4
μ (mm ⁻¹)	0.077
F(000)	824
Index ranges	h: ± 13 ; k: -16, 18; l: -10, 20
Goodness of fit, S	1.035
No. of reflections collected	24,831
No. of unique reflections	10,391
D_{calc} (g cm ⁻³)	1.227
Final R indices [$I > 2\sigma(I)$]	$R_1 = 0.0626$, $wR_2 = 0.1552$
R indices (all data)	$R_1 = 0.1003$, $wR_2 = 0.1742$
Largest difference peak and hole (e Å ⁻³)	0.299 and -0.275

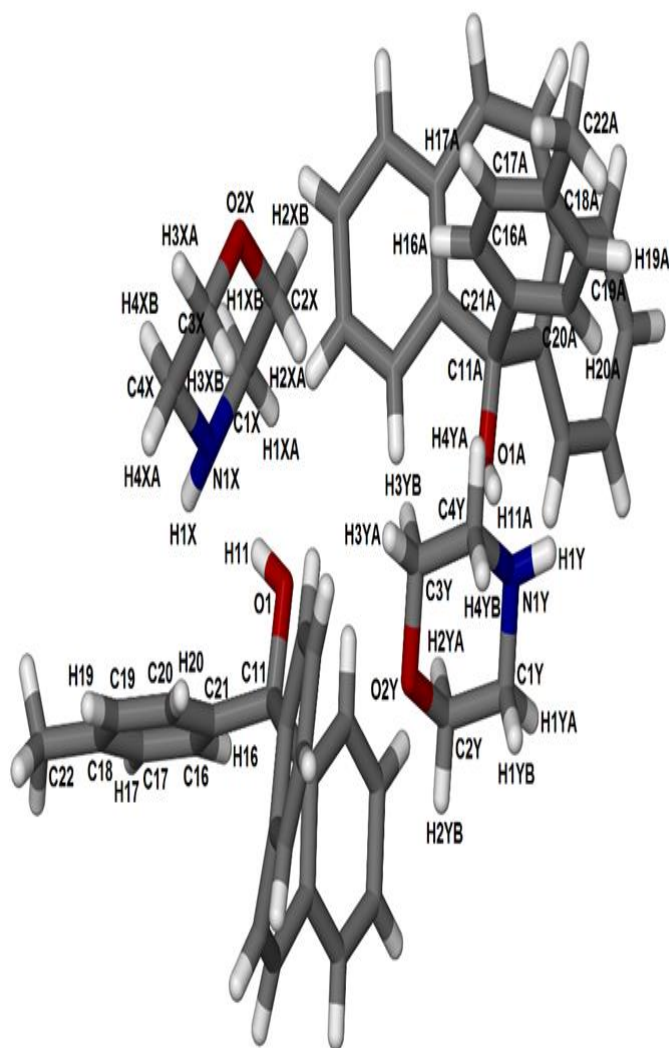


Figure 4.24: Asymmetric unit of H2·MORP, only the major component of the disordered guest is shown for clarity.

Each host molecule is hydrogen bonded to a morpholine molecule via (Host)–OH•••N (**MORP**) hydrogen bonds (Figure 4.25). Again there are C–H••• π contacts between the **MORP** molecules and the extensive host π network; C1X••• π (centroid): 3.636 Å, 152.7°; C4X••• π (centroid): 3.997 Å, 125.3°; C1Y••• π (centroid): 3.806 Å, 139.8° (Figure 4.26, the latter interaction is not indicated on the diagram because it involves the minor component of the disordered morpholine). The nitrogen atoms of the two morpholine guests are involved in very weak N–H••• π interactions with N1Y–H1Y directed towards the C7Y–C8Y double bond (3.720 Å, 144.1°) and N1X••• π : 3.994 Å, 126.6°. The ether oxygen of the morpholine is not involved in hydrogen bonding, this behaviour was also observed for inclusion compounds of morpholine with xanthenol hosts. ^[8]

Table 4.14: Hydrogen bonding details of **H2•MORP**.

Donor (D)–H	Acceptor (A)	D···A (Å)	D–H (Å)	H···A (Å)	D–H···A(°)
O1	N1X	2.745 (3)	0.75	2.01	167.9
O1A	N1Y	2.774(1)	0.84	1.95	164.5

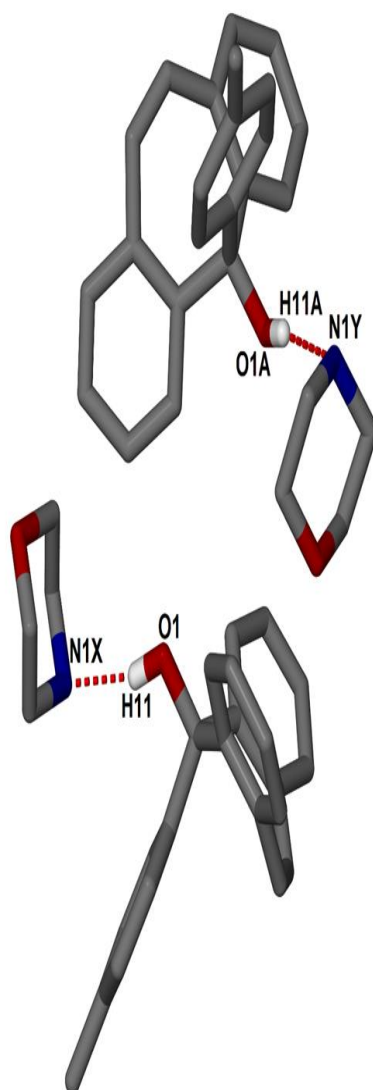


Figure 4.25: Hydrogen bonding in **H2•MORP**.

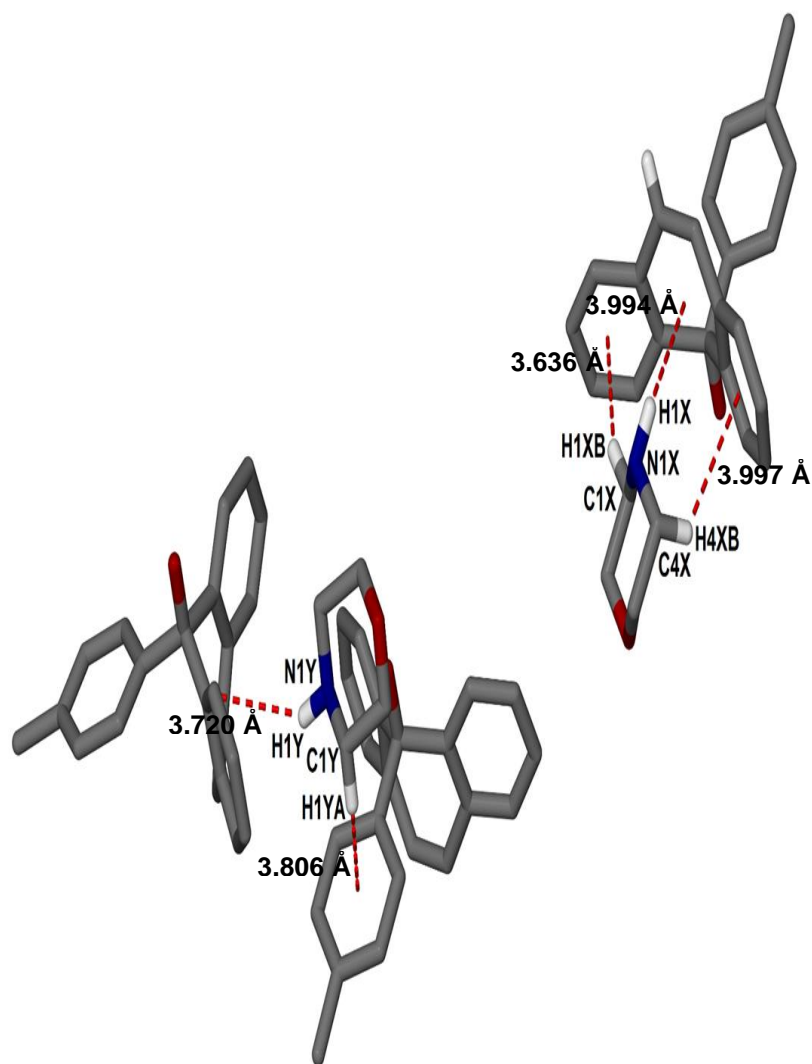


Figure 4.26: C/N-H... π (centroid) interactions in H2•MORP (only the interactions involving the major component of the disordered MORP guest are shown for clarity).

Two S-shape columns of host molecules are interleaved between two columns of **MORP** molecules, Figure 4.27 with **MORP** molecules occupying interconnected channels along [100] and [010], Figure 4.28 and Figure 4.29.

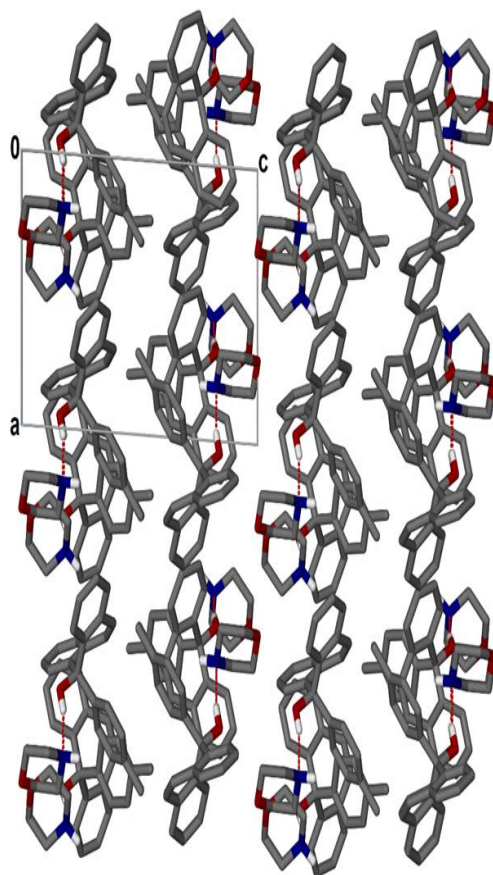


Figure 4.27: Packing diagram along [010], only the major component of the disordered MORP guest is shown for clarity.

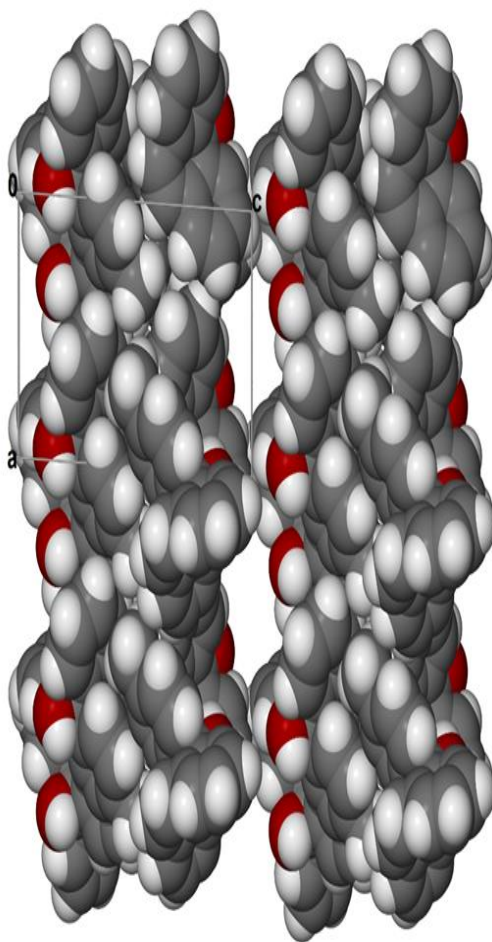


Figure 4.28: Space filling diagram along [010] with the MORP guests omitted.

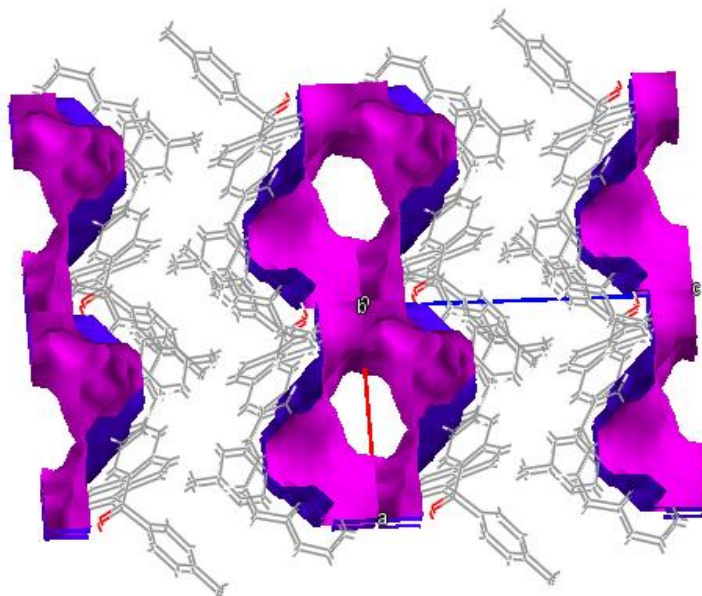


Figure 4.29: Channels in which the MORP guests are located.

4.4 Crystal structure analysis of the apohost H2

In an attempt to prepare the acetone inclusion compound by slow evaporation of a solution of the host in acetone, an unsolvated form of the host crystallised. An apohost structure (**H2**) was solved successfully in $P\bar{1}$ with two host molecules in the asymmetric unit ($Z = 4$), Figure 4.30.

Table 4.15: Crystal data and refinement parameters of H2.

Compound	H2
Molecular Formula	$C_{22}H_{18}O$
M_w (g mol ⁻¹)	298.36
Data collection temp (K)	173(2)
Crystal system	Triclinic
Space group	$P\bar{1}$
a (Å)	9.4207(19)
b (Å)	11.573(2)
c (Å)	16.075(3)
α (Å)	85.67(3)
β (Å)	79.73(3)
γ (Å)	67.49(3)
Volume (Å ³)	1593.1(6)
Z	4
μ (mm ⁻¹)	0.075
F(000)	632
No. of reflections collected	36592
No. of unique reflections	7277
D_c , (g cm ⁻³)	1.244
Index ranges	h: 0, 12; k: -13, 15; l: ± 20
Goodness of fit, S	1.028
Final R indices [$I > 2\sigma(I)$]	$R_1 = 0.0430$, $wR_2 = 0.1007$
R indices (all data)	$R_1 = 0.0576$, $wR_2 = 0.1104$
Largest peak and hole (eÅ ⁻³)	0.290 and -0.223

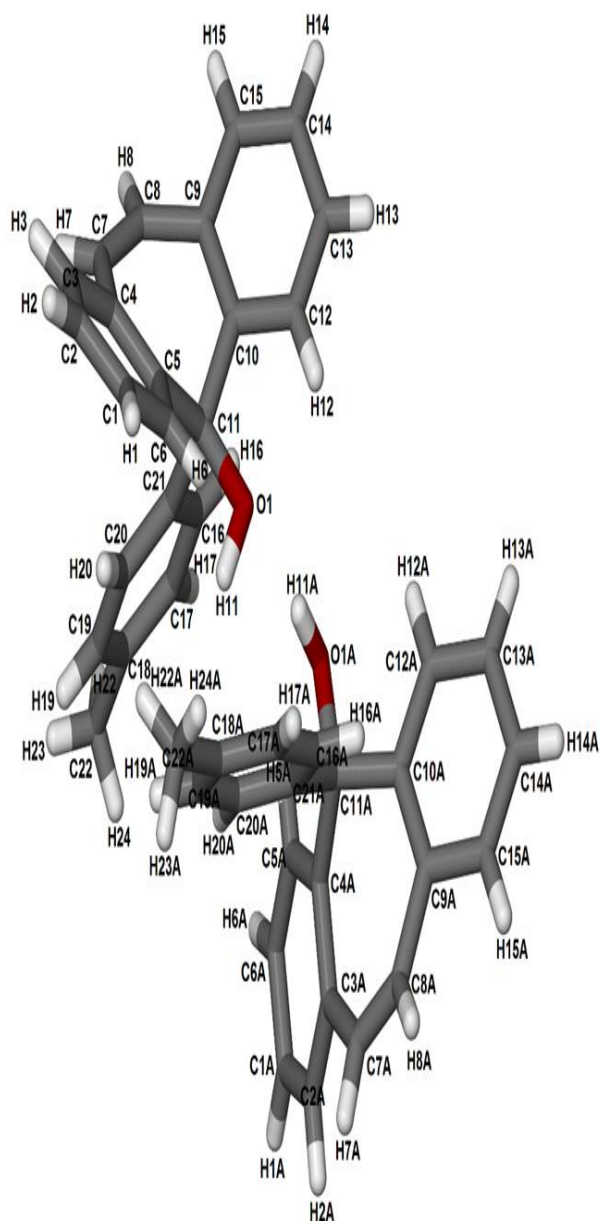


Figure 4.30: Asymmetric unit of H2.

The host molecules are linked via (Host)–OH•••O(Host) hydrogen bonds (Figure 4.31) and show a similar anti-parallel arrangement as observed for the structure of the related host 5-(4-methoxyphenyl)-5*H*-dibenzo[*a,d*]cyclohepten-5-ol.^[9] Short C–H••• π contacts are prevalent (Figure 4.32); C17••• π (centroid): 3.727(1) Å, 139°; C22••• π (centroid): 3.672(1) Å, 141° and C22A••• π (centroid): 3.735(1) Å, 159° as well as an O–H••• π interaction, O1••• π (centroid): 3,244 Å, 131°.

Table 4.16: Hydrogen bonding details of H2.

Donor (D)–H	Acceptor (A)	D···A (Å)	D–H (Å)	H···A (Å)	D–H···A (°)
O1A	O1	2.866(2)	0.91	1.96	172

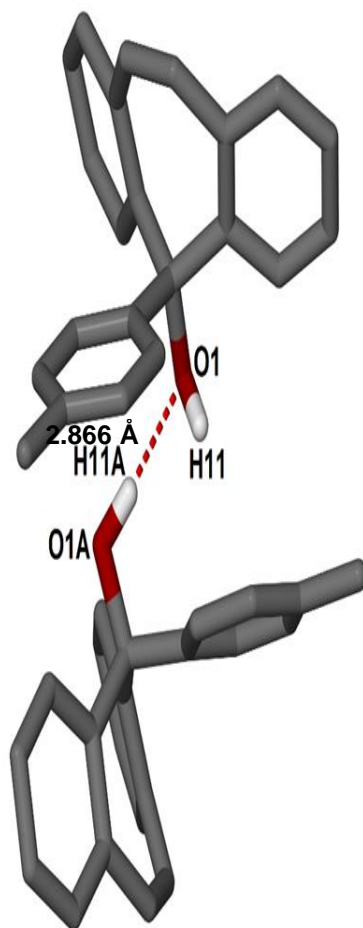


Figure 4.31: Hydrogen bonding in H2.

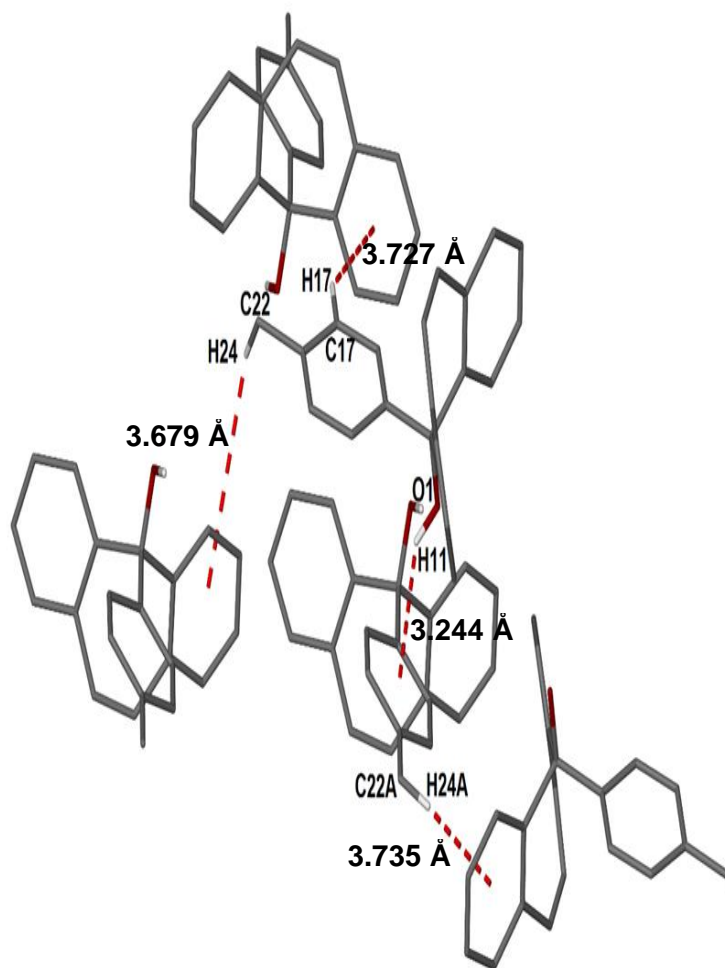


Figure 4.32: C-H $\cdots\pi$ (centroid) and O-H $\cdots\pi$ (centroid) hydrogen bonding in **H2**.

The packing diagram of **H2** along [100] is shown below in Figure 4.33.

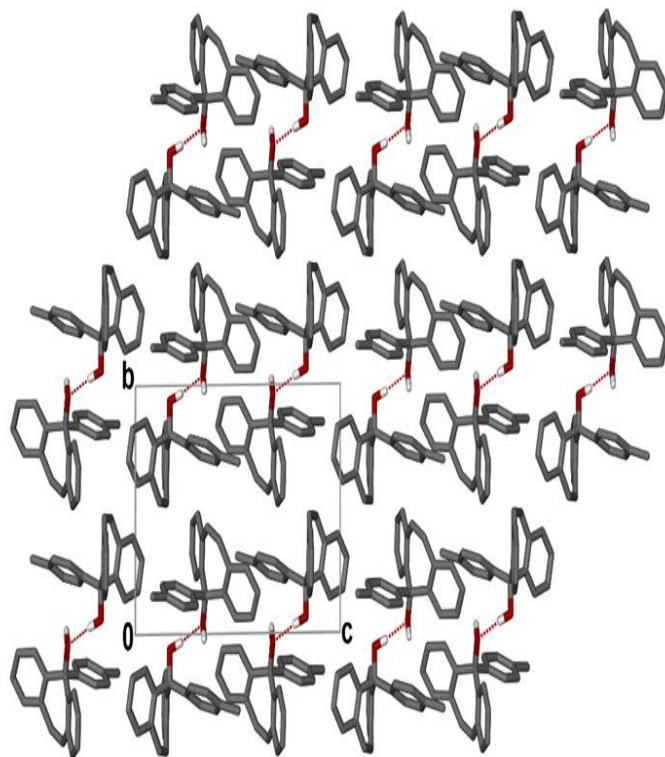


Figure 4.33: Packing diagram of H2 along [100].

Table 4.17: Summary of thermal analysis data of H2 and its inclusion compounds.

Compound	H2	H2•DMSO	H2•NMP	H2•MORP
H : G ratio	-	1:1	1:1	1:1
TG (Calc.%mass loss)	-	20.7	24.9	22.6
TG (Exp.% mass loss)	-	20.0	24.2	21.0
DSC Endotherm (T _{on} /K)				
Peak 1				
Peak 2	409.8	363.7 393.1	389.4	355.7
Normal boiling point of pure guest ^[18] (K)	-	462.2	475.0	401.2
(T _{on} -T _b)/K	-	-98.5	-85.6	-45.5

For all the inclusion compounds the guest is released at a lower temperature than the normal boiling points of the pure solvents.^[9] The (T_{on}-T_b) values suggest that the relative thermal stability of the inclusion compounds follows the trend **H2•MORP** > **H2•NMP** > **H2•DMSO**.

4.5 Selectivity experiments

Competition experiments were performed to determine the selectivity of the host compound **H2** towards mixtures of two guests. These were done for 1: 1 molar ratios of **DMSO: MORP**, **DMSO: NMP** and **NMP: MORP**. The total guest: host ratio was approximately 20: 1. The resultant crystals were analysed using TG or DSC (experimental results given in Appendix B1-B6). In each case only one product was found and the results are summarised below in Table 4.18.

Table 4.18: Summary of selectivity experiments.

Guest mixtures	Resultant inclusion compound
DMSO:MORP	H2•MORP
DMSO:NMP	H2•NMP
NMP:MORP	H2•NMP

Thus the selectivity trend is: **NMP>MORP>DMSO**. Both the relative thermal stability ($T_{on}-T_b$) and selectivity experiments showed agreement that the **H2•DMSO** compound was the least favoured. However the selectivity experiments show that **NMP** was preferentially included over **MORP** which is different from the trend observed from the ($T_{on}-T_b$) values.

4.6 Torsion angles for the host molecule H2

For all the structures of the inclusion compound with **H2**, the dibenzosuberonyl group adopts a concave shape. The torsion angles involving the seven membered ring (Figure 4.34) of the host molecule is summarised in Table 4.19. Overall there are small differences in all three of the torsion angles with τ_2 displaying the least variation ranging from -1.3 to 2.7° . A similar analysis was completed for the compound 10,11-dihydro-5-(4-methoxyphenyl)-5*H*-dibenzo[a,d]cyclohepten-5-ol, which displayed more flexibility in τ_1 due it having a single bond C12-C13.^[10] The dihedral angle between the least squares planes of the phenyl rings A and B was also determined (Figure 4.34).

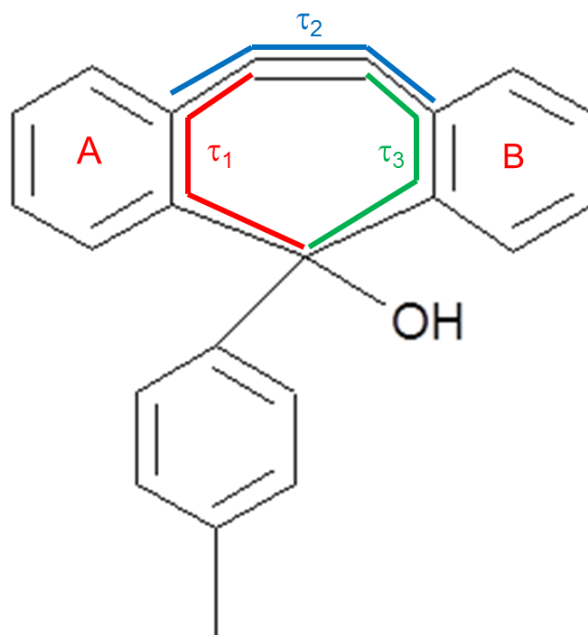


Figure 4.34: Torsion angles (τ_1 , τ_2 and τ_3) analyses for the host molecule H2.

Table 4.19: Selected geometrical parameters of the host molecule H2.

Torsion angle	H2	H2·DMSO	H2·NMP	H2·MORP
τ_1 (°)	-7.1; -3.7	-10.6	-7.6	-7.0; -7.0
τ_2 (°)	0.7; -1.3	2.7	-0.8	0.6; -1.2
τ_3 (°)	3.1; 5.9	4.1	7.9	3.3; 6.9
Dihedral angle between ring A and B	54.6; 51.5	48.9	57.2	55.9; 53.5

References

1. Yvon, K., Jeitschko, W. & Parth, E. (1977) *Appl. Crystallogr.*, 10: 73-74.
2. Jacobs, A., Nassimbeni, L.R. & Taljaard, B. (2004) *Acta Cryst.*, C60, 0668-0670.
3. Taljaard B., Taljaard J.H., Imrie C. & Caira M.R. (2005) *Eur J Org Chem.*, 12:2607-2619.
4. Sheldrick GM. (1997) SHELX-97, program for crystal structure refinement. University of Göttingen, Germany.
5. Barbour, L.J. (2001) Xseed, a software tool for supramolecular crystallography. *J. Supramol Chem.*, 1: 189.
6. Spek, A.L. (1990) *Acta Cryst.*, A46:C34.
7. Spek, A.L. (1998) PLATON, a multipurpose crystallographic tool. Utrecht University, Utrecht, The Netherlands.
8. Sayed, A., Jacobs, A. & Taljaard, J.H. (2013) *J. Chem. Cryst.*, 43:325-330.
9. Lide, D.R. (2003) CRC handbook of chemistry and physics, 84th edn. CRC Press, Boca Raton.
10. Nassimbeni, L.R., Ramon, G. & Taljaard, J.H. (2009) *Cryst. Growth Des.*, 9:88-94.

5. CHAPTER 5 – HIRSHFELD SURFACES ANALYSIS OF THE INCLUSION COMPOUNDS OF H1

Hirshfeld surface analysis was used to quantify the intermolecular interactions present in all the inclusion compounds. It is a new way of exploring packing modes and intermolecular interactions in molecular crystals, and has become a valuable tool in comparison of crystal structures. [1, 2]

The distance d_e on the Hirshfeld surface represents the distance from the surface to the nearest external atom (outside) and d_i represents the distance from the surface to the nearest internal atom (inside). Both the d_e and d_i are used to produce a fingerprint plot, [3] which is a 2D representation of all the intermolecular interactions in a crystal structure with intercontacts of the type, C...H which is due to the C-H... π interaction, C...C due to the π ... π interactions, O...H, N...H and H...H. The program CrystalExplorer w

s used to obtain the Hirshfeld surfaces for the host molecules in the crystal structures and generate the resulting fingerprint plots. Table 5.1 summarises the percentage contribution of individual intermolecular contacts to the Hirshfeld surface of **H1** in each of the inclusion compounds. The fingerprint plots are given in Figures 5.1- 5.5.

Table 5.1: Summary of the percentage of various intermolecular contacts contributed to the Hirshfeld surface contacts of H1 in its inclusion compounds.

Structures	C...H (%)	O...H (%)	N...H (%)	H...H (%)	C...C (%)
H1•PYR	30.2	6.5	2.1	57.3	1.9
H1•NMP	27.6	10.1	-	60.7	-
H1•DMA	27.2	9.2	-	61.3	-
H1•MORP1	28.8	8.8	1.1	60.1	-
H1•MORP2	29.2	9.4	1.2	58.5	1.5

For all the structures, it was observed that the major contribution to the Hirshfeld surface was from the H...H intercontact. This is followed by the % C...H interactions which is consistent with the C-H... π contacts found in all of the crystal structures and indicates the importance of these weak interactions in stabilising the structures. **H1•NMP** shows the

highest % O...H (10.1%) with H1•PYR the lowest (6.5 %). The low values obtained for the % C...C suggests that there are no significant $\pi \cdots \pi$ interactions in the crystal structures.

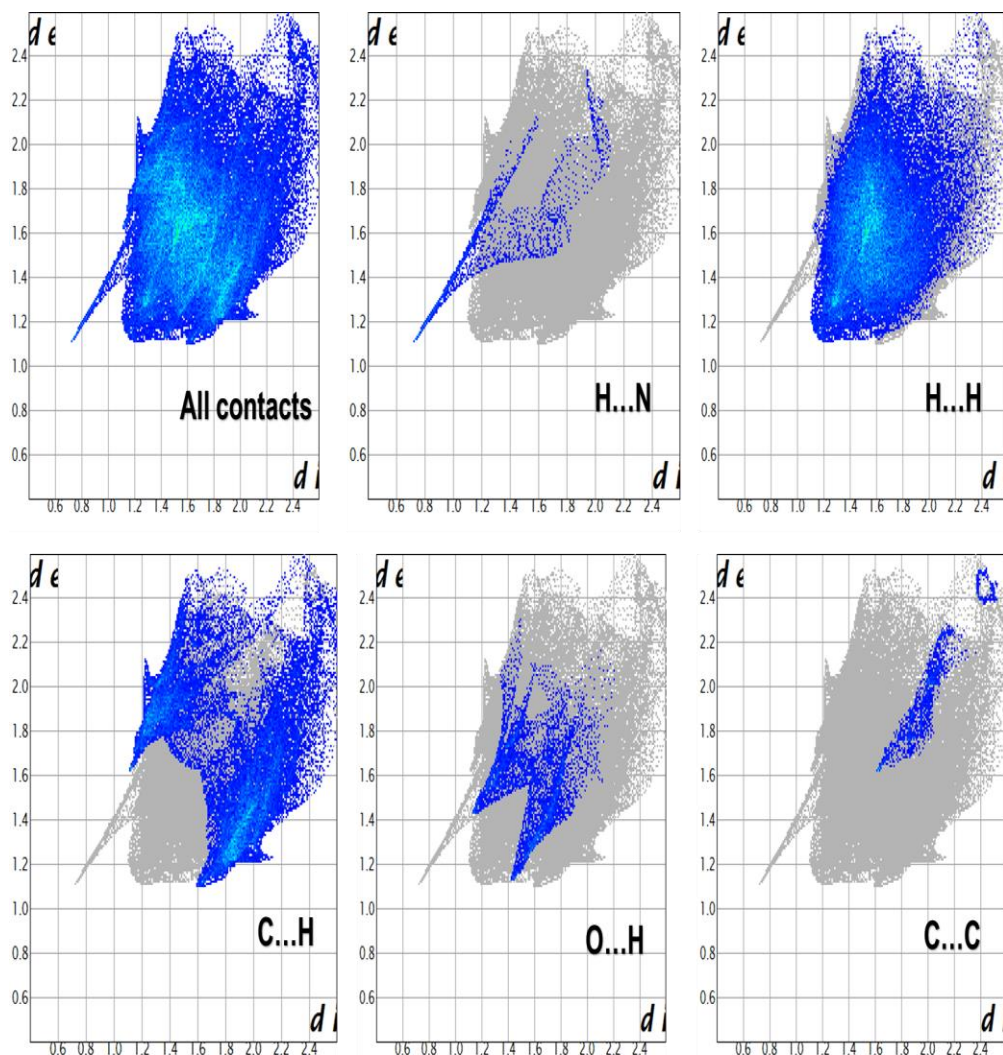


Figure 5.1: Fingerprint plots for different interactions present in H1•PYR.

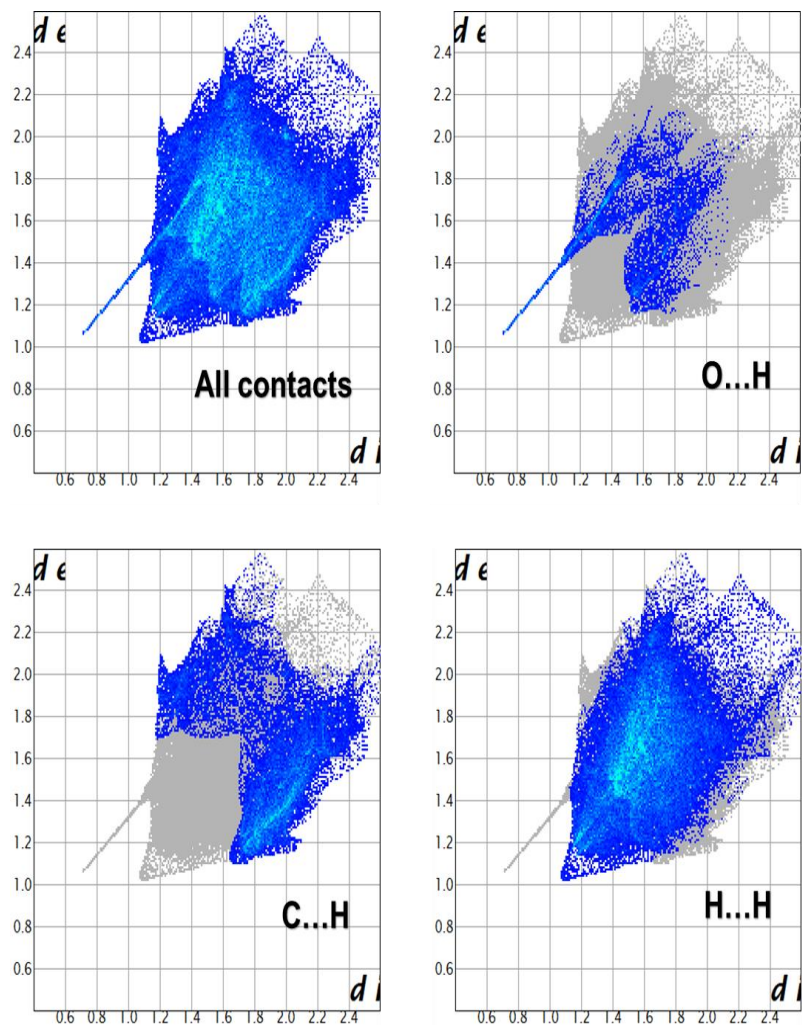


Figure 5.2: Fingerprint plots for different interactions present in H1•NMP.

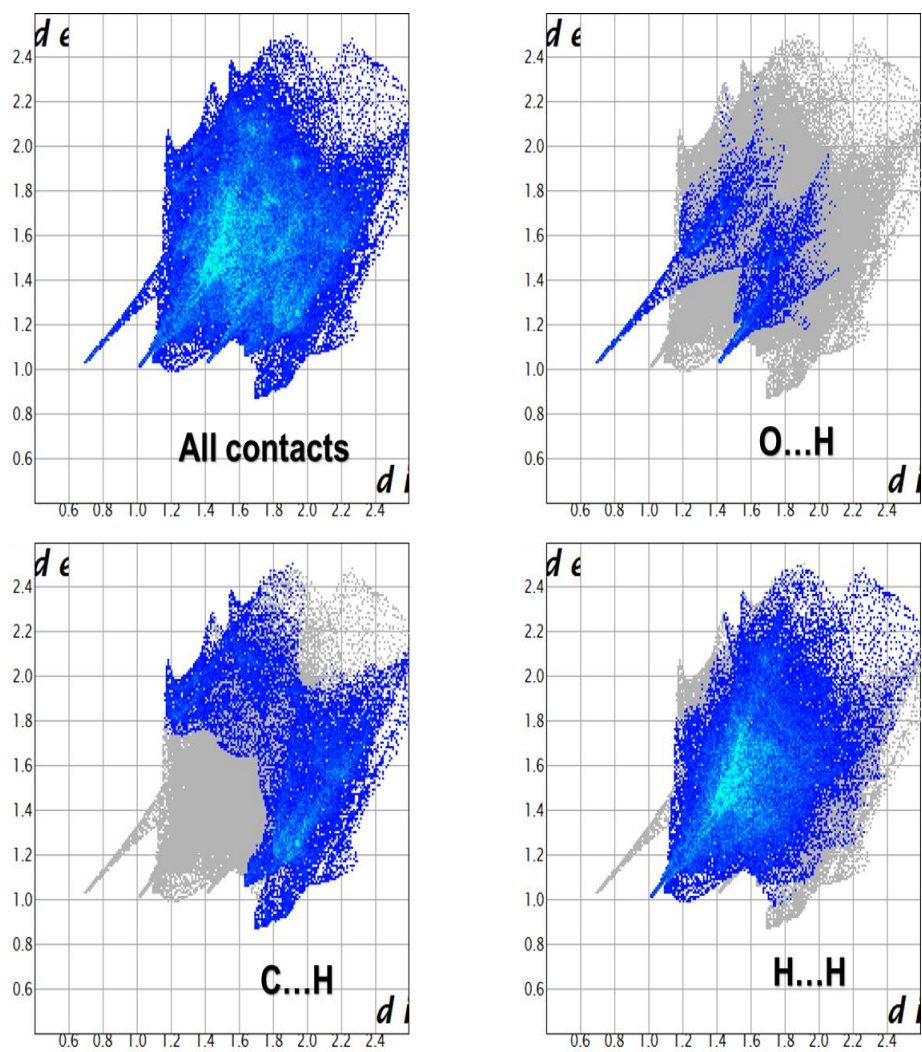


Figure 5.3: Fingerprint plots for different interactions in H1•DMA.

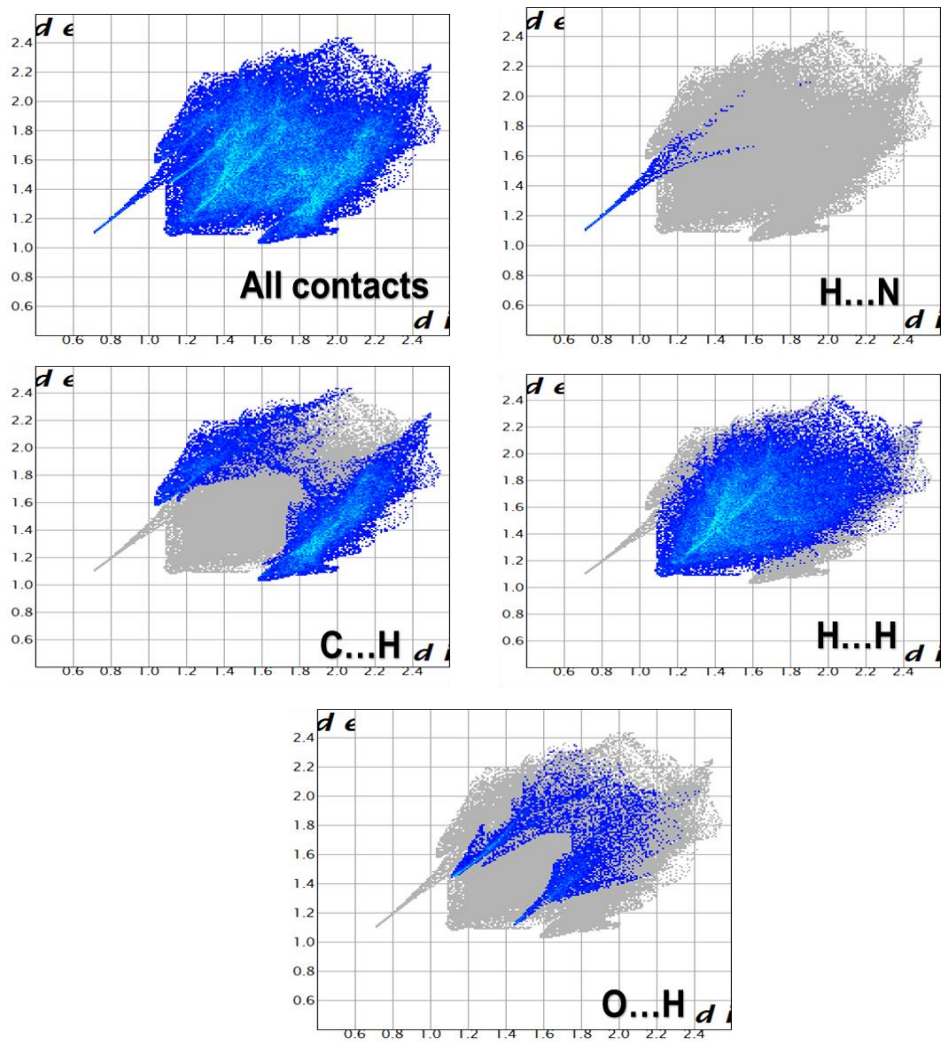


Figure 5.4: Fingerprint plots for different interactions in H1-MORP1.

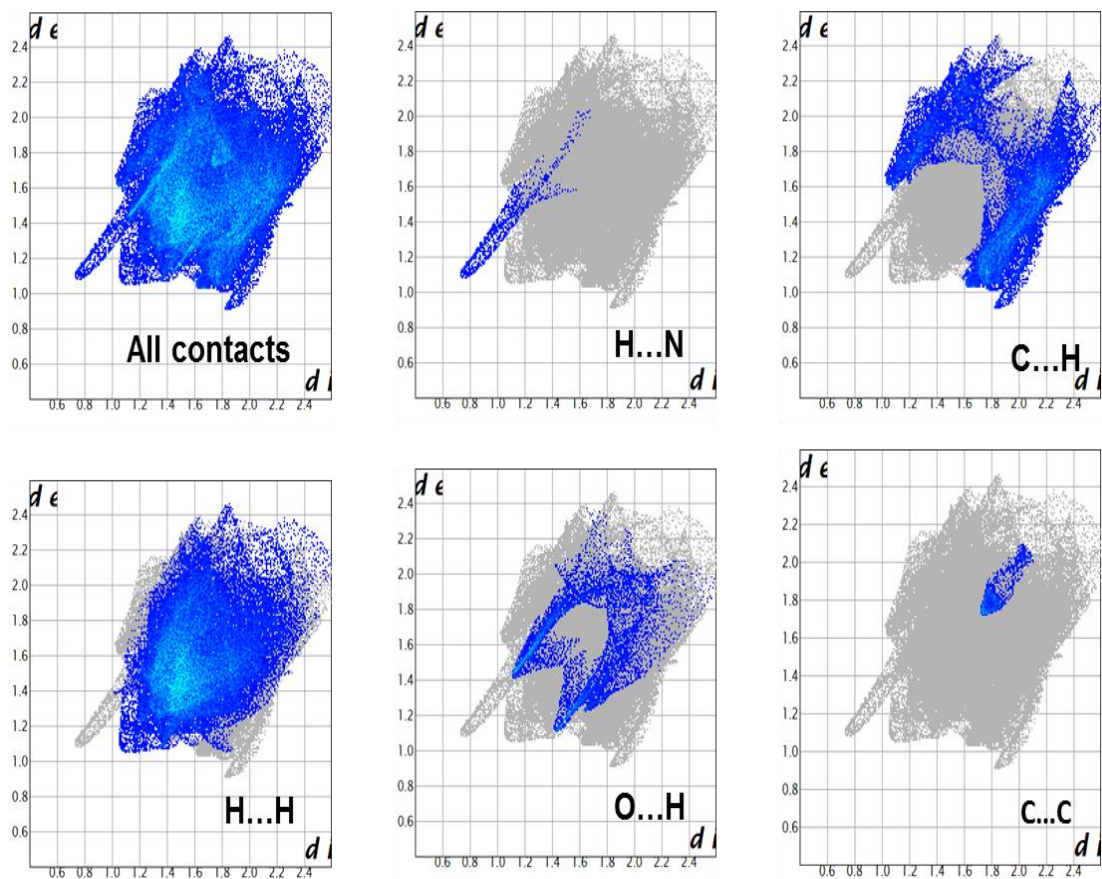


Figure 5.5: Fingerprint plots for different interactions in H1-MORP2.

References

1. McKinnon, J.J., Jayatilaka, D. & Spackman, M.A. (2007) *Chem. Comm.*, 37: 3814-3816.
2. McKinnon, J.J., Spackman, M.A. & Mitchell, A.S. (2004) *Acta Cryst.*, 60:637-668.
3. Spackman, M.A. & McKinnon, J.J. (2002) *CrystEngComm.*, 4:378-392.

6. CHAPTER 6 – HIRSHFELD SURFACE ANALYSIS OF THE INCLUSION COMPOUNDS OF H₂

Here again, all of the intermolecular interactions in the crystal structures were analysed using the Hirshfeld surface by looking at the fingerprint plot for the different interactions. This is a unique tool to represent the intermolecular interactions present in the crystal structure.^[1] The results are summarised in Table 6.1 and the fingerprint plots are given in Figures 6.1-6.3.

Table 6.1: Summary of the percentage of various intermolecular contacts contributed to the Hirshfeld surface of H₂ in its inclusion compounds.

Structures	O...H (%)	C...H (%)	H...H (%)	H...N (%)
H ₂ •DMSO	8.3	23.9	65.7	-
H ₂ •NMP	6.9	20.9	71.6	-
H ₂ •MORP	2.6	25.0	71.2	1.2

As was observed for the Hirshfeld surface analysis of the inclusion compounds of **H1**, the highest % contributions are from the H...H intercontacts, followed by the C...H interactions. The % O...H interactions vary from 8.3 % for **H₂•DMSO** to 2.6 % for **H₂•MORP**. No C...C contributions were found for the inclusion compounds involving **H₂**.

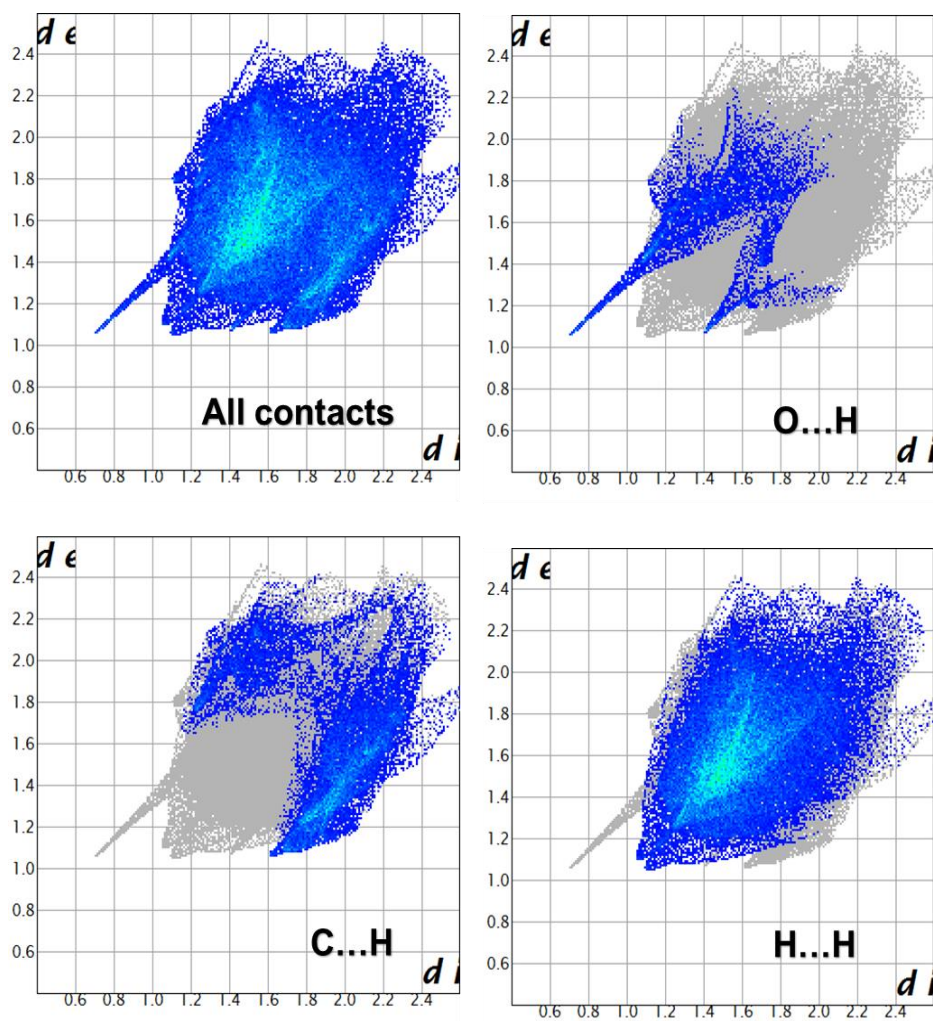


Figure 6.1: Fingerprint plots for all the interactions in H₂•DMSO.

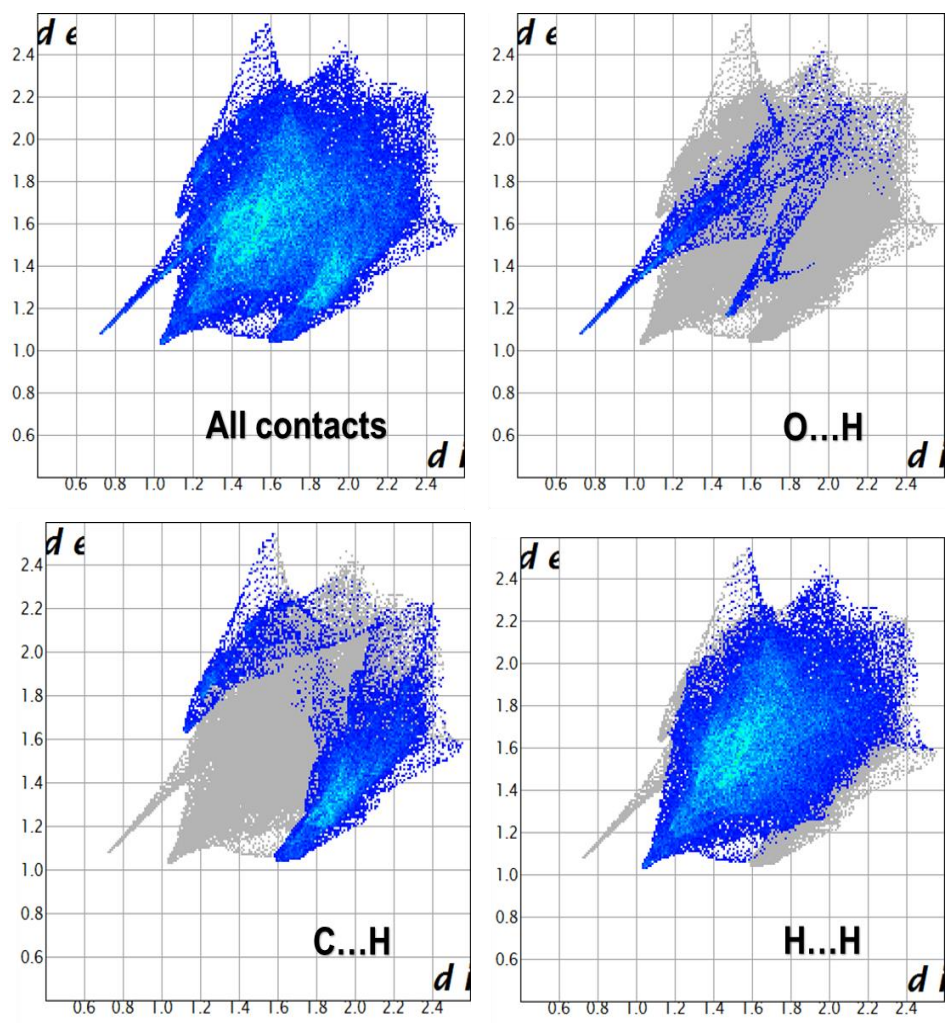


Figure 6.2: Fingerprint plots for all the interactions in H2•NMP.

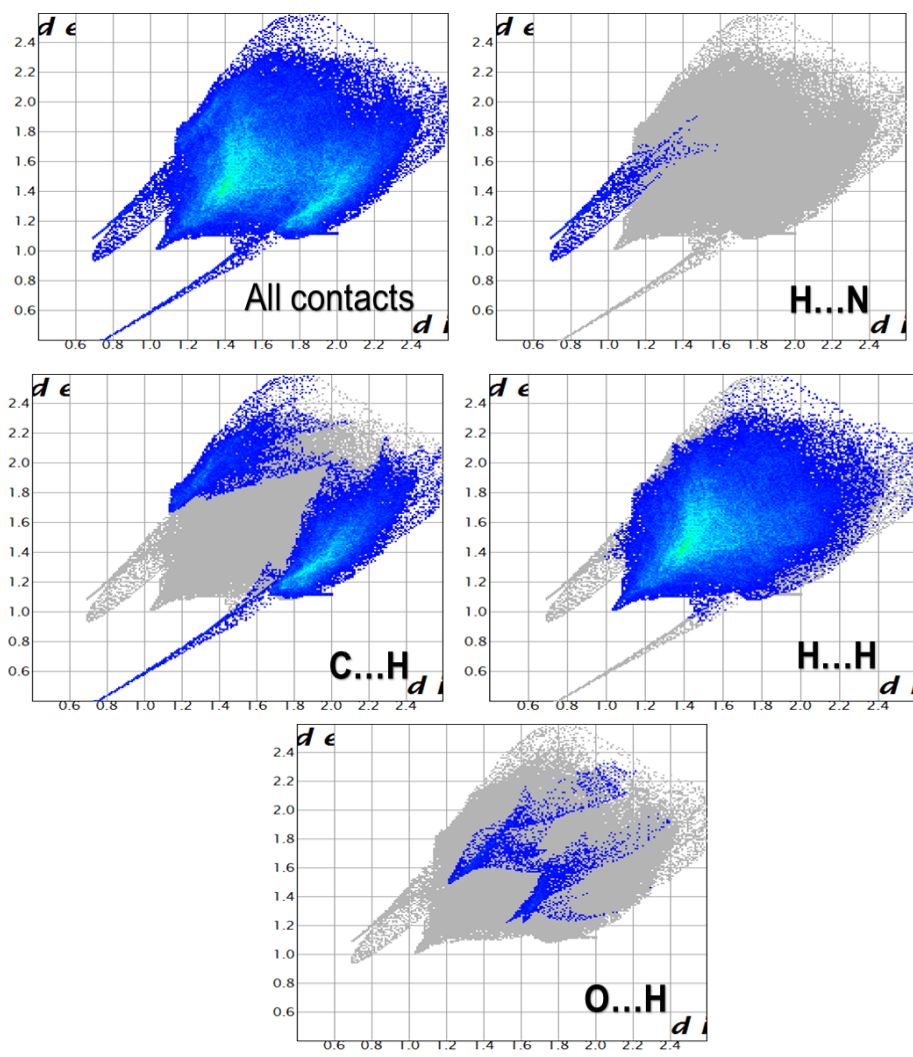


Figure 6.3: Fingerprint plots for all the interactions in H2-MORP.

References

1. Spackman, M.A. & Jayatilaka. D. (2009) *CrystEngComm.*, 11:19-32.

7. CHAPTER 7- SUMMARY AND CONCLUSION

Inclusion compounds of two hydroxyl hosts with a variety of guests have been investigated in this study. The host 9-(1-naphthyl)-9*H*-xanthen-ol (**H1**), forms inclusion compounds with pyridine (**PYR**), *N,N*-dimethylacetamide (**DMA**), morpholine (**MORP**) and *N*-methyl-2-pyrrolidinone (**NMP**). All of the inclusion compounds except **H1•MORP1** ($1: \frac{3}{2}$) demonstrated a host: guest ratio of 1 : 1. In addition a 1: 1 **H1: MORP** compound, **H1•MORP2**, resulted from dissolution of **H1** in a 1:1 molar ratio of **MORP: DMA**. **H1** interacts with pyridine and morpholine via (Host)O-H...N(Guest) hydrogen bonds and via (Host)OH...O(Guest) hydrogen bonds with *N*-methyl-2-pyrrolidinone and *N,N*-dimethylacetamide. The structures are further stabilised by C-H... π interactions formed between the Host...Host and the Host...Guest. Competition experiments were performed to determine the selectivity of the host compound **H1** towards mixtures of two guests. These were done for 1: 1 molar ratios of **PYR: NMP**, **PYR: MORP**, **MORP: NMP**, **DMA: NMP**, **DMA: PYR** and **DMA: MORP**. The selectivity trend was found to be **NMP > MORP > DMA > PYR**.

The host 5-(4-methylphenyl)-5*H*-dibenzo[a,d]-cyclohepten-5-ol (**H2**) forms inclusion compounds with dimethylsulfoxide (**DMSO**), morpholine (**MORP**) and *N*-methyl-2-pyrrolidinone (**NMP**). All of the inclusion compounds demonstrated a host: guest ratio of 1:1. The guests are hydrogen bonded to the host via (Host)-OH...O(Guest) interactions for the dimethylsulfoxide and the *N*-methyl-2-pyrrolidinone inclusion compounds and via (Host)-OH...N(Guest) hydrogen bonds for the inclusion compound involving morpholine. An apohost structure was also determined for **H2** with the host molecules interacting via (Host)-OH...O(Host) linkages. Furthermore all the structures are stabilised by C-H... π interactions involving the extensive aromatic system of the host and for the morpholine inclusion compound, weak N-H... π interactions are also present. For the apohost structure an additional O-H... π contact plays a role in the packing arrangement of the host molecules. Selectivity experiments were performed involving 1:1 molar ratios of **DMSO: MORP**, **DMSO: NMP** and **NMP: MORP**. The selectivity trend was found to be **NMP > MORP > DMSO**.

The inclusion compounds were also prepared using neat grinding methods and characterized using powder X-ray diffraction (PXRD) which shows that the compounds can be obtained using a different technique (grinding) by using a small quantity of the solvent. Fourier transform infrared (FTIR) spectroscopy was also used for the molecular characterization of compounds.

Thermogravimetry was used to measure the percentage mass loss due to the loss of guests from the inclusion compounds upon heating. There was good agreement between the calculated percentage weight loss and the experimental percentage weight loss for all the compounds.

Differential scanning calorimetry was used to measure the onset temperatures for the various thermal events. For all the inclusion compounds the guests were released at a lower boiling point than the normal boiling point of the pure liquid guest.

The relative stabilities ($T_{on} - T_b$) of all the inclusion compounds were also calculated. The order of thermal stability determined in this way for the inclusion compounds of **H1** was **H1•MORP2 > H1•PYR > H1•DMA > H1•MORP1 > H1•NMP**. For the inclusion compounds of **H2** the order was found to be **H2•MORP > H2•NMP > H2•DMSO**. There was no correlation between the ($T_{on} - T_b$) values and the selectivity experiments except for the case of **H2•DMSO** which was found to be the least favoured.

Hirshfeld surfaces of the host moieties were generated using CrystalExplorer software for all the crystal structures and the resulting fingerprint plots analysed. For all the inclusion compounds the major contribution to the Hirshfeld surface was from the H•••H intercontact. This was followed by the C•••H interactions which is due to the C–H••• π contacts found in the crystal structures. For the inclusion compounds of **H1**, the low values for the % C•••C suggests that there were no significant π ••• π interactions in the crystal structures and no C•••C contributions were found for the inclusion compounds of **H2**.

In conclusion, both host compounds employed in this study are capable of forming inclusion compounds with different guests. **H1** and **H2** are effective host compounds due to their bulky structure which result in voids that can accommodate small guests, and the presence of the hydroxyl moiety that can interact with suitable guests.

Appendix A: DSC RESULTS FOR SELECTIVITY EXPERIMENTS OF H1

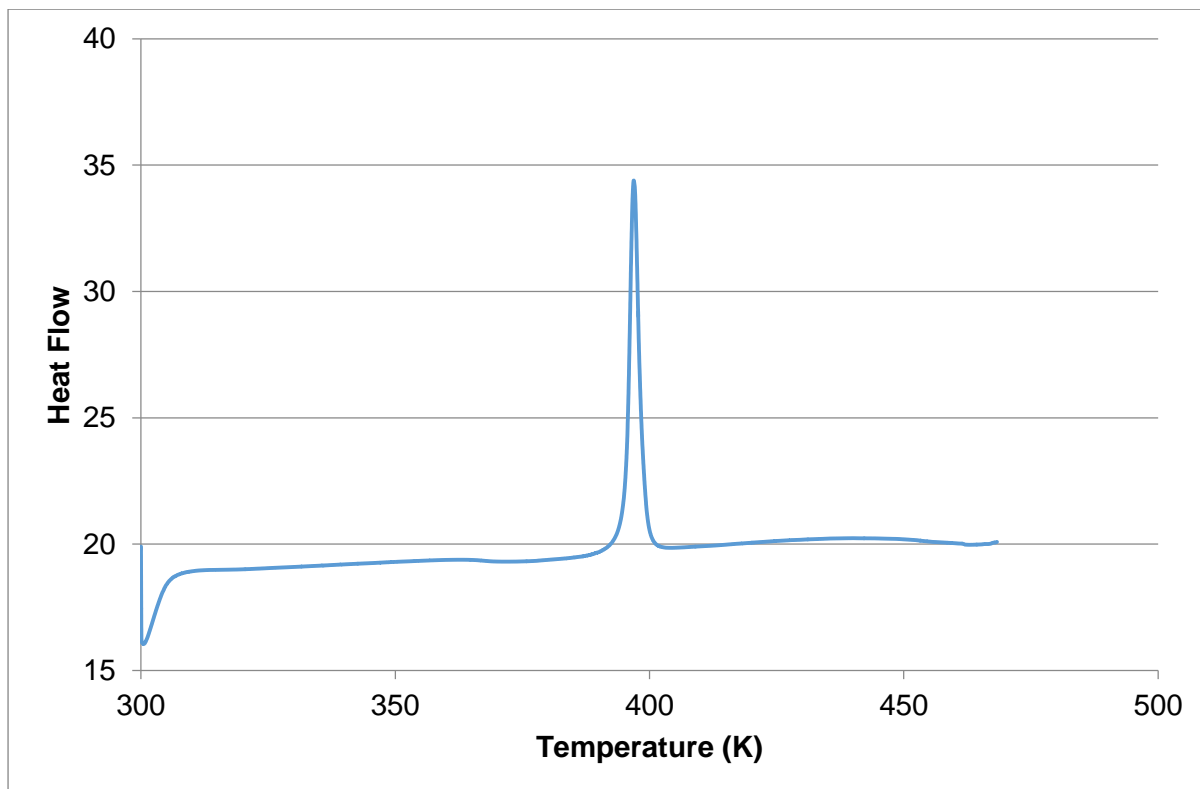


Figure A1 DSC curve for H1: PYR/NMP.

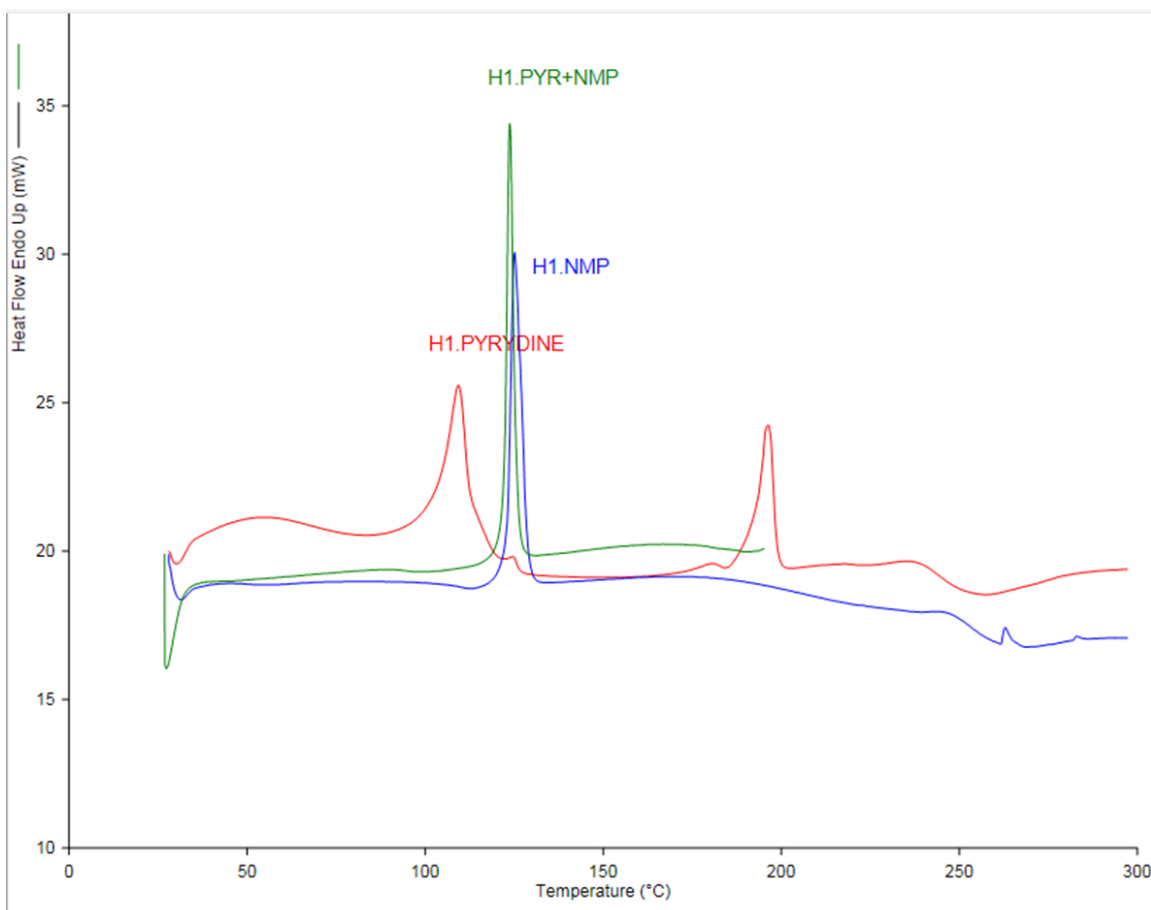


Figure A2 DSC of H1•PYR (red), H1•NMP (blue) and H1: PYR/NMP (green).

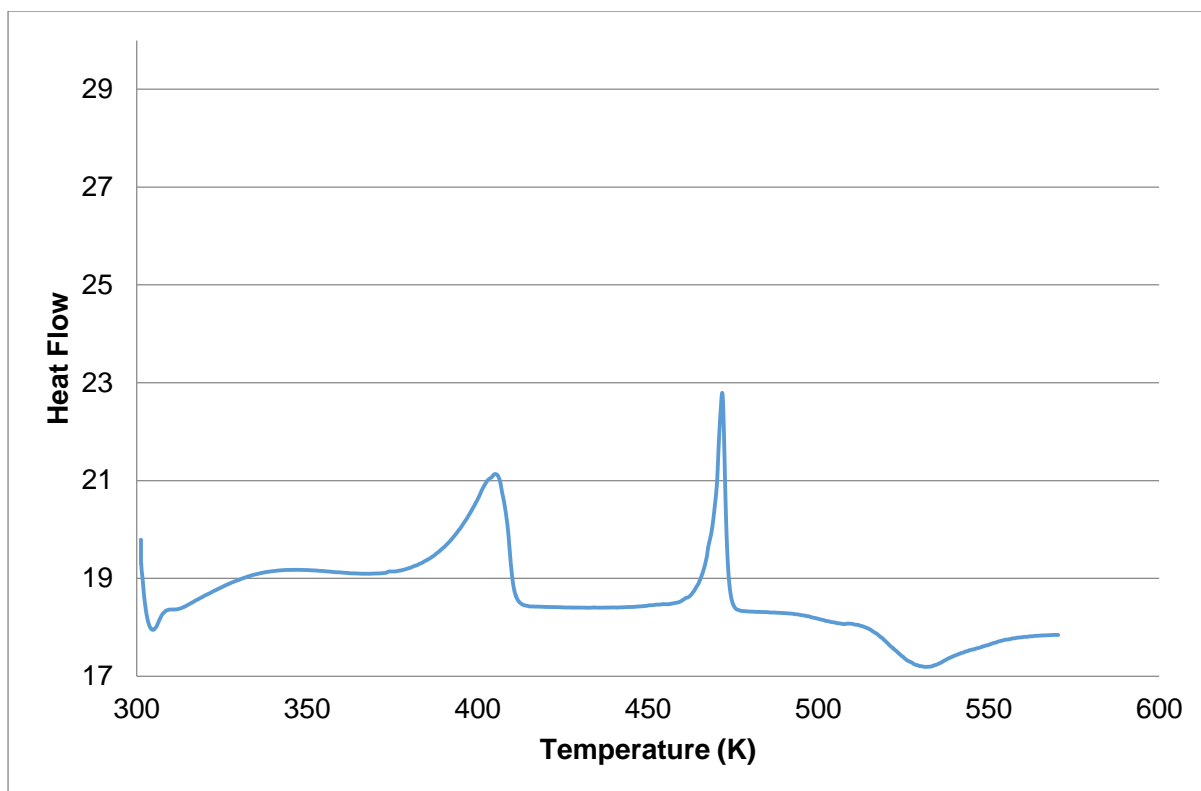


Figure A3 DSC for H1: PYR/MORP.

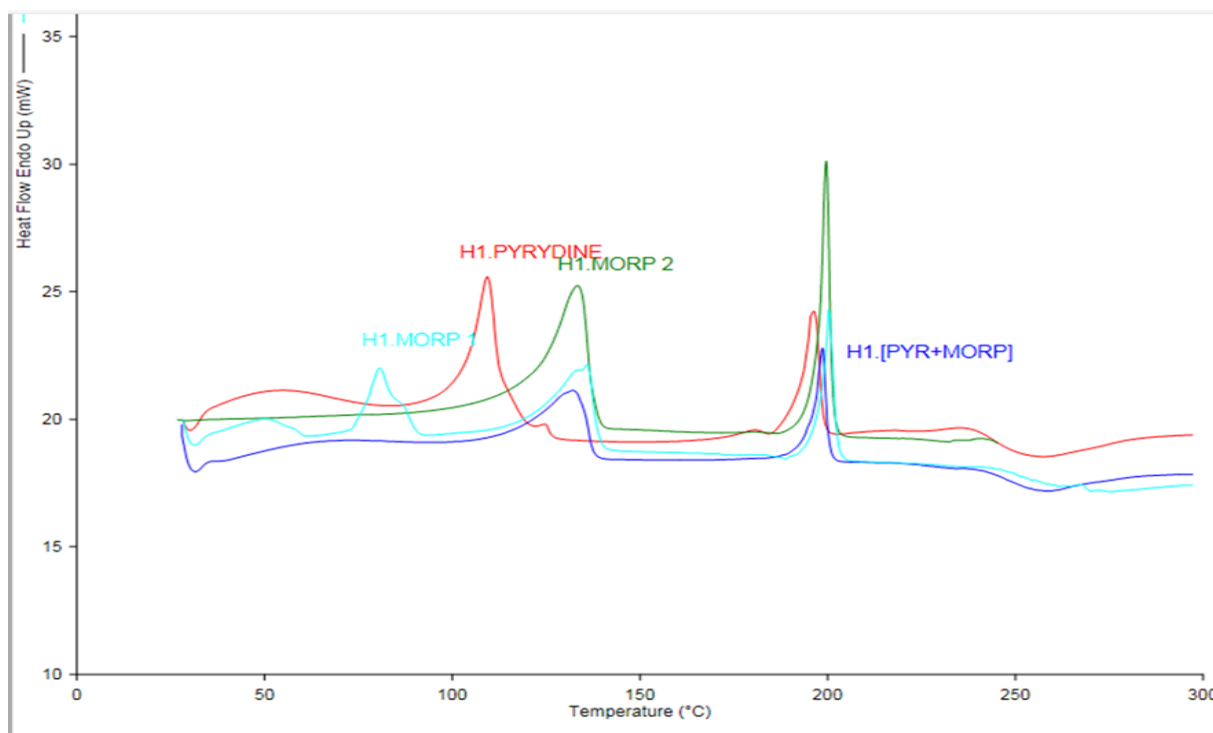


Figure A4 DSC of H1•MORP1 (turquoise), H1•MORP 2 (green), H1•PYR (red) and H1: PYR: MORP (blue).

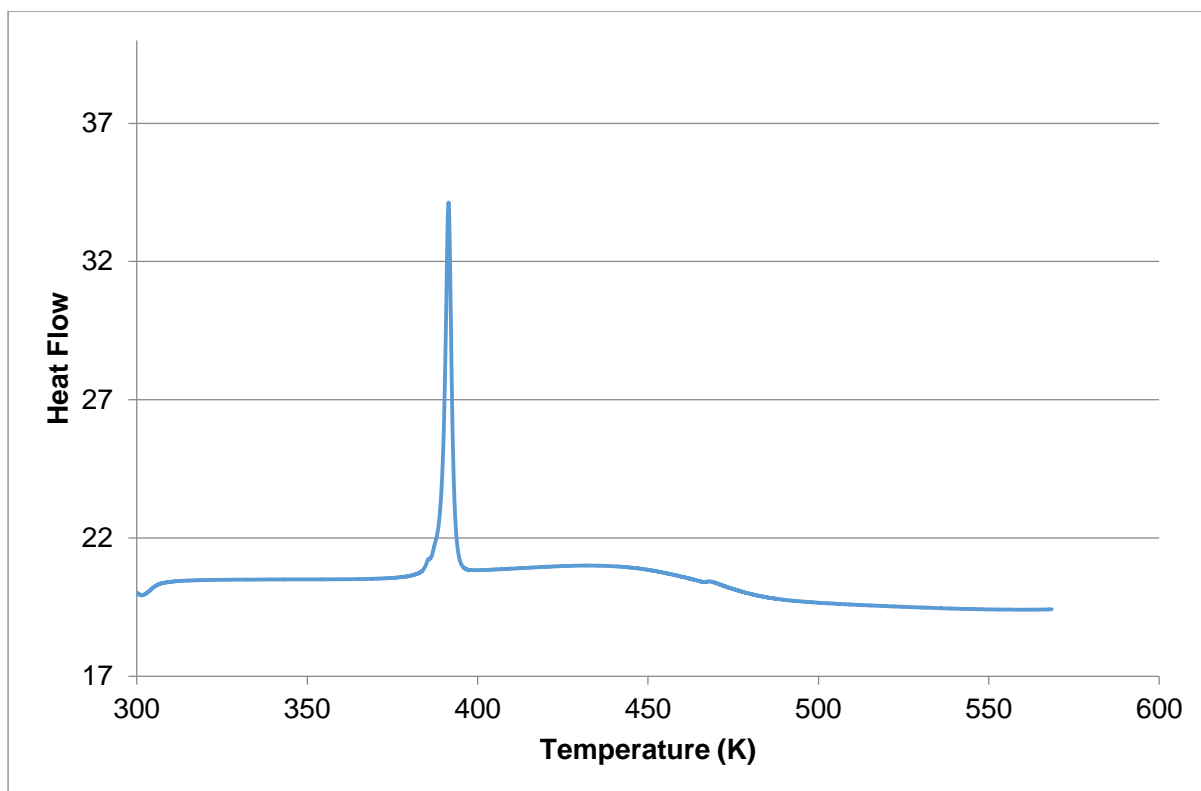


Figure A5 DSC of H1: MORP/NMP.

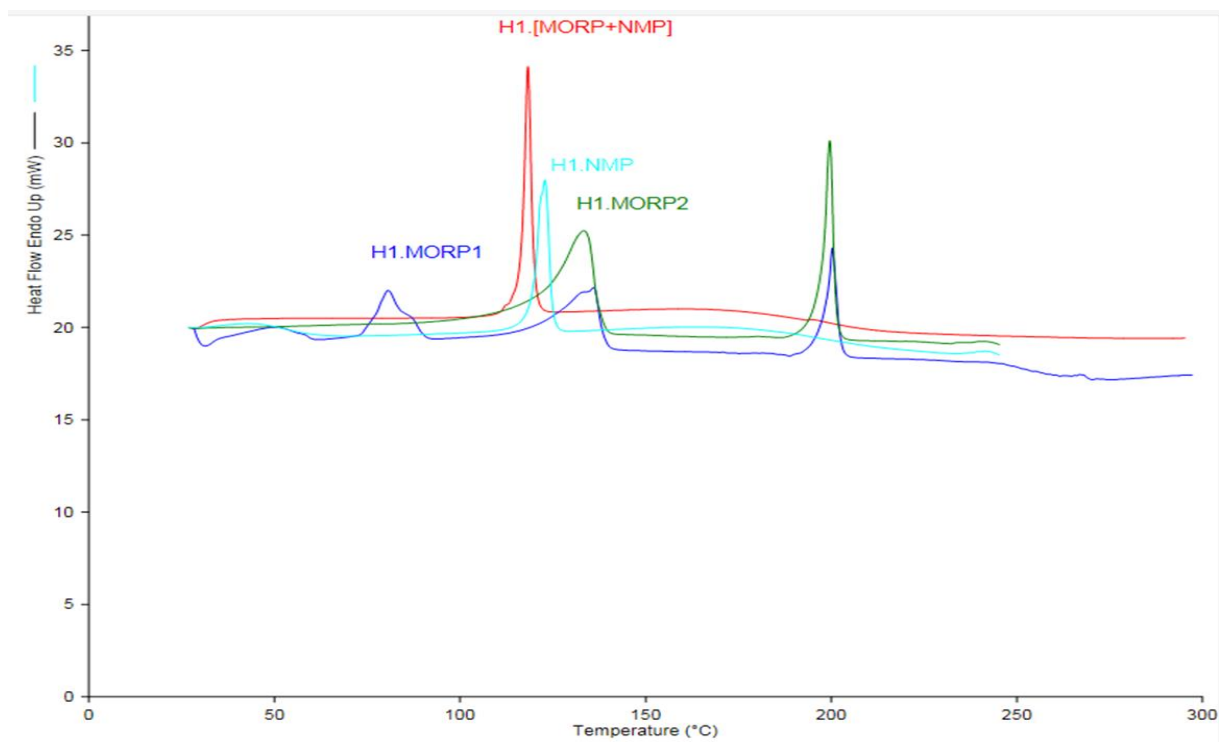


Figure A6 DSC of H1·MORP1 (blue), H1·MORP2 (green), H1·NMP (aqua) and H1: MORP/NMP (red).

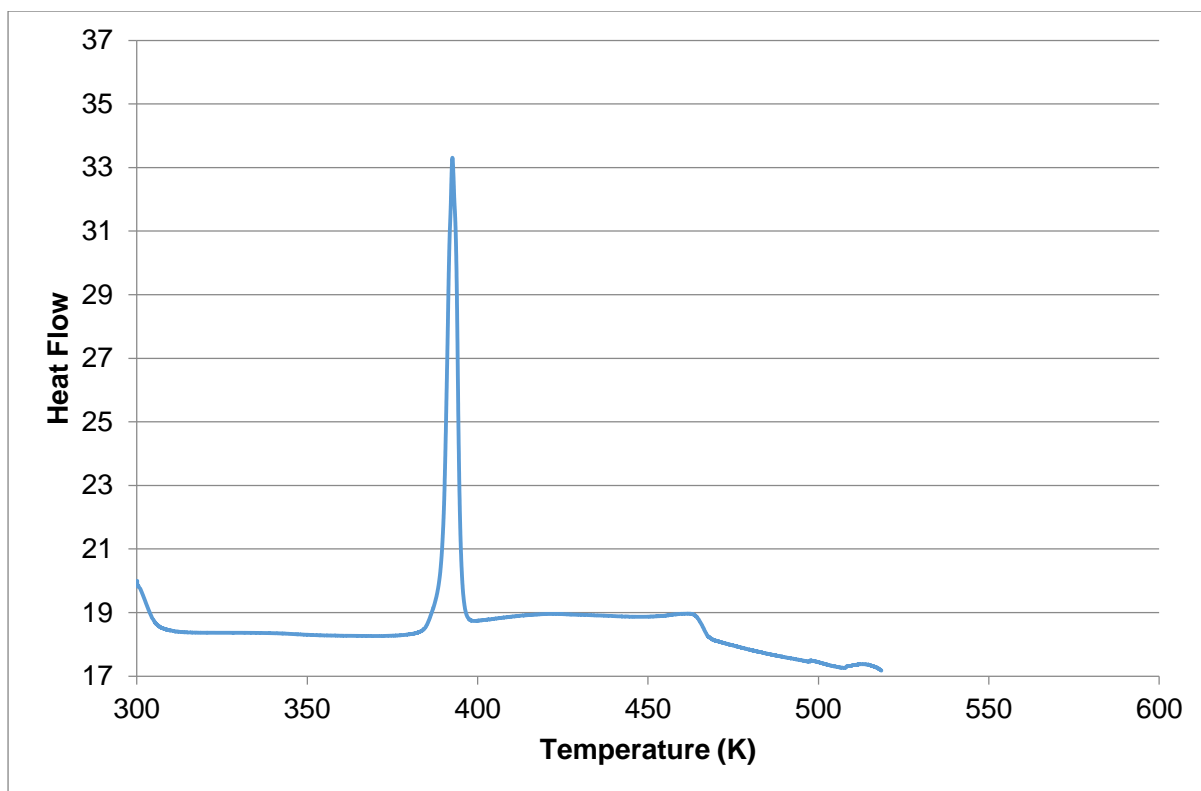


Figure A7 DSC of H1: DMA/NMP.

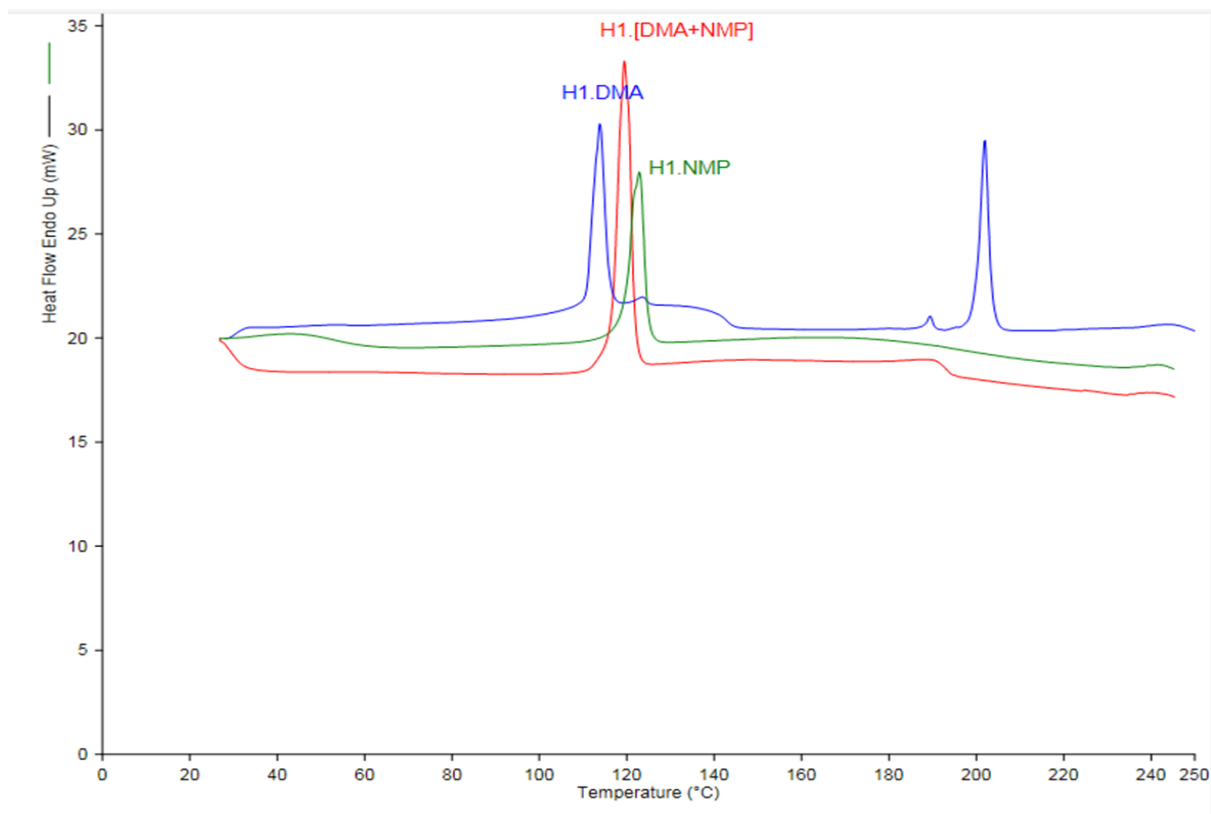


Figure A8 DSC of H1•DMA (blue), H1•NMP (green) and H1: DMA /NMP (red).

It was observed from the DSC curve overlays in Figure A8 that there was a small shift between the DSC obtained for **H1•NMP** and the one obtained for the precipitate of the **H1: DMA/NMP** selectivity experiment. This could be due to particle size differences between the samples analysed. Thus the PXRD pattern of the precipitate of the **H1: DMA/NMP** selectivity experiment was determined and compared to the calculated PXRD pattern for **H1•NMP** obtained from LAZYPULVERIX (Figure A9). There was overall agreement between the two PXRD's, which confirms that the selectivity experiment resulted in the formation of **H1•NMP**.

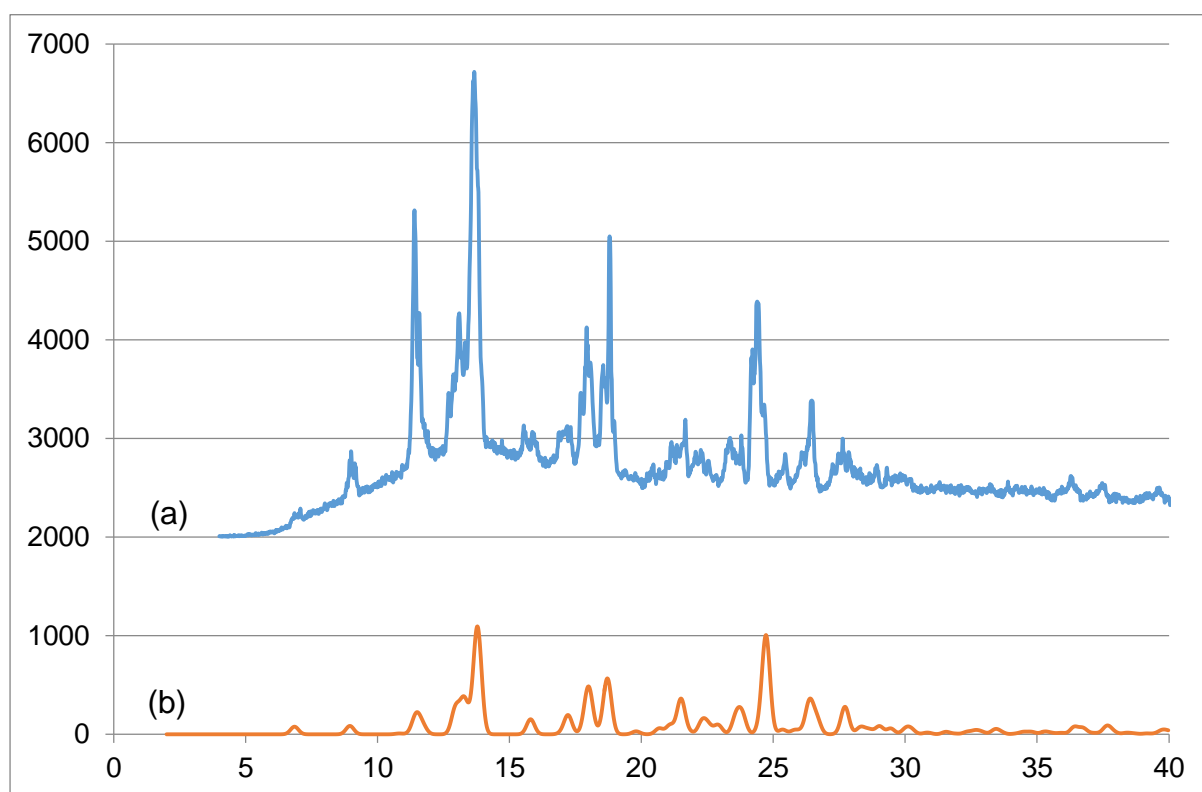


Figure A9 PXRD patterns of (a) H1: DMA/NMP and (b) H1•NMP calculated from LAZYPULVERIX.

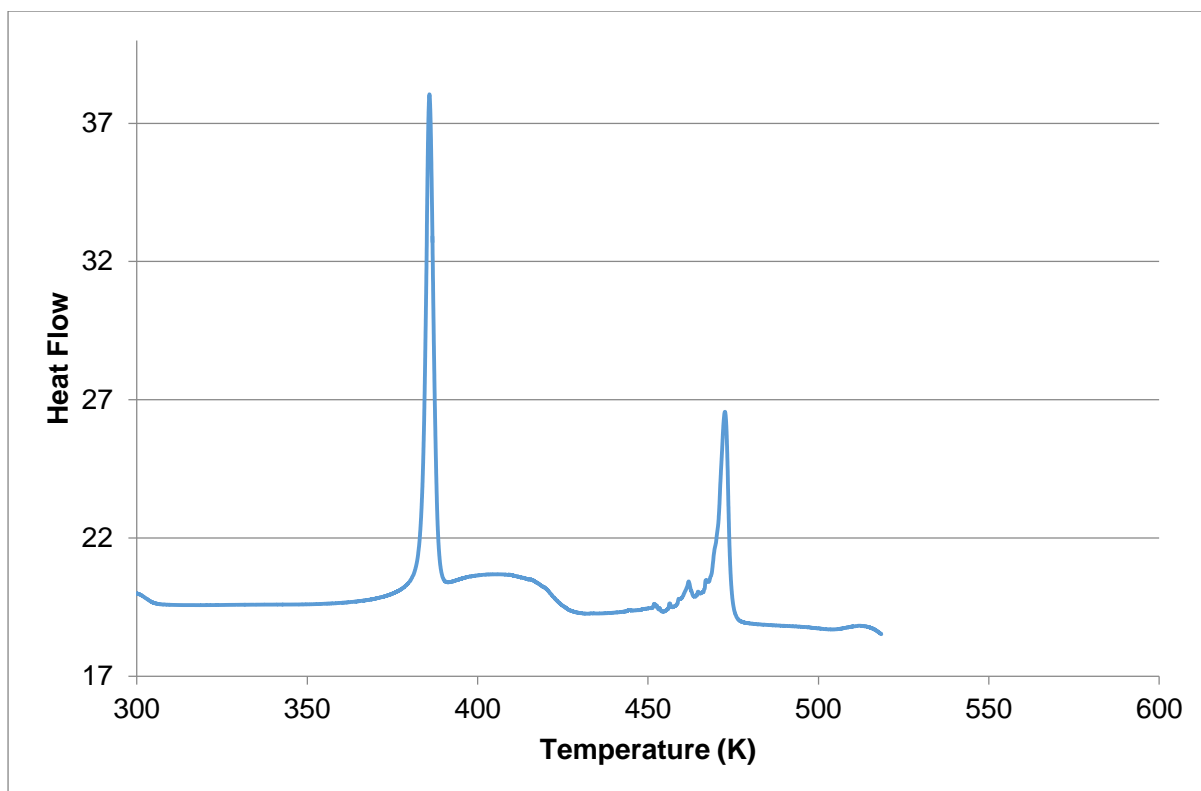


Figure A10 DSC of H1: DMA/PYR.

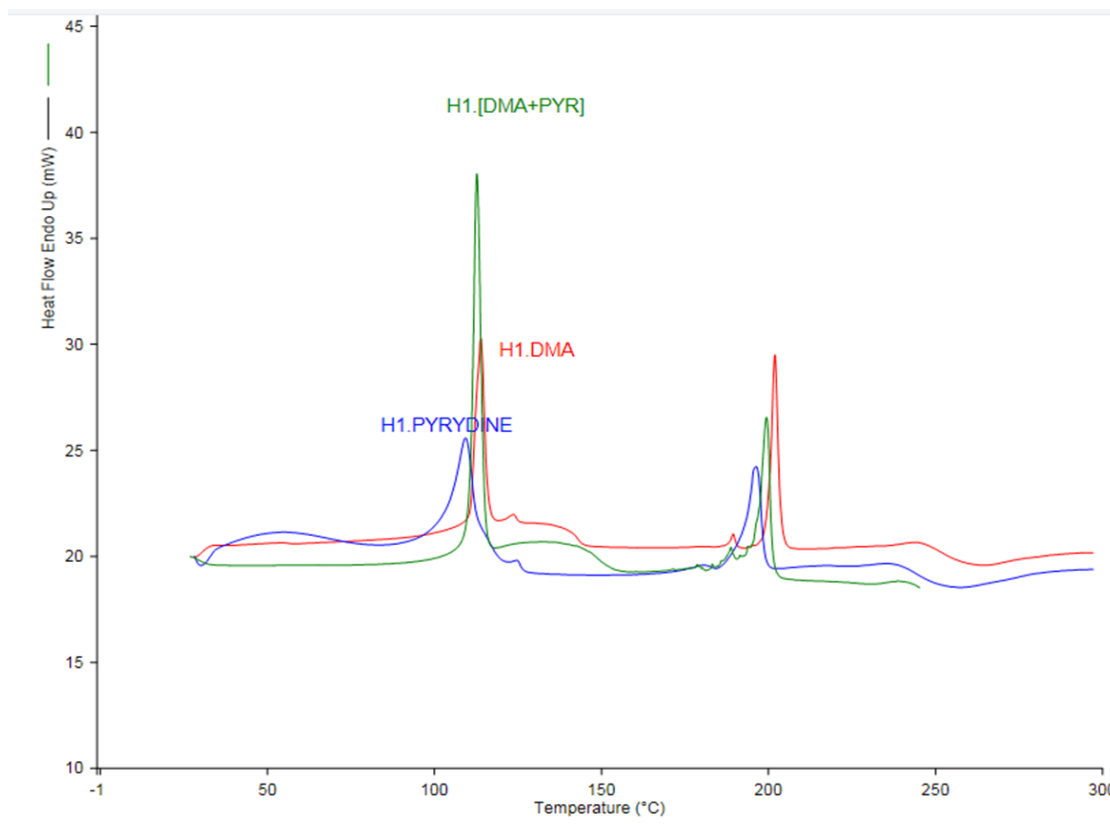


Figure A11 DSC of H1•PYR (blue), H1•DMA (red) and H1: DMA/PYR (green).

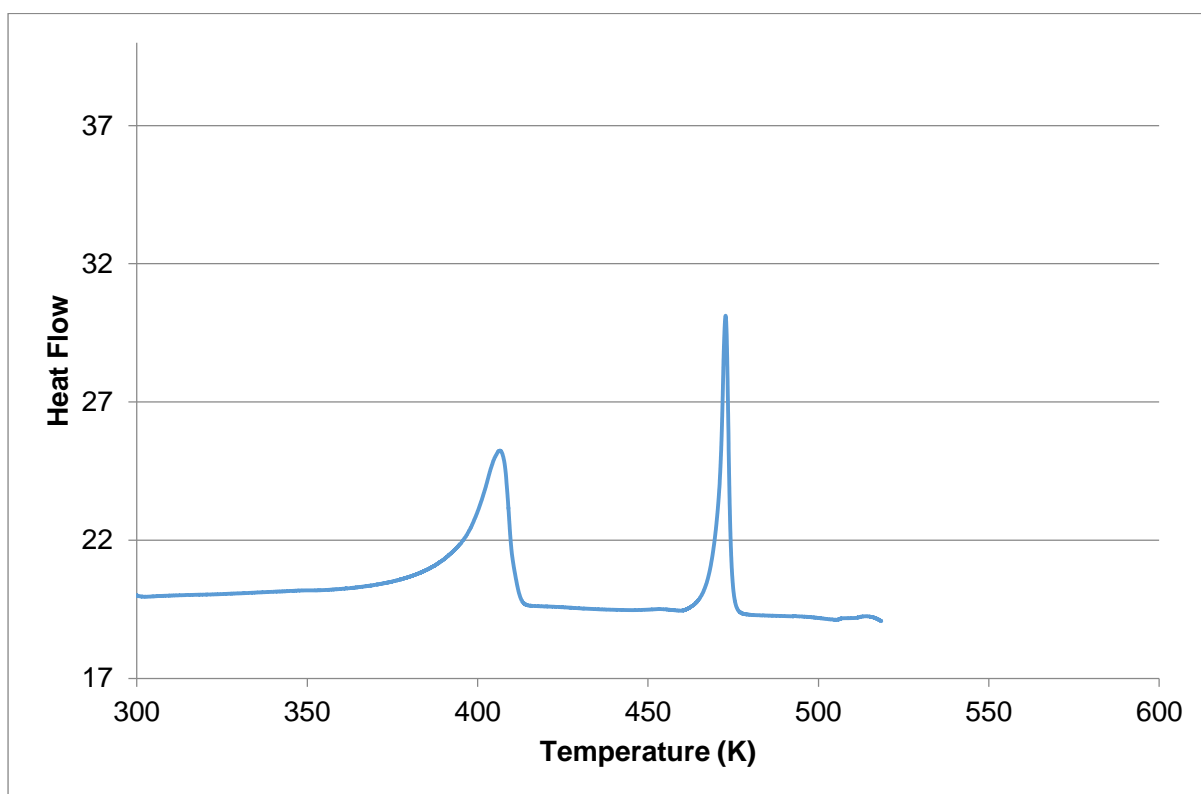


Figure A12 DSC of H1: DMA/MORP.

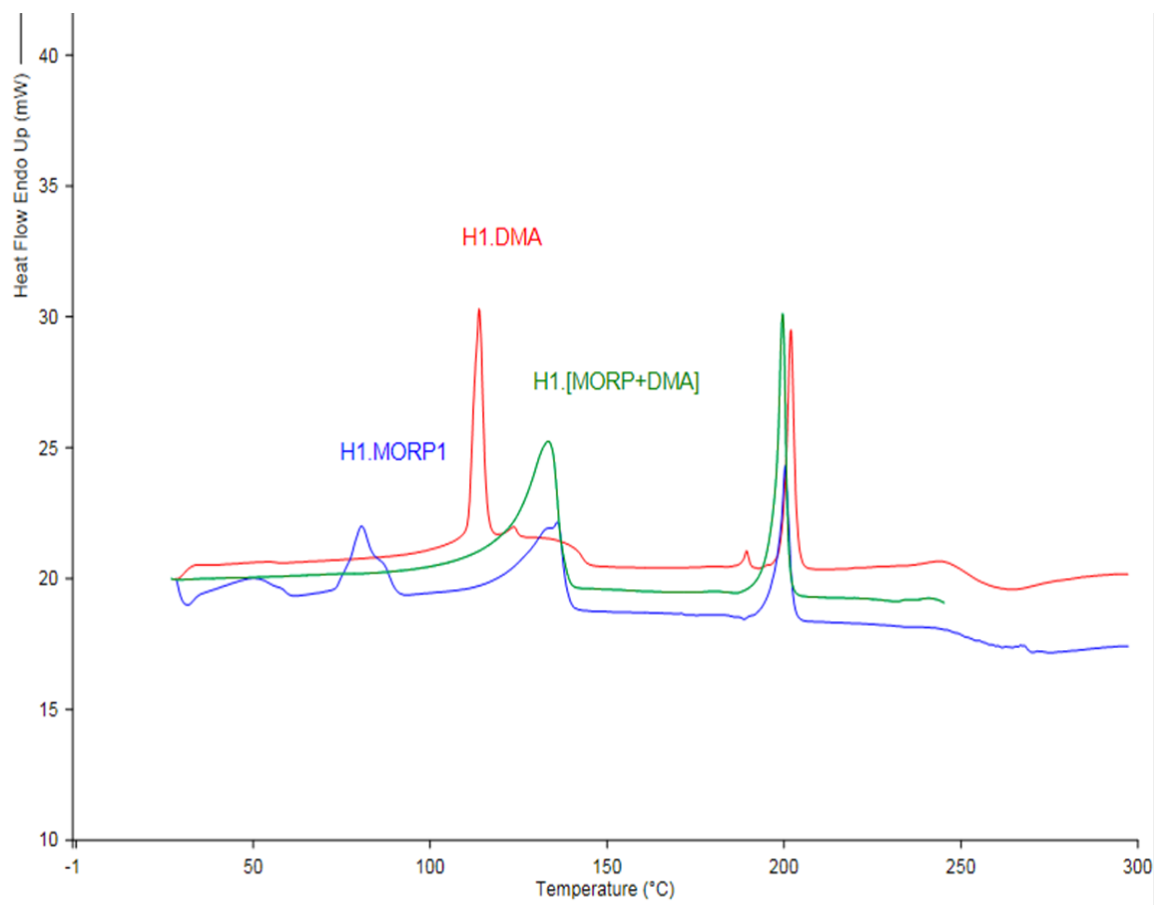


Figure A13 DSC of H1•MORP1 (blue), H1•DMA (red) and H1: MORP/DMA (green).

Appendix B: SELECTIVITY EXPERIMENTS OF H2

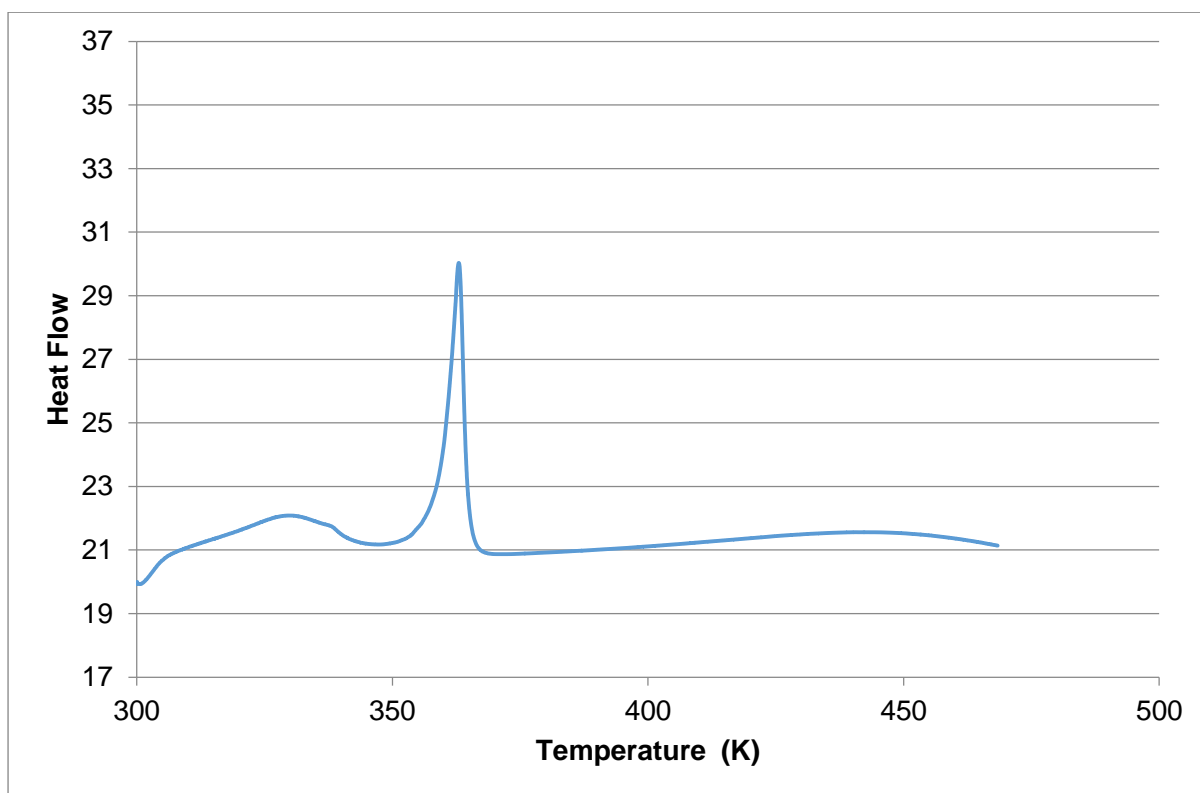


Figure B1 DSC of H2: DMSO/MORP.

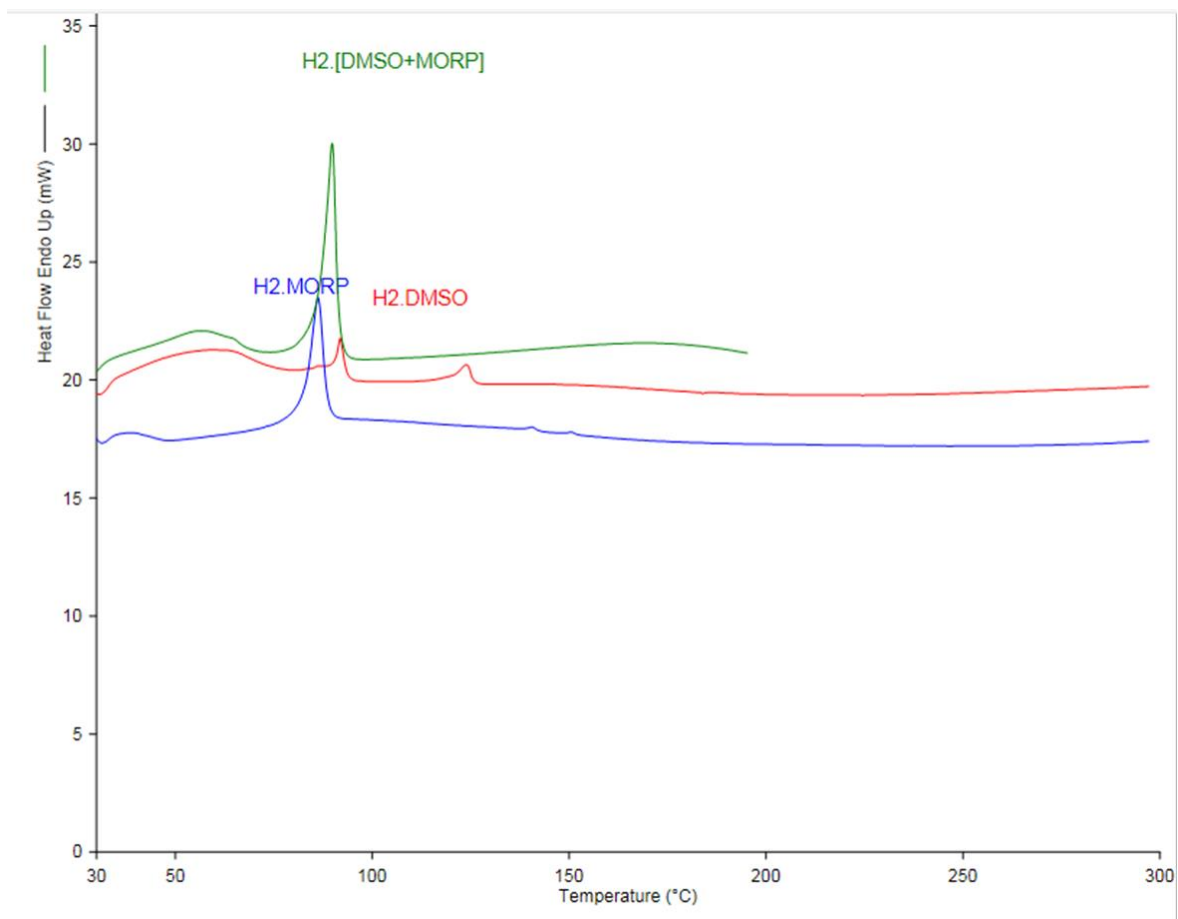


Figure B2 DSC of H2•MORP (blue), H2•DMSO (red) and H2: DMSO/MORP (green).

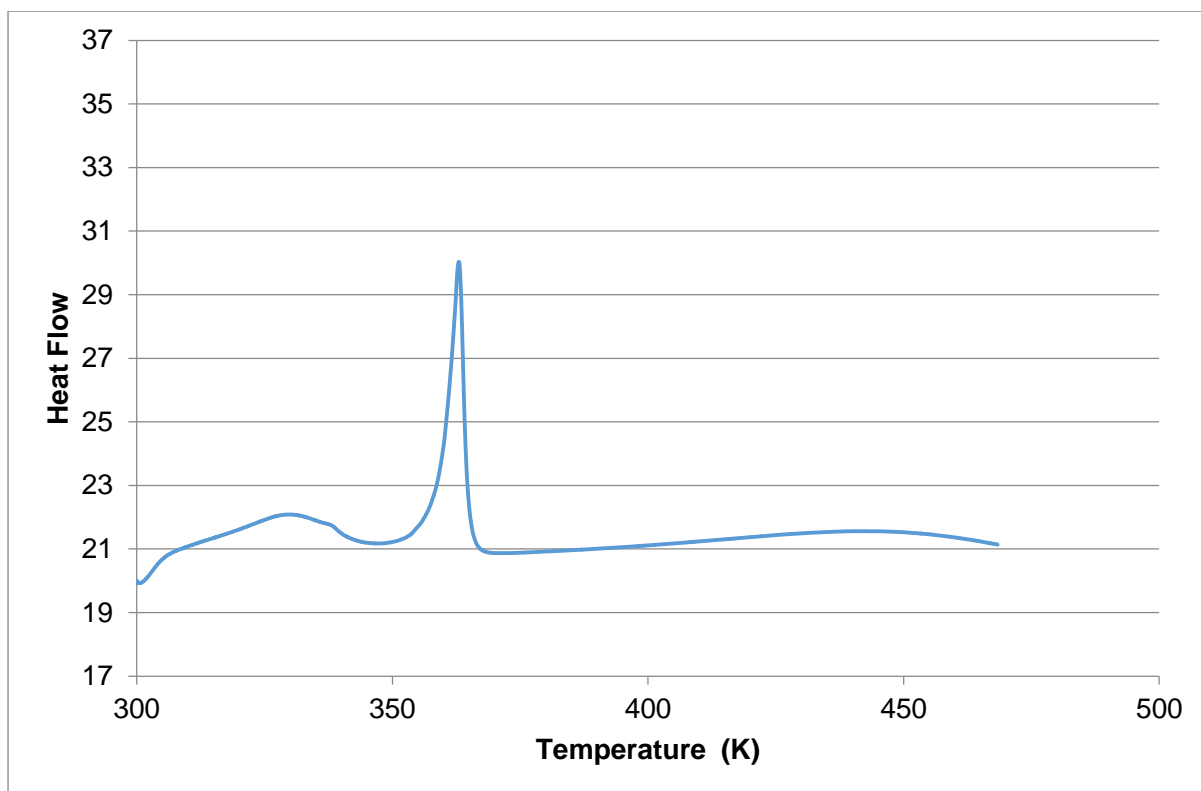


Figure B3 DSC of H2: DMSO/NMP.

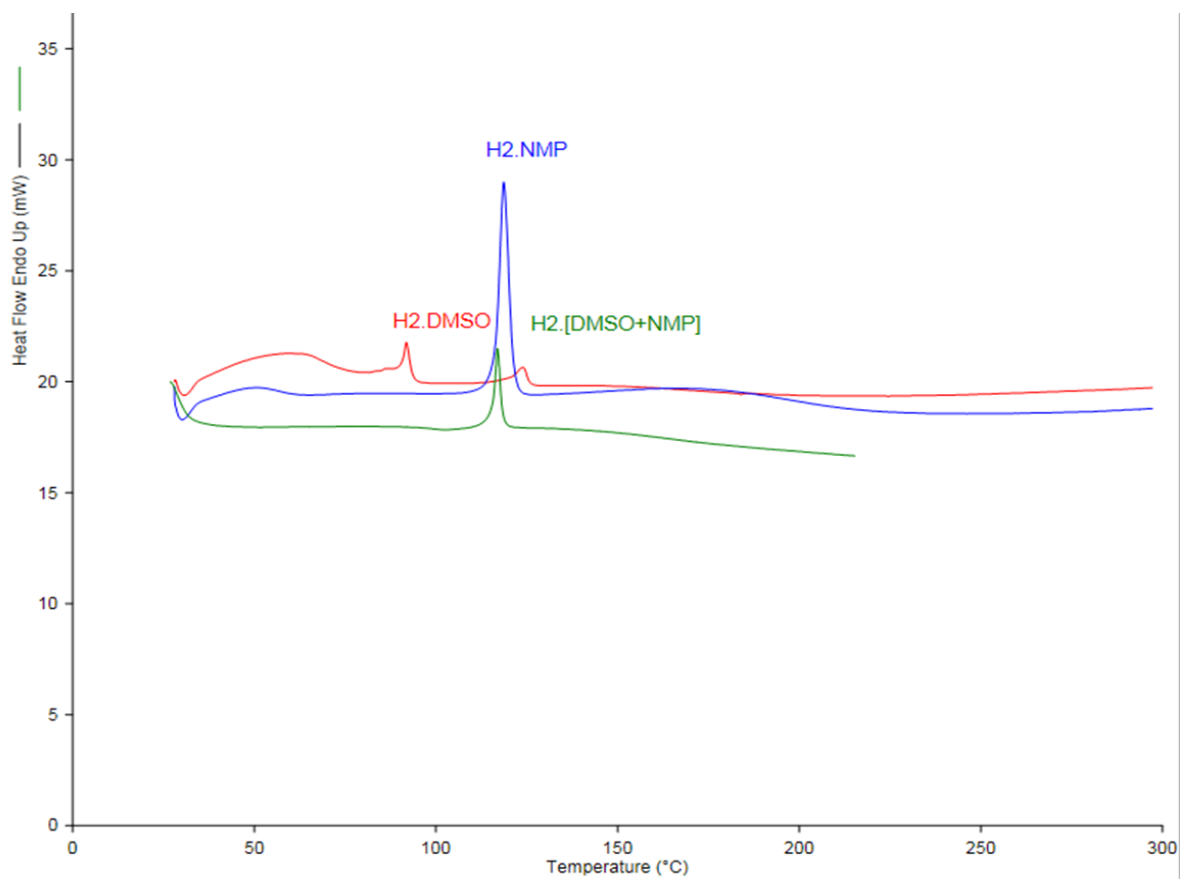


Figure B4 DSC of H2·DMSO (red), H2·NMP (blue) and H2: DMSO/NMP (green).

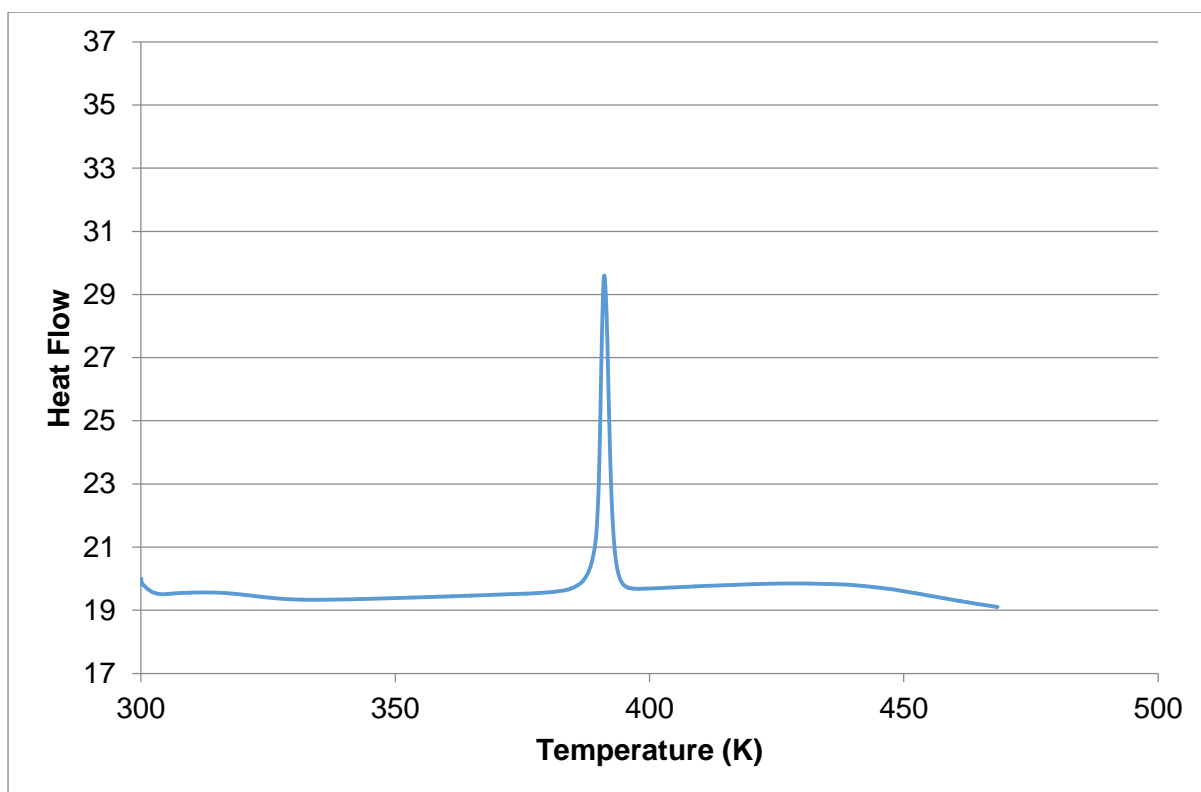


Figure B5 DSC of H2: NMP/MORP.

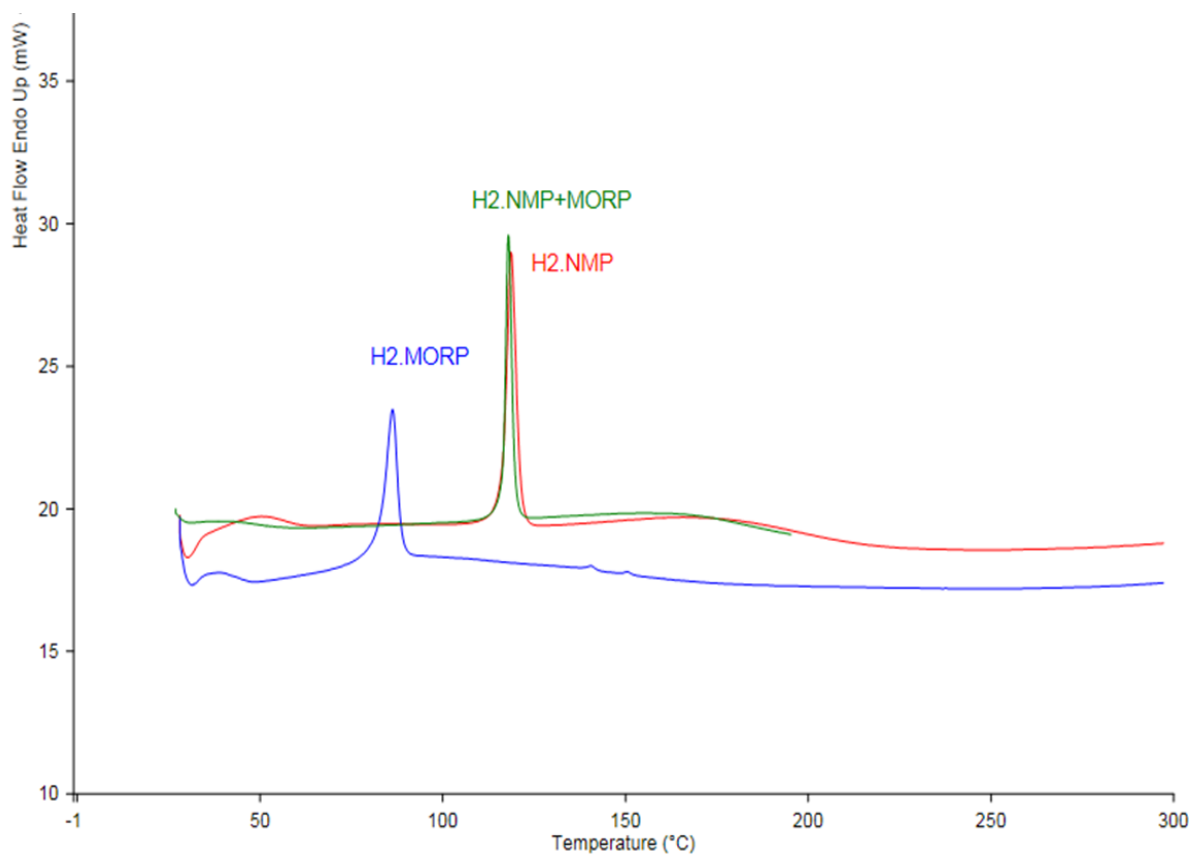


Figure B6 DSC of H2•MORP (blue), H2•NMP (red) and H2: NMP/MORP (green).